Georgia State University
ScholarWorks @ Georgia State University

Mathematics Dissertations | Department of Mathematics and Statistics

12-10-2018

A Computation Study of Biofilm Development and Dispersal

Howard Smith
Georgia State University

Follow this and additional works at: https://scholarworks.gsu.edu/math_diss

Recommended Citation
Smith, Howard, "A Computation Study of Biofilm Development and Dispersal." Dissertation, Georgia State University, 2018.
https://scholarworks.gsu.edu/math_diss/59

This Dissertation is brought to you for free and open access by the Department of Mathematics and Statistics at ScholarWorks @ Georgia State University. It has been accepted for inclusion in Mathematics Dissertations by an authorized administrator of ScholarWorks @ Georgia State University. For more information, please contact scholarworks@gsu.edu.

A COMPUTATIONAL STUDY OF BIOFILM DEVELOPMENT AND DISPERSAL

by

HOWARD SMITH

Under the Direction of Yi Jiang, PhD

ABSTRACT

Bacterial biofilms are a structured population of bacteria adhered to a biotic or abiotic surface. Bacteria establish a biofilm by encasing themselves in a self-secreted matrix of extra polymeric substance. The matrix, composed primarily of polysaccharides and protein, confers to the individual bacterium enhanced protection from environmental insults. These insults would otherwise be detrimental to the bacteria if they were not part of the biofilm. To properly time when it is most beneficial to establish a biofilm and carry out other process, bacteria have developed a means to communicate using signaling molecules termed autoinducers. These signaling molecules help bacteria to make coordinated decisions.

One such decision is phenotype switching, where some bacteria in the colony change their phenotypes to ensure their survival or the survival of an entire colony. Some species of

bacteria exhibit a clear delineated spatiotemporal pattern of changing their phenotype. In particular, Bacillus Subtilis forms a biofilm that exhibits spatiotemporal patterning during its development. Using an agent-based model that includes thresholds on environmental cues we reproduced the spatiotemporal behavior observed from experiments. Specifically, we incorporate thresholds on the concentration on the level of nutrient and autoinducer to reproduce the experimental pattern. This model represents the first attempt using an agent-based model to reproduce the spatiotemporal pattern exhibited experimentally where phenotype switching is induced by both nutrient and the autoinducer. The model allows us to gain an understand of the interrelatedness between autoinducer levels and nutrient availability.

The end stage of biofilm development inevitably leads to some members of the community dying or leaving through a variety of dispersal mechanisms. We developed another agent-based model to study biofilm dispersal. Dispersal is caused by the weakening of cohesive bonds within the biofilm. We study dispersal under the condition where cohesive forces are weakened to induce dispersion. The weakening of cohesive force allows us to gain insight on the benefits if any dispersal has on the development of a biofilm.

INDEX WORDS: Cellular Potts Model, Biofilm, Agent-Based Model, Quorum Sensing, Autoinducer, Compucell3D, Dispersal, Detachment, Glazier-Graner-Hogeweg

A Computation Study of Biofilm Development and Dispersal

by

HOWARD SMITH

A Thesis/Dissertation Submitted in Partial Fulfillment of the Requirements for the Degree of

Doctor of Philosophy

in the College of Arts and Sciences

Georgia State University

2018

Copyright by
Howard Smith
2018

A Computation Study of Biofilm Development and Dispersal

by

HOWARD SMITH

Committee Chair: Yi Jiang

Committee: Vladimir Bondarenko

Eric Gilbert

Xin Qi

Electronic Version Approved:

Office of Graduate Studies

College of Arts and Sciences

Georgia State University

Dec 2018

DEDICATION

This dissertation is dedicated to my family and friends, without whom none of my success would be possible.

ACKNOWLEDGEMENTS

I would like to express my most profound gratitude to my advisor and committee chair Dr. Yi Jiang for believing in me, supporting and guiding me during all these years. I would like to acknowledge and thank the rest of my dissertation committee members: Dr. Eric Gilbert, Dr. Vladimir Bondarenko, and Dr. Xin Qi for their time, guidance, and recommendations. I would also like to thank Dr. Xiaoling Wang for providing the experimental data for the first part of the dissertation, always being kind, and helpful. I would like to acknowledge the great people that I worked with in Dr. Jiang's Lab over the past few years. They have always been inspiring, supporting, and helpful. I would like to thank especially the GSU CURVE for allowing me to use the facilities extensively for my research. In addition, I am immensely indebted to the staff of the Mathematics and Statics department. Thank you all.

TABLE OF CONTENTS

ACKNOWLEDGEMENTS V

LIST OF TABLES VIII

LIST OF FIGURES IX

LIST OF ABBREVIATIONS XI

1 INTRODUCTION 1

1.1 Motivation 1

1.2 Biofilm Review 2

1.2.1 Biofilm Formation. 2

1.2.2 The Role of EPS. 4

1.2.3 Quorum Sensing Molecules. 6

1.3 Models of Biofilm Development 9

1.4 Cellular Potts Model (CPM) 11

2 MODELING SPATIOTEMPORAL DYNAMICS 17

2.1 Spatiotemporal Dynamics of Bacillus Subtilis 17

2.2 Model 24

2.2.1 Model Description 24

2.3 Results 30

3 A COMPUTATIONAL MODEL OF BIOFILM DETACHMENT 49

3.1 Biofilm Dispersal 49

3.1.1 Background 49

3.1.2 Mathematical Models of Detachment 51

3.2 Agent Based Model of QS Induced Biofilm Dispersal 57

3.2.1 Cellular Potts Implementation 57

3.3 Results 63

3.3.1 Aim of Study 63

3.4 Conclusion 77

4 CONCLUSIONS AND FUTURE WORK 79

4.1 Conclusion 79

4.2 Future Work 82

REFERENCES 83

LIST OF TABLES

Table 2.2-1 Simulation Values 27

Table 2.2-2 Parameter Values for Thresholds 29

Table 3.2-1 Parameter Values..... 62

Table 3.3-1 Total Number of Dispersal Events 72

LIST OF FIGURES

Figure 1.2-1 Stages of Biofilm Formation. 4

Figure 1.2-2 Function of EPS. 6

Figure 1.2-3 Threshold and Quorum Sensing. 8

Figure 1.3-1 Continuum and Discrete Approaches Modeling Biofilms. 12

Figure 1.3-2 Illustration Valid and Invalid Pixel Copy Attempts. 15

Figure 2.1-1 B. Subtilis Phenotypes. 18

Figure 2.1-2 Spatiotemporal Dynamics Experiment. 19

Figure 2.1-3 Hierarchical Description of Microbial Systems. 22

Figure 2.2-1 Illustration of EPS Production in CPM. 26

Figure 2.2-2 Flow Chart Model. 29

Figure 2.3-1 Spatial and Temporal Dynamics Using One Autoinducer. 31

Figure 2.3-2 Chemical Gradient Using One Autoinducer Low EPS Production. 32

Figure 2.3-3 Chemical Gradient Using One Autoinducer Medium EPS Production. 33

Figure 2.3-4 Chemical Gradient Using One Autoinducer High EPS Production. 34

Figure 2.3-5 Fractional Composition of Different Phenotypes Using One Autoinducer. 37

Figure 2.3-6 Spatial and Temporal Dynamics Using Two Auto Inducers. 38

Figure 2.3-7 Cell Lineage Using One and Two Autoinducers. 39

Figure 2.3-8 Fractional Composition Using Two Autoinducers. 40

Figure 2.3-9 Chemical Gradient Using Two Autoinducers Low EPS Production. 42

Figure 2.3-10 Distance from the Center of Biofilm of the Three Major Phenotypes. 45

Figure 3.1-1 Active vs Passive Dispersal. 50

Figure 3.1-2 Detachment Rules Used in Baclab. 54

Figure 3.1-3 Biomass Detachment as Implemented in the Particle Based Model. 55

Figure 3.2-1 Biofilm Detachment. 60

Figure 3.3-1. Initial Attempt to Initiate Dispersal Using Individual Adhesion Terms. 64

Figure 3.3-2 $upregulated\ +$ and $upregulated -$ Using Equal Values on Both Thresholds. . 65

Figure 3.3-3 Biofilm Morphology. 67

Figure 3.3-4 $Upregulated\ +$ Using and Increased Value for Second Threshold. 69

Figure 3.3-5 Loss of Biomass. 71

Figure 3.3-6 Fractional EPS Composition. 74

Figure 3.3-7 $EPS +$ VS $PS -$ 76

LIST OF ABBREVIATIONS

EPS	Extracellular polymeric Substance
CPM	Cellular Potts Model
CC3D	Compucell3D
B. Subtilis	Bacterium Species Bacillus Subtilis
QS	Quorum Sensing
GGH	Glazer-Graner-Hogeweg
MCS	Monte Carlo Step

1 INTRODUCTION

1.1 Motivation

A biofilm is defined as an assemblage of microbial cells irreversible attached to a surface encased in a extra polymeric substance (EPS) [1]. The EPS plays a central role in the development of a biofilm first aiding in the initial attachment of the biofilm to a surface and later providing protection and hydration to the cells within the biofilm[2]. The protection provided by the EPS leads to the recalcitrant property often exhibited by biofilms. Gaining an understanding of biofilms is an active area of study in many different fields. Of particular interest, is the study of biofilms as they relate to biomedicine and human well-being. Biofilms forming on indwelling medical devices cause bloodstream and urinary tract infections [3]. In addition to forming on medical devices, biofilm are often formed on chronic wounds causing delayed healing and further infections[4]. Patients suffering from cystic fibrosis are susceptible to biofilms formed by Pseudomonas aeruginosa leading to lung infections in these patients[5]. According to the World Health Organization 30% of all diseases and 40% of all deaths throughout the world is due to polluted water, leading to waste water treatment plants using biofilms to aid in bioremediation [6]. The use of biofilm as another tool in water treatment is crucial Given the wide range of fields and application of biofilms it seems imperative to gain a better understanding of the mechanism underlying its development.

Despite many models developed in the past few decades that aim to better understand biofilms there is still a lot unknown about the spatial and temporal dynamics that govern the phenotypic heterogeneity exhibit in developing biofilms, [7]. Specifically, the interactions between a biofilm and signal in its environment that lead to the dynamics observed in vitro. Bacteria are known to use many different environmental ques such Quorum sensing (QS),

nutrient, and Ph levels that are threshold dependent to control their behavior. Yet, the interaction of the different thresholds and how they lead to spatiotemporal heterogeneity have not been incorporated into models.

Mature biofilms are known to disperse once certain thresholds on environmental ques are reached [8]. Specifically, environmental ques that suggest low nutrient availability or autoinducer levels above or below a given threshold can lead to dispersal. Models of dispersal have focused on detachment mechanism due to outside forces, cell lysis or detachment dependent on the thickness of a biofilm or other pre-specified functions. Most models do not include QS or the effect of cohesion on the dispersal exhibited in biofilms.

1.2 Biofilm Review

1.2.1 Biofilm Formation.

For millions of years bacteria constituted the only life on earth. The biofilm mode of growth is said to have evolved has a means for bacteria to survive the harsh environment they must have encountered [9]. A biofilm is defined as a multicellular community of bacteria that is held together by a self-produced extracellular polymeric substance (EPS) [2]. Within the biofilm bacteria form a community where they are able to respond to changing environmental conditions by communicating through QS [10]. QS is used by bacteria to regulate gene expression as a response to cell-density [10, 11]. The regulation of genes as a response to environmental ques enables bacteria to switch to different phenotypes as a survival mechanism [12, 13].

Biofilm are ubiquitous and can be found in medical devices, sewage bioremediation, plant growth promotion, chronic infections and industrial biofouling [14]. For the aforementioned reasons, it is important that we gain a better understanding of the development process that occurs during the establishment of a biofilm. I will discuss some of the important features and implications of bacteria and their associated biofilms.

Biofilm formation is a multi-stage process as illustrated in figure 1.2-1. The first step in the formation of a biofilm is the forming of a conditioning layer. The conditioning layer forms on a surface that is either biotic or abiotic facilitates the attachment of cells to a substratum. The conditioning layer is created by organic or inorganic material from the environment. The process of biofilm formation continues as bacterium in their planktonic state becoming irreversible attaching to the condition surface. The attachment is mediated by secretion of adhesins and appendages located on the surface of the bacterium. The adhesins used are target specific allowing the bacterium to colonize a wide variety of surfaces. Planktonic bacterium use appendages located on their surface to form an initial attachment to the condition layer. The appendages are species specific and can include flagella, fimbriae and pili. Other environmental factors contribute to bacterial adhesion, these include available energy, surface functionality, bacterial orientation, temperature and pressure conditions [15].

Once bacterium attach to a surface they rapidly start to proliferate and secrete EPS to increase cell-cell cohesion. At this stage of development, the bacteria have formed a biofilm and start to take on the mushroom like structure associated with biofilms. The formation of the biofilm now confers enhanced protection against environmental insults allowing for the cells in the biofilm to communicate with each other using QS to regulate their gene expression. The final stage of development is dispersal where cells are released from within. The dispersal is due to

enzymes released by the cells that break down the cohesive forces within the biofilm. Due to the importance of QS and EPS production in the development of a biofilm, each will be discussed in more detail.

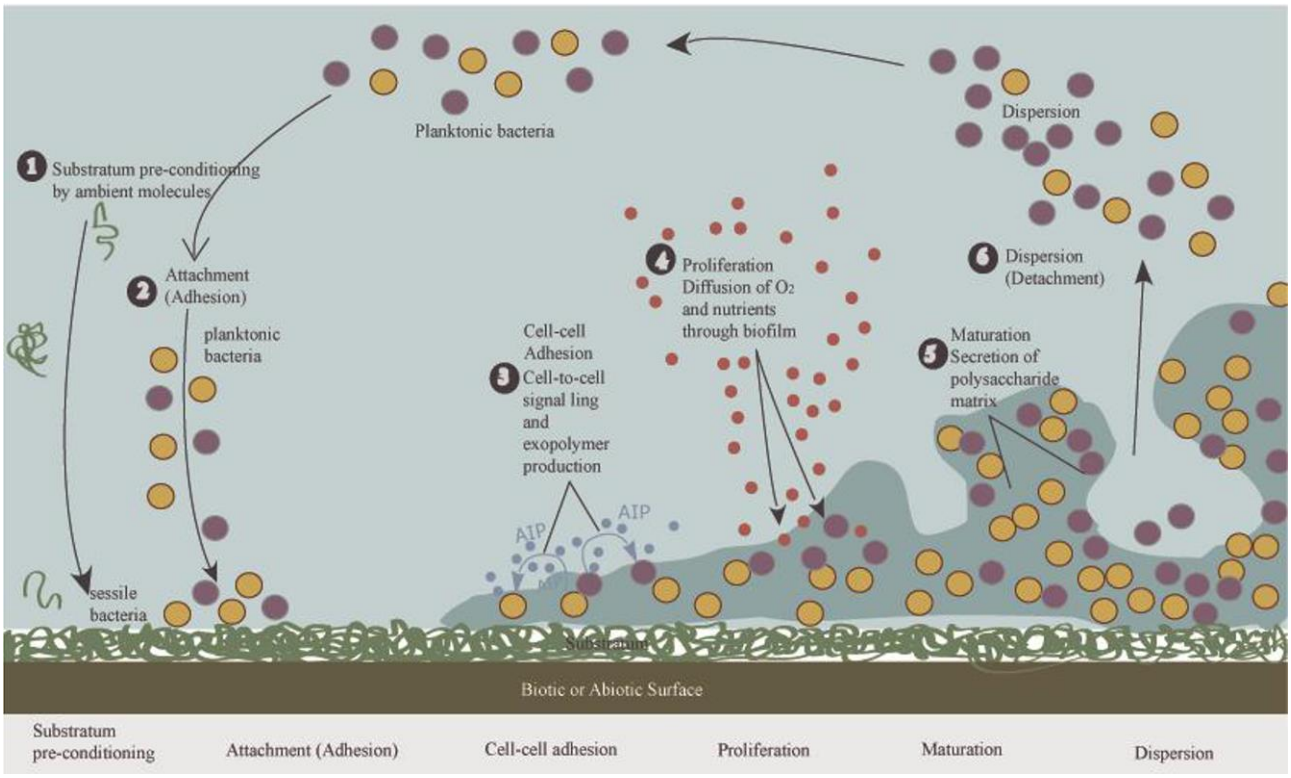

Figure 1.2-1 Stages of Biofilm Formation.
The stages of biofilm development begin with the pre-conditioning of a substratum followed by attachment to the surface. Bacteria then reach a quorum and start producing an extracellular matrix to encase the bacteria and form a biofilm. Within the biofilm the cells consume nutrient and proliferate until a mature biofilm if formed. The next step is the dispersal of some cells from the biofilm in order recolonize. Figure reproduced [16]with the permission of the authors.

1.2.2 The Role of EPS.

EPS encasing bacteria are mostly composed of polysaccharides, proteins and Extracellular genomic DNA (eDNA) [17]. Although the polysaccharides, proteins and eDNA can vary across species and environment the function of the EPS does not change. Across species EPS provides not only structural integrity to the biofilm but also serves as a protective layer [14]. A complete

list of the functions of EPS is provided in figure 1.2-2. A central role of EPS is to improve adhesive and cohesive forces within the biofilm. Specifically, EPS enhances adhesion to solid surfaces and the cohesive forces between microbes to increase their accumulation leading to the formation of a mature biofilm[18]. The increased adhesive and cohesive force conferred by EPS has been proven as one of the reasons biofilms are difficult to remove[19]. The increased cohesive and adhesive forces caused by secreted EPS also contributes to the mushroom like structures associated with biofilms [20, 21]. EPS occupies a majority of the space in a biofilm. The occupancy affects the diffusion of signals that in turn produce chemical and nutrient gradients within the biofilm. The gradients lead to distinct environmental niches in the biofilm. The microenvironments in turn lead to spatial organized gene expression and spatial heterogeneity[18].

Function	Relevance for biofilms	EPS components involved
Adhesion	Allows the initial steps in the colonization of abiotic and biotic surfaces by planktonic cells, and the long-term attachment of whole biofilms to surfaces	Polysaccharides, proteins, DNA and amphiphilic molecules
Aggregation of bacterial cells	Enables bridging between cells, the temporary immobilization of bacterial populations, the development of high cell densities and cell–cell recognition	Polysaccharides, proteins and DNA
Cohesion of biofilms	Forms a hydrated polymer network (the biofilm matrix), mediating the mechanical stability of biofilms (often in conjunction with multivalent cations) and, through the EPS structure (capsule, slime or sheath), determining biofilm architecture, as well as allowing cell–cell communication	Neutral and charged polysaccharides, proteins (such as amyloids and lectins), and DNA
Retention of water	Maintains a highly hydrated microenvironment around biofilm organisms, leading to their tolerance of dessication in water-deficient environments	Hydrophilic polysaccharides and, possibly, proteins
Protective barrier	Confers resistance to nonspecific and specific host defences during infection, and confers tolerance to various antimicrobial agents (for example, disinfectants and antibiotics), as well as protecting cyanobacterial nitrogenase from the harmful effects of oxygen and protecting against some grazing protoza	Polysaccharides and proteins
Sorption of organic compounds	Allows the accumulation of nutrients from the environment and the sorption of xenobiotics (thus contributing to environmental detoxification)	Charged or hydrophobic polysaccharides and proteins
Sorption of inorganic ions	Promotes polysaccharide gel formation, ion exchange, mineral formation and the accumulation of toxic metal ions (thus contributing to environmental detoxification)	Charged polysaccharides and proteins, including inorganic substituents such as phosphate and sulphate
Enzymatic activity	Enables the digestion of exogenous macromolecules for nutrient acquisition and the degradation of structural EPS, allowing the release of cells from biofilms	Proteins
Nutrient source	Provides a source of carbon-, nitrogen- and phosphorus-containing compounds for utilization by the biofilm community	Potentially all EPS components
Exchange of genetic information	Faciliates horizontal gene transfer between biofilm cells	DNA
Electron donor or acceptor	Permits redox activity in the biofilm matrix	Proteins (for example, those forming pili and nanowires) and, possibly, humic substances
Export of cell components	Releases cellular material as a result of metabolic turnover	Membrane vesicles containing nucleic acids, enzymes, lipopolysaccharides and phospholipids
Sink for excess energy	Stores excess carbon under unbalanced carbon to nitrogen ratios	Polysaccharides
Binding of enzymes	Results in the accumulation, retention and stabilization of enzymes through their interaction with polysaccharides	Polysaccharides and enzymes

Figure 1.2-2 Function of EPS.
The EPS serves many roles in the biofilm from the initial adhesion on a surface, to building the biofilm by forming the needed architecture and protective barrier. Once the biofilm has formed the EPS recruits and aids in the digestion of nutrients. In the later stage of the biofilm the EPS weakens allowing the release of cells from within the biofilm. Figure reproduced with permission from [22].

1.2.3 Quorum Sensing Molecules.

QS is the language used by microbes to communicate and regulate gene expression. Specifically, it is a form of density dependent cell-cell signaling mediated by an autoinducer. Bacteria are able to secrete autoinducers, which are small molecules that freely diffuse through the environment. The autoinducers then accumulate in the environment until a “quorum” is

reached. Once the threshold determining a "quorum" is reached the cells become up-regulated and produce autoinducer at an increased rate. Once an autoinducer threshold is reached, genes under control of a particular QS system become activated or deactivated [23]. QS systems in bacteria have been generally divided into three classes: (1) LuxI/LuxR–type QS in Gram-negative bacteria, which use acyl-homoserine lactones (AHL) as signal molecules; (2) oligopeptide-two-component-type QS in Gram-positive bacteria, which use small peptides as signal molecules; and (3) luxS-encoded autoinducer 2 (AI-2) QS in both Gram-negative and Gram-positive bacteria[11]. QS is necessary to multiple stages of biofilm development since QS allows a bacterium to change its phenotype [24]. In particular, during the early stage of development, bacteria are able to switch to different phenotypes to establish a biofilm. For example, B. Subtilis express the $tapA - sipW - tasA$ operon and start secreting matrix encasing the bacteria and increasing the adhesive force to the substratum[25]. At a later stage QS is responsible for dispersal by altering genes as a response to environmental ques or chemical signals produced by an aging biofilm [26].

Bacteria also use QS to collectively produce virulence factors in eukaryotic hosts causing a myriad of biofilm related diseases and infection [23]. Biofilm related diseases and infection such as cystic fibrosis, bacterial endocarditis and corneal ulcers are notoriously difficult to treat because of the matrix [27], which confers enhanced protection against antibiotics and other environmental insults that would kill a bacterium in a planktonic state. Several mechanisms have been put forth to explain the resistance exhibited by biofilms. One such mechanism is that resistance to antibiotics is due to slow or incomplete penetration of antibiotic into the biofilm due to the presence of EPS[27]. Another is that within a biofilm they are altered microenvironments of low metabolic substrate. In these environments, cells do not grow and are therefore immune to

penicillin that cannot act on such cells. It is also been proposed that a subpopulation within the biofilm form a protected phenotype that enable them to survive treatment with antibiotics [28]. This enhanced protection from antibiotics makes biofilm associated diseases such as cystic fibrosis, periodontitis and other biofilm associated diseases difficult to treat. Due to the recalcitrant behavior of biofilm researchers are searching for alternative methods to remove biofilms. These alternative strategies include bactericidal, the use of antiadhesion agents, and the manipulation of dispersal signals.

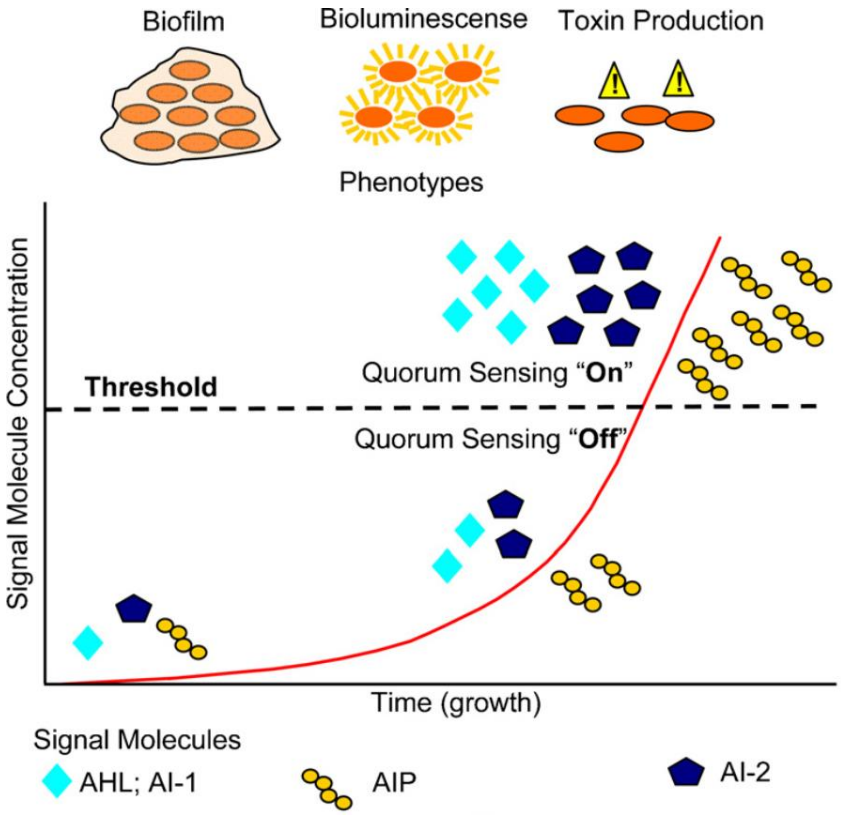

Figure 1.2-3 Threshold and Quorum Sensing.
Schematic representation of switching resulting from signaling molecules reaching threshold. Once a signaling molecule reaches a threshold concentration. Bacterium can express genes leading to the formation of biofilm by switching to an EPS secreting phenotype. The phenotypes under the control of QS varies from species to species and include biolumiscense, toxin production, and motility. Figure reproduced with permission from [29].

1.3 Models of Biofilm Development

Mathematical and computational models have become complementary to lab experiments. Mathematical models of biofilms are used to study many of the process in the development of a biofilm. Specifically, mathematical and computational models of detachment, chemical signaling, competition, cooperation, EPS production and other properties of biofilm growth have been developed [30-34]. Models of biofilms are categorized as either discrete or continuum models. Figure 1.3-1 gives a graphical illustration of the difference and similarities between the two approaches used when modeling biofilm. We will briefly discuss both types of models and do not attempt to give a full review since an up to date and recent review already exist [7].

The earliest models of biofilm were 1-D continuum models were the processes involved in the evolution of the biofilm were modelled using ordinary or partial differential equations. Specifically, early attempts at describing the development of the biofilm modelled. However, the 1-D models could not reproduce the morphology observed in experiments. This led to the development of multidimensional continuum models that gave modelers a closer representation of the complex morphology observed in experiments. Continuum models were modified to include a wide variety of biofilm phenomena that include detachment, antimicrobial penetration, the viscoelastic properties of biofilms, chemical signaling and pattern formation. An advantage of this modelling approach for researchers is that they are deterministic allowing for easy interpretation. Although multidimensional models gave a better representation of biofilm morphology than a 1-D model. Multidimensional continuum models could not account for the contribution of individual cells to the morphology of a biofilm or how cell-cell interactions led to the complex morphology of biofilms.

To overcome the shortcomings of continuum modeling researchers developed discrete models. Discrete models improved on the shortcomings of continuum models by enabling the modeler to assign properties and rules to individual cells. This approach allowed a researcher to interpret the morphology of a biofilm, as a consequence of a cell's interaction with its environment or its interaction with other cells. Discrete models are classified as either cellular automata, hybrid (discrete and continuous) or individual based. Although broadly classified together as discrete models, the approach used to represent biomass differ in each modelling framework.

Briefly, In CA models, the biomass is represented in an array of small compartments, as opposed to the agent-based representation of the individual based models that use particles located anywhere in space and characterized by essential state variables like cell mass and volume[35]. CA models are grouped in to three classes: (1) deterministic or Eulerian automata; (2) lattice gas models; and (3) solidification models[36]. With each class having a slightly different approach when it comes to modeling. In Eulerian automata, the evolution of the biofilm is modelled on a fixed lattice with each lattice point having a state associated with and the following state determined by the earlier state of a cell and its neighbor[35]. Lattice gas models are suited for modelling at the mesoscopic scale since each cell is large enough to contain a considerable number of microscopic particles but small compared to the macroscopic length scale in the system [37]. The solidification model takes a similar modeling approach as the lattice gas model with the exception that the cells can be in a bound state. Although, the cellular automata models give a more realistic model of cells these models cannot account for the contribution a cell's shape might have on the formation of a biofilm. To overcome the limitation of the CA models we use the Cellular Potts Model.

1.4 Cellular Potts Model (CPM)

We choose the Cellular Potts Model since it is able to describe an individual cell and its contribution to the overall development of the biofilm. Furthermore, we would like to account for the contribution if any the cells shape has on the patterning and spatiotemporal distribution of cells during the development of the biofilm. The CPM also called the Glazier-Graner-Hogeweg model takes an approach to modeling biological system that is most similar to the individual based model in its representation of biomass.

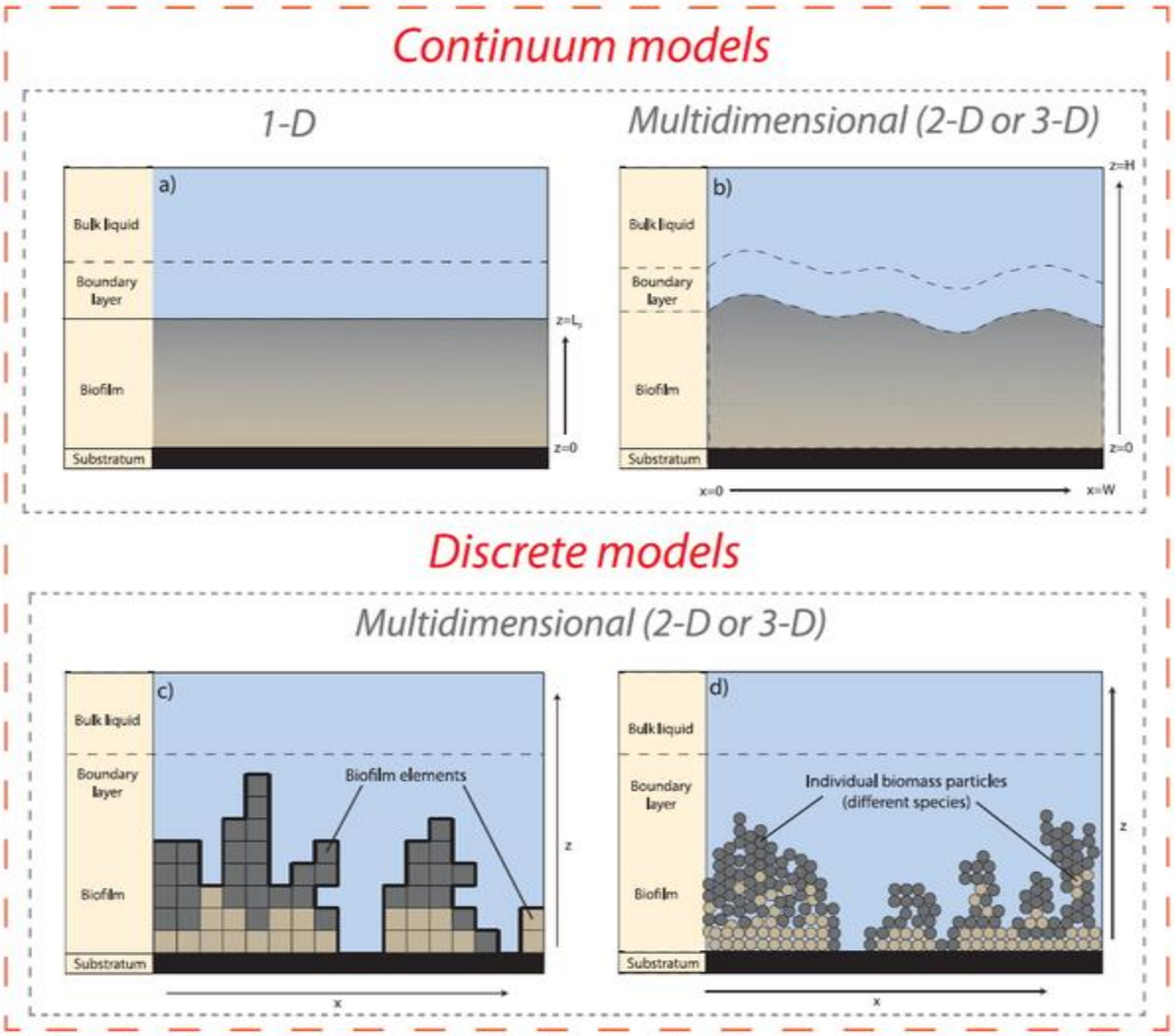

Figure 1.4-1 Continuum and Discrete Approaches Modeling Biofilms.
In (a) the biomass can only spread in one direction vertical to the substratum (b) the biomass is can spread in both the vertical and horizontal directions giving a better understanding of its morphology. (c) A discrete cellular automata representation of biomass. The biomass is represented as rectangles (d) takes the approach of the individual based model representing biomass as spherical agents each having a set of attributes. Figure reproduced with permission from [35].

The CPM model is a lattice-based model that combines the individual representation of cells with molecular level behaviors. The CPM model was first used to study cell sorting due to different cohesive or adhesive forces between different types of cells[38]. The objects in the CPM model are either discrete or continuous, therefore the CPM model can be thought of as a hybrid model. The domains is a *d*-dimensional lattices $\Omega \subseteq \mathbb{R}^d$, where d =1,2,3 [39]. A cell in

the CPM model is made up of a collection of lattice site $\vec{\imath}$ with a unique index $\sigma(\vec{\imath}) \in \mathbb{N}$. In the CPM, the border between different indices represent the cell membrane and σ is interpreted as a degenerate spin from the original Ising approach[40].

Each cell in the GGH model has an associated cell type denoted by $\tau(\sigma)$ and a set of attributes, including a cells volume, surface, cell-cell and cell-environment interactions. These cell attributes along with the cell-cell and cell-environment interactions are implemented in the effective energy of the system through a Hamiltonian *H*:

$$H(t) = H_{adhesion}(t) + H_{constraint}(t) + H_{force}(t)$$

$H_{adhesion}$ models the adhesive/cohesive forces between cells based on Steinberg's Differential Adhesion Hypothesis[41]. The Differential Adhesion Hypothesis states that different cell types adhere to each other with different strengths. The GGH model accounts for differential adhesion by including the term below. The adhesion term $H_{adhesion}$ is at the core of the GGH approach and is usually included in every model.

$$H_{adhesion} = \sum_{(i,j)neighbors} J(\tau(\sigma(\boldsymbol{i})), \tau(\sigma(\boldsymbol{j})))(1 - \delta(\sigma(\boldsymbol{i}), \sigma(\boldsymbol{j})))$$

The energy coefficients $J(\tau(\sigma(\boldsymbol{i})), \tau(\sigma(\boldsymbol{i})))$ are symmetric and represent the binding forces per unit area, $(\boldsymbol{i}, \boldsymbol{j})$ represent a pair adjacent lattice sites. The summation takes place over a predefined neighbor order that is typically set between 1st and 4th nearest neighbors. The Kronecker delta function $\delta(\sigma(\boldsymbol{i}), \sigma(\boldsymbol{j})) = 1\ if\ \sigma(\boldsymbol{i}) = \sigma(\boldsymbol{j}), 0\ if\ \sigma(\boldsymbol{i}) \neq \sigma(\boldsymbol{j})$ assures that only links between different objects contribute to the energy.

The constraint term $H_{constraint}(t)$ incorporates an agent's geometric attributes such as volume and surface area or length in the general form:

$$H_{constraint} = \sum_{\sigma} \sum_{i-constraint} \lambda_{\sigma}^{i}(t)[a_{\sigma}^{i}(t) - A_{\sigma}^{i}(t)]^2,$$

where $a_\sigma^i(t)$ and $A_\sigma^i(t)$ represents the actual and target value of an attribute respectively. The term $\lambda_\sigma^i(t) \in \mathbb{R}_+$ is the Lagrange multiplier, corresponding to elastic modulus of the cell. For low values of $\lambda_\sigma^i(t)$, the actual and target values are allowed to deviate more from values satisfying the constraint, for high values the penalty is large for deviations.

$H_{force}(t)$ describes the point force $\boldsymbol{F}^k$acting on a lattice site *i* with strength u_σ^k at a certain position $\boldsymbol{r}_x = (x_i, y_i, z_i)^T$ on the lattice.

$$H_{force}(t) = -\sum_{i\in\sigma}\sum_{k-force} u_\sigma^k(t)\boldsymbol{F}^k(t)\cdot\boldsymbol{r}_x$$

The GGH model seeks to minimize the energy of the total effective energy on the lattice by using the Metropolis algorithm[42]. The steps in the algorithm are.

1. At each simulation time step, select a lattice site *i* belonging to $\sigma(\vec{\imath})$ and call it the source voxel.
2. Then select another site in its neighbor list at random and call it the target voxel.
3. Calculate the current configuration energy of the system $H_{initial}$ and the energy if the source voxel were changed to the target voxel H_{final}.
4. Calculate change $\Delta H = H_{final} - H_{initial}$
5. Accept change with the probability:

$$P\left(\sigma(\vec{\imath}) \to \sigma(\vec{J})\right) = \begin{cases} e^{-\Delta H/T} \; if & \Delta H > 0 \\ 1 \quad if & \Delta H \leq 0 \end{cases}$$

6. Then go to step 1

In the GGH model, $T \in \mathbb{R}_+$ represents the Boltzmann temperature and simulates the membrane fluctuations due to cell activity. *T* determines the probability of a configuration in the GGH model. For example, for very large values of *T*, all copy attempts are accepted while for very small values the system will almost not change. The unit of time in the GGH model is the

MCS, where one MCS is denoted as N copy attempts. In the CPM a MCS has to be translated into an actual unit of time. Making a direct correspondence between the model and the actual time scale not be straightforward. However, a realistic correspondence is usually set by fitting a posteriori the temporal dynamics of the simulated phenomenon with the relative experimental counterparts[43].

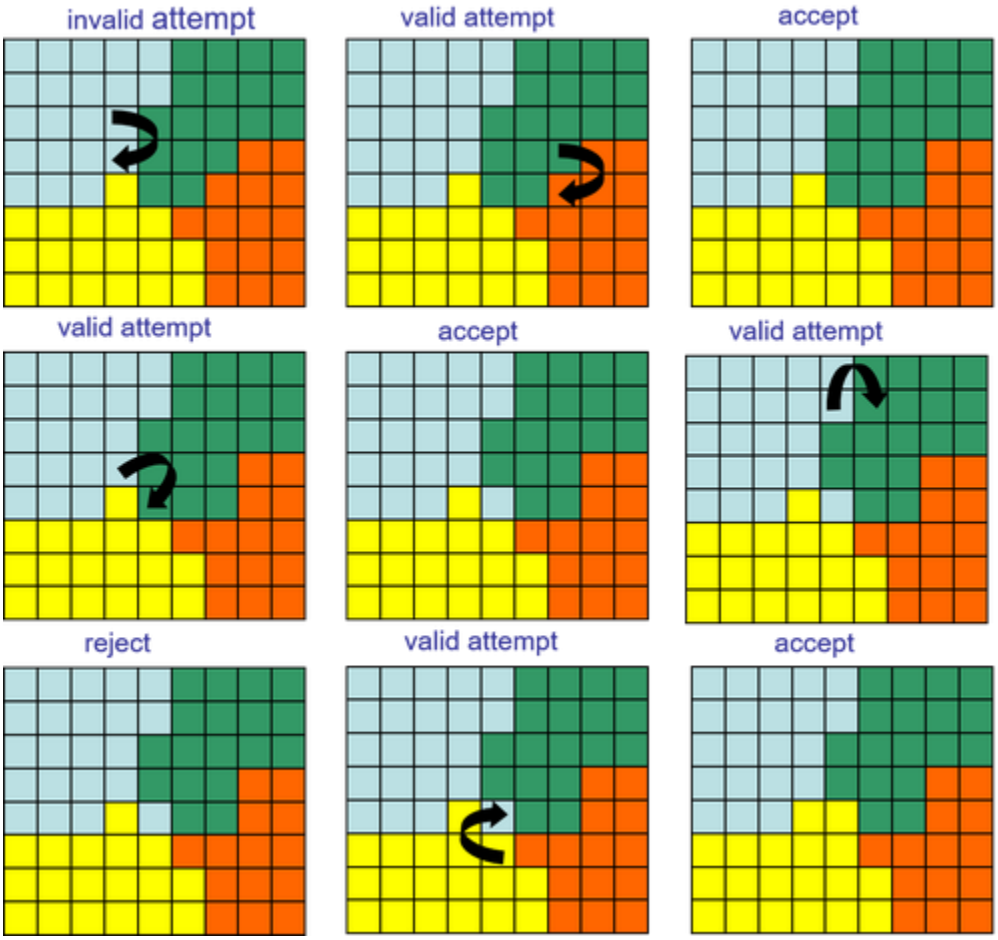

Figure 1.4-2 Illustration Valid and Invalid Pixel Copy Attempts.
A successful pixel copy attempt $\Delta H < 0$ will lead to the source pixel replacing the target pixel.
Figure reproduced with permission from authors.

In the CPM framework, continuous objects such chemical signals that lie within discrete objects (as DNA, RNA, cytosolic ions, and proteins) or its external environment (as nutrients,

growth factors, matrix proteins, matrix metalloproteinases) are modeled using reaction diffusion equations[43], which have the general form

$$\frac{\partial c(i,t)}{\partial t} = \nabla \cdot [D_c(i,t)\nabla c(i,t)] + F(c).$$

In the equation, $c(i,t)$ denotes the concentration at a site i on the lattice of a chemical species, D_c represents the diffusion coefficient and F the reaction term. The equation can either apply to the entire domain or selected regions in the domain.

The CPM models are implemented in the open-source software modeling environment CC3D. The software allows users to easily develop multiscale models that are reusable and shareable. The ease of modeling is due to the use of XML and python scripting to control attributes of the cells. CC3D also integrates subcellular modelling by using the system biology markup language (SBML).

In this dissertation, we present two novel methods to study biofilm formation using the CPM modeling framework. We first present a CPM model that incorporates threshold on environmental signals to study the spatiotemporal distribution of specific phenotypes in a developing biofilm. To the best of our knowledge this has not been done before and presents some insight on the factors that lead to phenotypic differentiation. We next use the CPM to model the final stage of biofilm development. Specifically, dispersal in our model is a result of QS and weakening of cohesion within the biofilm using the CPM. Our model presents the first attempt at incorporating QS and weakening of cohesive forces to model dispersal.

2 MODELING SPATIOTEMPORAL DYNAMICS

2.1 Spatiotemporal Dynamics of Bacillus Subtilis

In their planktonic state, bacteria are susceptible to being treated with antibiotics allowing for the reversal of harmful effects caused by bacterial infection[44]. Bacteria can however form a biofilm as a defense mechanism against antibiotic treatment and other environmental insults[16, 28, 44, 45]. A meaningful definition of a biofilm is that they are a community of tightly associated bacteria encased in an extracellular matrix[17, 46, 47]. Once bacteria switch from the planktonic mode to form a biofilm their protection to treatment of antibiotics increase by a factor of 1000 [48]. The biofilm mode of growth provides more resistant to antimicrobials and physical removal[19]. It is this recalcitrant property of biofilm that leads to them being one of the leading causes of infection in medical devices, injured tissue and costly to a myriad of industries due to biofouling[49, 50].

Matrix production is one of the many mechanisms used by bacteria to ensure their survival[28, 47, 51]. Another mechanism is phenotypic heterogeneity[52-54]. This allows for what are termed “nonconformist” cells to coexist within an isogenic population[53]. Phenotypic heterogeneity affects many aspects of the bacterial lifestyles, and is assumed to increase bacterial fitness and survival of the whole population or smaller subpopulations in unfavorable environments[53, 55]. The Gram-positive Bacterium B. Subtilis has been shown to exhibit multiple phenotypes during colony development. In particular, B. Subtilis is capable of differentiating into motile, matrix producing cells, spores, competent, surfactin producing, miner, and cannibal cells [12, 56, 57]. Differentiation into the distinct cell types is in response to extracellular signaling molecules produced either by itself, or present in its environment[13]. Although B. Subtilis exhibits a wide variety of phenotypes, the majority of cells in a colony of B.

Subtilis are comprised of three cell types: motile, matrix producing, and spore forming cells [58-61]. Each of these phenotypes play a crucial role ensuring the success of the biofilm.

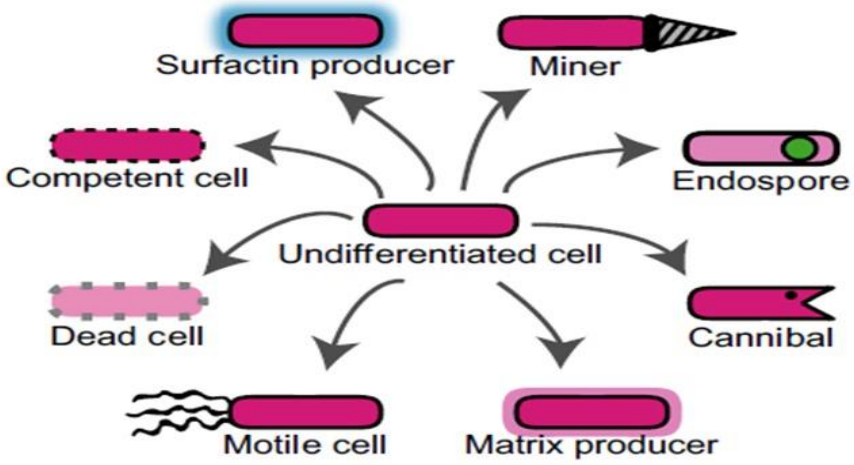

Figure 2.1-1 *B. Subtilis Phenotypes.*
Each cell type has a critical role and occur at different times during the development of the biofilm. However, the majority of cells in the biofilm are either matrix producers, motile or endospore cells. The different phenotypes follow a defined spatiotemporal pattern of occurrence. Early in the development of the biofilm most cells are motile, this is then followed by a switch to matrix producing cells that establish the biofilm. When the biofilm becomes mature some of the cells die or become endospores. Figure reproduced with permission from [62].

Motile cells are responsible for the initial attachment to a substrate [46, 63]. Later in the development process, matrix producing cells produce and secrete EPS composed of protein and exopolysaccharides providing structural integrity to the biofilm [46, 61, 63-66]. Later in the development as the biofilm matures and nutrients become scarce, certain members of the biofilm community initiate the process of sporulation and form endospores [46, 61, 63-65]. Endospore formation allows the bacterium to become resistant to additional external stresses, ensuring survival until more favorable conditions occur[67].

Microbiologist have used several methods to study the phenotypic differentiation exhibited in B. Subtilis and other microbe species[13]. The methods allow for the analysis of a biofilm but with disadvantages. For example, flow cytometry although fast and able to track a

large number of cells it does not offer spatial information[58]. Another method is the thin sectioning of colonies, which offers a limited 2D view of the spatial organization[58, 61]. These methods have proving useful but with the disadvantage that neither is capable of tracking a single colony's development over time. Furthermore, they have fluorescent reporters on no more than two phenotypes[58].

Figure 2.1-2 Spatiotemporal Dynamics Experiment.
Images captured using the non-destructive method. The colors represent fluorescent reporters for motile (yellow), matrix (green), spore forming (blue) and low fluorescent(purple) at different time periods. Time increases from left to right. The first image represents the early stage of biofilm development where most of the cells are motile. The second image represents a later stage in the development where the motile cells are localized to the center of the biofilm and the outer layer. In the final stage the biofilm is comprised mostly of spore forming cells and low fluorescent material. Used with permission of authors.

Therefore, the methods are not able to capture the diverse composition of a biofilm and the spatiotemporal dynamics during development. Recently, Wang et al, develop a nondestructive method for the analysis of biofilm growth based on optical transmission and fluorescence microscopy using a triple-labeled B. subtilis strain NCIB3610[58]. This method is capable of revealing the spatial and temporal distribution of the motile, matrix, and spore forming phenotypes within the biofilm. This method presents an advancement in the study of biofilm colonies since researchers can now track the distribution of the three different phenotypes over space and time.

Although an improvement on current methodology, the method developed in [58] does not give insight on the microenvironment factors that lead to phenotype differentiation during the colony development. Furthermore, it does not distinguish between dead cells and extracellular polymeric substance and instead groups them into one class of low fluorescent material. The method is valid for time intervals less than six hours. Specifically, early in the colony development the fluorescence signal is too weak for the method to accurately determine the composition. While, later in the colony development the method is not able to classify the different phenotypes with great accuracy due to the amount of material with low or no fluorescence becomes significant making estimates based solely on fluorescence become increasingly worse[58]. To gain further understanding of the morphology of the biofilm we use a computational model to simulate the whole process biofilm formation.

The practice of using mathematics and computation to study bacteria and their associated biofilms have been used for decades especially for model species such as B. Subtilis. There have been studies on the genetic networks leading to sporulation, matrix production, virulence and competence [68-73]. Computational and mathematical models have also been proposed to study phenotypic differentiation in B. Subtilis[74-76], and colony patterns [77]. However, to the best of our knowledge there does not exist a model that explains the spatiotemporal organization of B. Subtilis due to changing microenvironmental inputs.

As pointed out in [62] spatiotemporal structures within bacterial communities exhibit diverse morphologies and functions. Studies of self-organization mechanisms and microbial population control strategies have reported on gene networks supporting cell differentiation[46]. Conversely, isolated features of community morphology have been examined to assess the roles of individual genes in community development[78]. However, morphological responses of

bacterial communities to environmental variations are too diverse to be understood only at the molecular and cellular levels. In this work, we use an agent-based modeling approach to elucidate possible environmental cues that lead to the spatiotemporal dynamics demonstrated during the formation and growth of a B. Subtilis biofilm. We use a threshold on the environmental signals to study the dynamics of B. Subtilis. The threshold mechanism serves as a proxy for cellular behavior and allows for cells to switch their phenotypes based on environmental cues such as nutrient and autoinducer levels.

A biofilm, like any other complex system, interacts at multi-scales. Therefore, to gain a comprehensive understanding of the organization of B. Subtilis, it is imperative that we incorporate the useful interactions that take place on different scales. Our model includes molecular scale behaviors such as chemical secretions. At the cellular scale, we examine cell level behaviors such as adhesion/cohesion, growth and division that affects the organization and development of the colony. At the multicellular scale, we examine the overall spatiotemporal dynamics of the biofilm as a consequence of individual agent behavior.

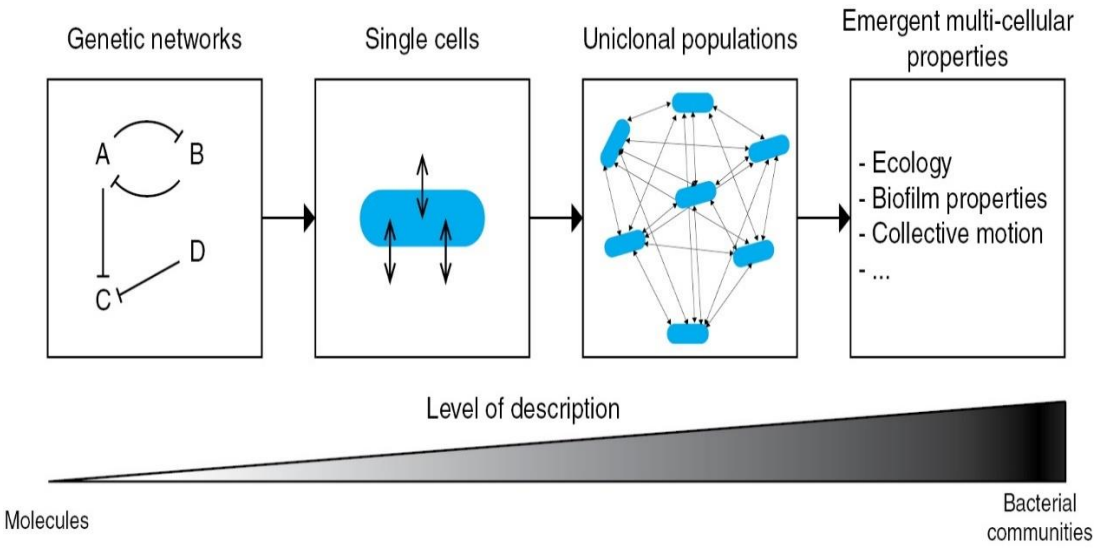

Figure 2.1-3 Hierarchical Description of Microbial Systems.
The lowest level of description the focus is on biochemical reaction networks and involves modelling the genetic networks that lead to the emergent multi-cellular properties. At a higher level than modeling the genetic network, is modelling single cell and their behavior that result in multicellular properties. Single cell modelling is often done using cellular automaton or individual agent based models. We can then use the single cell models to study uniclonal populations to determine how their interactions lead to multi-cellular properties. Figure reproduced with permission from [79].

In the experiments carried out in [58], B. Subtilis demonstrates a clear pattern of spatiotemporal organization figure 2.1-2. It is observed that motile cells differentiate to matrix-producing cells as the biofilm matures. The motile and matrix producing cells then go on to differentiate to either endospores or dead cells as indicated by the low fluorescent at the end of the experiment. Furthermore, these cell types localize to specific area in the biofilm. Motile cells form at the center, while matrix producing cells are distributed throughout the biofilm and spore forming cells that form later are located at the interior[61].

In our model, we focus on two environment signals, QS and nutrient, to aid in understanding of the observed dynamics. We focus on QS since QS has a well-established and central role in establishing a biofilm and controlling the phenotype within through gene networks. For example, the PhrA-RapA QS system controls sporulation in B. Subtilis by

stabilizing the master regulon Spo0A in its phosphorylated form Spo0A~P [56, 80, 81]. Similarly, the matrix producing phenotypes is also under the control of QS through paracrine signaling [82]. Paracrine signaling in B. Subtilis is governed in a sequential manner. Specifically, ComX a peptide pheromone is sensed by a membrane kinase ComP, which then phosphorylates a response regulator ComA [56, 83-85]. Once phosphorylated ComA activates the expression of the operon responsible for surfactin production[56, 83-86]. Surfactin then triggers matrix production in a subpopulation of cells [82, 87]. Matrix production then leads to the establishment of the biofilm.

Likewise, nutrient availability also leads to phenotypic changes and the initiating of matrix producing and sporulation phenotypes[88-90]. In B. Subtilis and other Gram-positive bacteria, CodY, a global transcriptional regulator, is responsible for the adaptive mechanism of cells in response to different levels of nutrient availability[91-93]. The importance of nutrient and QS as signals, which control behavior make them an ideal candidate to investigate the environmental signals that lead to phenotypic heterogeneity. Using these two environmental factors, we aim to reproduce the morphological development observed in[58] and shed some light on the biofilm formation at the mesoscopic level.

2.2 Model

2.2.1 Model Description

Our model of biofilm growth employs the CPM model implemented in CompuCell3D software environment[94, 95]. In this model, as previously described the Hamiltonian *H* describes the interactions and constraints of the cellular system as a total effective energy.

$$H = \sum_{(i,j)neighbors} J(\tau(\sigma(\boldsymbol{i})),(\tau(\sigma(\boldsymbol{j})))(1-\delta(\sigma(\boldsymbol{i}),\sigma(\boldsymbol{j}))) + \sum_{\sigma} \lambda_{vol}(\sigma)(v(\sigma)-V_t\,(\sigma))^2 + \sum_{\sigma} \lambda_{surf}(\sigma)(s(\sigma)-S_t\,(\sigma))^2$$

The first term describes phenomenologically the cell type dependent adhesion between two cells, where $\sigma(i)$ is the cell index of a cell occupying pixel i, $\tau(\sigma(i))$ the cell type, and δ is the Kronecker delta function. The second and third terms represent the volume and surface constraints respectively. The Lagrange multiplier λ determines the constraint strength.

In CPM, the default dynamical algorithm is the modified Metropolis algorithm in which we evaluate the changes in *H* due to the attempted index copy and accept the index-copy attempt with probability:

$$P\left(\sigma(\vec{\imath}) \to \sigma\left(\vec{\imath'}\right)\right) = \begin{cases} e^{-\Delta H/kT} & if \;\; \Delta H > 0 \\ 1 & if \;\; \Delta H \leq 0 \end{cases}$$

where T represents the effective amplitude of cell-membrane fluctuations.

Model Assumptions

In our model cells can be either motile, matrix producers capable of producing EPS, sporulating cells capable of forming endospores or dead. Depending on their phenotype cells in our model are capable of (i) growing due to available nutrient, (ii) dividing once a target volume is reached, (iii) producing and excreting EPS into their environment, (iv) responding to autoinducers and nutrient, and (v) switching their phenotypes.

Cell growth, division, and death

We model each cell's growth by increasing the cell's target volume by a constant ρ proportional to the concentration of nutrient c in the microenvironment.

$$\frac{dV_t(bacteria)}{dt} = \rho * c$$

In our model, a cell performs binary fission when its volume V_d doubles. When division occurs, the cell divides in two equal sized cells along a randomly chosen division axis and assign a new index value to either one of the newly created cells. The cells in our simulation can also die when the nutrient in their microenvironment are depleted. This corresponds to $c = 0.0$. When a cell dies in our simulation it becomes immobile and does not participate in index copy attempts.

EPS production

The EPS in our simulation are represented as a generalized cell type with varying cell size proportionally to the target volume of a cell in our simulation. Experimental values of EPS:Bacteria ratio varies widely from 10:1 to 1:2 [96]. To examine the effect EPS production has on the biofilm, we varied the production rate from $12\ \mu m^2$ (low) to $25\ \mu m^2$ (medium) to $100\ \mu m^2$(high).

The production rate of EPS is:

$$r_{EPS} = \alpha * bacterium\ volume$$

The production of EPS is simulated as follows: a boundary pixel is randomly selected from a cell, the location of that pixel is then used as a new EPS cell type with a predetermined target volume and surface area constraints. This process is illustrated in figure 2.2-1.

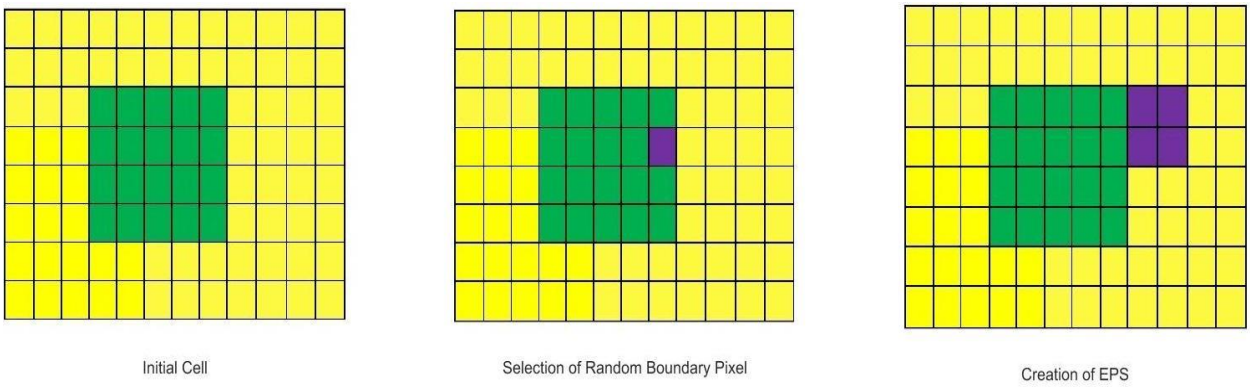

Figure 2.2-1 Illustration of EPS Production in CPM.
A random boundary pixel is selected from a cell that has reached the necessary threshold. Once a random pixel is selected it then becomes the center of the EPS cell type with a predetermined cell with a predetermined cell volume and surface constraints.

Reaction Diffusion Dynamics of Extracellular Molecules

Cells interact with the biochemical signals in their microenvironment by regulating cellular behavior due to environmental ques. Cells in our simulation interact with glucose the nutrient used in our model and the autoinducers released by cells. The spatiotemporal dynamics of nutrient and autoinducer signals are governed by the reaction-diffusion equations below:

$$\frac{\partial G}{\partial t} = D_1 \nabla^2 G - \lambda_1 G$$

$$\frac{\partial A}{\partial t} = D_2 \nabla^2 A - \lambda_2 A + \gamma A$$

Where $G = G(x,t)$is the glucose concentration at location x at time t. D_1 is the diffusion coefficient for glucose and λ_1 is the rate of glucose consumption. Similarly, $A = A(x,t)$ denotes

the concentration of an autoinducer, λ_2 the decay rate of A, and γ gives the secretion rate. The values for these parameters are in table 2.2.1.

Table 2.2-1 Simulation Values

Parameter	Symbol	Model Value	Reference
Glucose Diffusion	D_{Gluc}	$6.7 \times 10^{-6} cm^2/s$	[97]
Glucose Uptake	λ_1	2	Estimated
Autoinducer Diffusion	$D_{A.I.}$	$2.2 \times 10^{-6} cm^2/s$	[98]
Decay Autoinducer	λ_2	$0.693/h$	[98]
Secretion Autoinducer	γ	$1 \times 10^3 nM/h$	[98]
Cell-Cell adhesion for each microbe phenotype	$J_{Bac,Bac}$	4	Estimated
Cell-EPS adhesion for each microbe	$J_{Bac,EPS}$	4	Estimated
Medium-All other cell Types Adhesion	$J_{Med,EPS}$ or $J_{Med,Bac}$	0	Estimated
EPS production rate	r_{EPS}	varies	[96]

Model Parameters and Simulation Domain

The simulation domain corresponds to the 2-D lattice allowing us to make comparison to the experiments[58]. The parameter values used in our simulations are listed in Table 2.2.1. They were obtained from literature or fitted by fine-tuning the model to the observed morphology exhibited in the experiment. Specifically, we estimated the glucose uptake rate so that at the later stage of biofilm development the amount of nutrient on the lattice is zero. This is done to ensure that the biofilm doesn't grow into the boundaries of the domain. We set the surface energies based on the empirical evidence and the accepted current understanding that cell-EPS cohesion is stronger than cell-cell cohesion[15, 99-103]. This led us to choose values of $J_{Bac,EPS} < J_{Bac,Bac}$. Using the generation time of *B.* Subtilis 2 h and equating to the time a cell in

our simulation takes to divide [104], we obtained that one MCS in our simulation is equal to 12 minutes (720s) under conditions of optimal nutrient. The values of λ and the effective membrane fluctuation T were chosen to prevent the cells from disappearing or freezing during the simulation [39]. We set 1 pixel to $2\mu m$, the initial cell occupies a 5×5 grid on the lattice. The simulation domain is 350×350 pixels, corresponding to $700\mu m$ x 700um. In both the vertical and horizontal directions we impose no flux boundary conditions to reproduce the conditions of a biofilm grown on a agar. The lattice is initially saturated with glucose to simulate an agar surface, with an initial concentration set to $15\ mg/cm^3$ as in the experiments[105].

Threshold Conditions

We control phenotypic changes due to environmental ques by placing thresholds on nutrient and autoinducer. The threshold represent a cell-fate decision mechanism and can be used to discriminate between different hypotheses regarding the mechanistic basis of decisions[80]. Figure 2.2-2 illustrates the flow chart of the model. Initially, a motile cell is placed at the center of the lattice. At each Monte Carlo step, the cell consumes nutrient and secretes an autoinducer. A check is made to examine if the cell has reached V_d the doubling volume; if so it divides. In addition, the cell senses its local environment to determine the level of nutrient and autoinducer. If a threshold is reached the cell will switch its phenotype accordingly.

Four different thresholds are used in our model $T_1, T_2, T_3, and\ T_4$. The first three of these threshold couple nutrient and autoinducer while $T_4$is based only on nutrient. T_1 corresponds to a threshold when reached causes a motile cell to switch to the matrix producing phenotype. T_2 is used by matrix producing cells to determine whether the conditions warrant the production of EPS. T_3 corresponds to either a motile or matrix producing cell switching phenotypes to a spore cell. While T_4 is the condition necessary for cells to die.

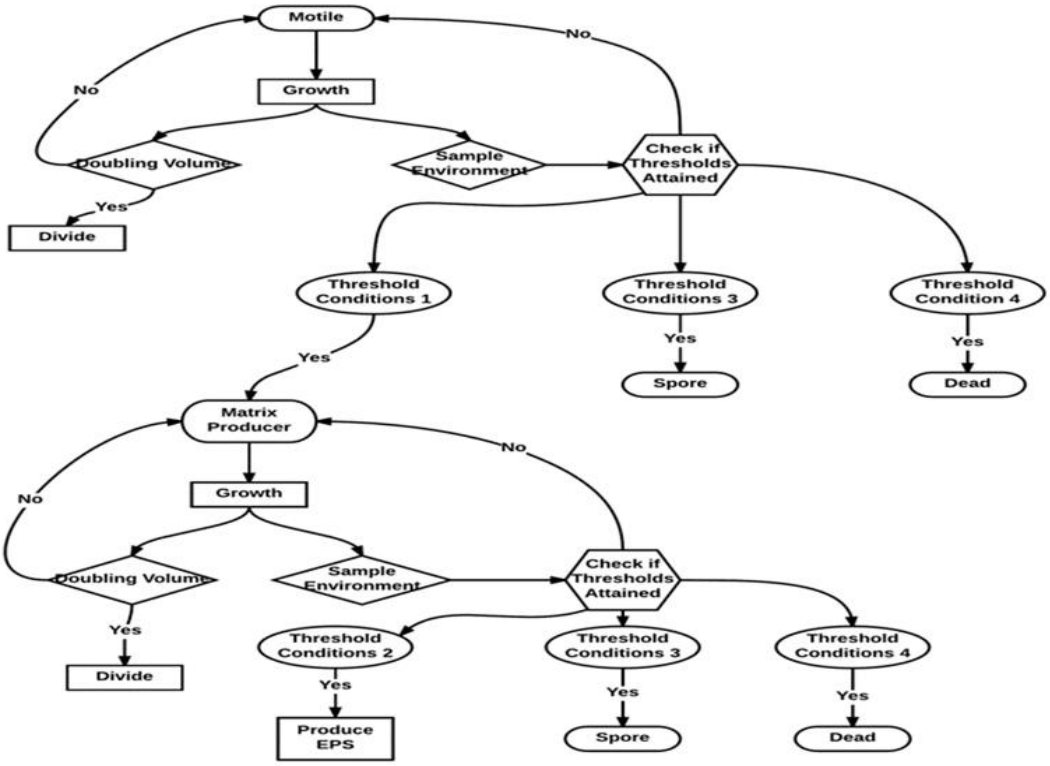

Figure 2.2-2 Flow Chart Model.
Schematic of the different decisions made during the establishment of a colony. Each cell initially starts as a motile cell, their fate during the establishment of the colony is determined by the thresholds on nutrient and autoinducer. The decision to produce EPS is also dependent on a threshold value.

Table 2.2-2 Parameter Values for Thresholds

Cell Type	Glucose (G)	Autoinducer 1 (A1)	Autoinducer 2 (A2)	Threshold
Matrix	$14\ mg/cm^3 \leq G$	$3.75\mu M \leq A1$		T_1
Spore	$4\ mg/cm^3 \leq G \leq 5\,mg/cm^3$	$4\,\mu M \leq A1 \leq 6\,\mu M$	$A2 \geq 3.5\mu M$	T_3
EPS	$7.0\ mg/cm^3 \leq G$	$A1 \geq 4.0\mu M$		T_2
Dead	$0.0 = G$			T_4

2.3 Results

The baseline model utilizing one autoinducer and low EPS production is capable of reproducing the spatiotemporal dynamics exhibited in[58]. Specifically, a subpopulation of motile cells differentiates to matrix producing cells. The matrix producing cells then produce EPS throughout the biofilm. The development of the biofilm then concludes with spore cells, EPS and dead cells composing the biofilm.

To reproduce this spatiotemporal sequence of biofilm development, we start with a single motile cell at the center of the simulation domain. As illustrated in the flow-chart Figure 2.2-2, the cell then grows and divides, forming a colony of motile cells. The growth and division continues altering the cell's microenvironment. Once the local threshold $T_1$is reached, a cell then differentiates and become matrix-producing cells. The matrix producing cells grow and divide until threshold condition T_2 is reached, when matrix producing cells start to produce EPS. From the baseline simulations, we observe that EPS starts being produced by the matrix producing cells closest to the center of the colony at t=29 hours. The onset of matrix producing cells occurs later than the observation time of 25 hours in the experiment[58]. We next observe the emergence of spore forming cells at t=34 hours as T_3 is reached a value in agreement with what was observed in experiments. Spores continues to radially expand until t=36 hours. After t=36, some motile cells start to become either spores or dead cells. In the later stages of development, cells within the matured biofilm start to die due to depleted glucose leaving a small cluster of dead cells at the center and spore forming cells throughout the biofilm. The spatial and temporal dynamics of the biofilm is illustrated in figure 2.3-1.

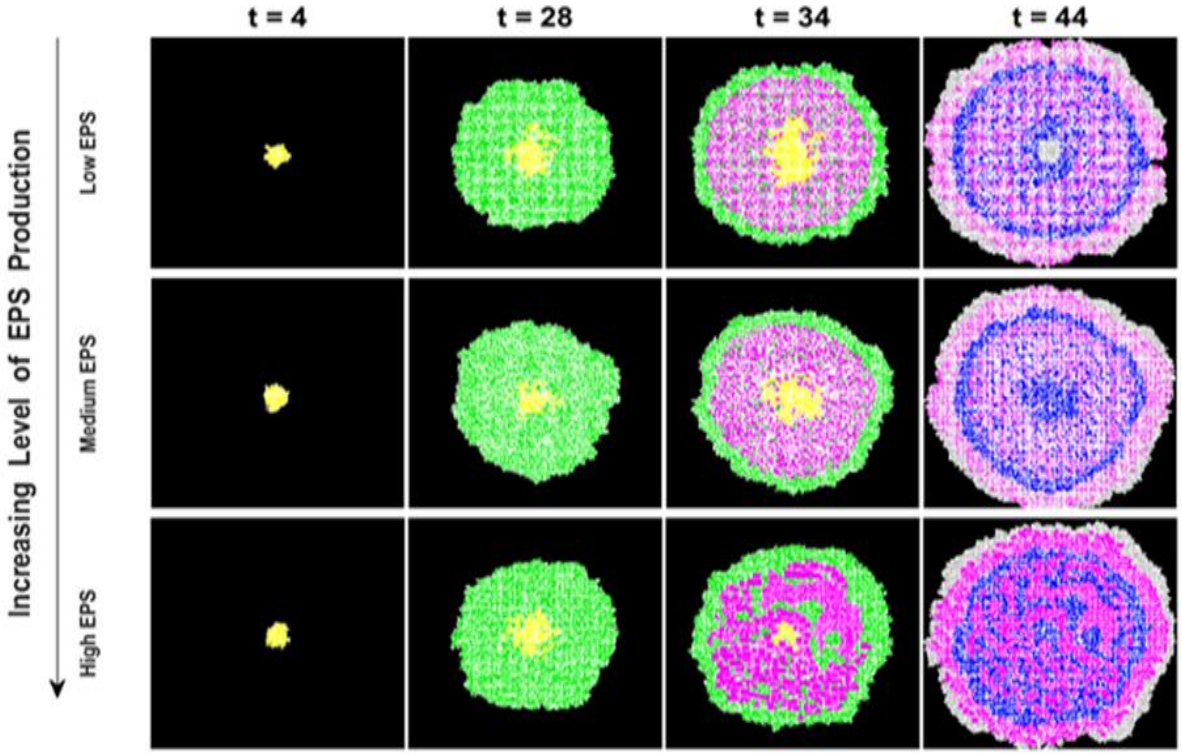

Figure 2.3-1 Spatial and Temporal Dynamics Using One Autoinducer.
For the case of low, medium, and high EPS production. Initially, the motile cells (yellow) occupy the center of the biofilm and is solely responsible for the expansion of biofilm until t=12 hrs. Once the matrix producing phenotype is introduced they become responsible for the expansion of the colony. At t= 28 hrs, we can see that most of the expansion is due to the matrix producing phenotype with the motile (yellow) phenotype still residing at the center of the biofilm. The result holds for all three EPS production levels. The expansion of the colony due to matrix producing cells continues until the threshold to sporulate is reached or the level of nutrient is depleted leading to dead cells. The case of high EPS production leads to patterning not consistent with the experimental results. Specially, the EPS is not distributed equally throughout the biofilm but localized in certain areas. The difference in patterning suggest that the level of EPS production plays a role in the dynamics of the biofilm development.

To quantify the temporal dynamics, we measured the fractional composition of the different cell types over time figure 2.3.5 The ratios obtain from the simulation agree with the experimental ratios and follow the temporal dynamics observed in the experiments. Specifically, motile cells occupy the largest fraction of cells in the biofilm during the early stage of development. As the biofilm grow matrix producing cells occupy a higher fraction of the biofilm.

When matrix producing cells reach their highest value spore forming cells and cells belonging to the group of low fluorescent material (EPS and dead cells) start to appear in the biofilm. At the end of the simulation low fluorescent material occupy the highest fraction. It should be noted that there are some discrepancies in the simulation motile cells occupy close to zero percent whereas in the experiments the number of motile cells is close to ten percent.

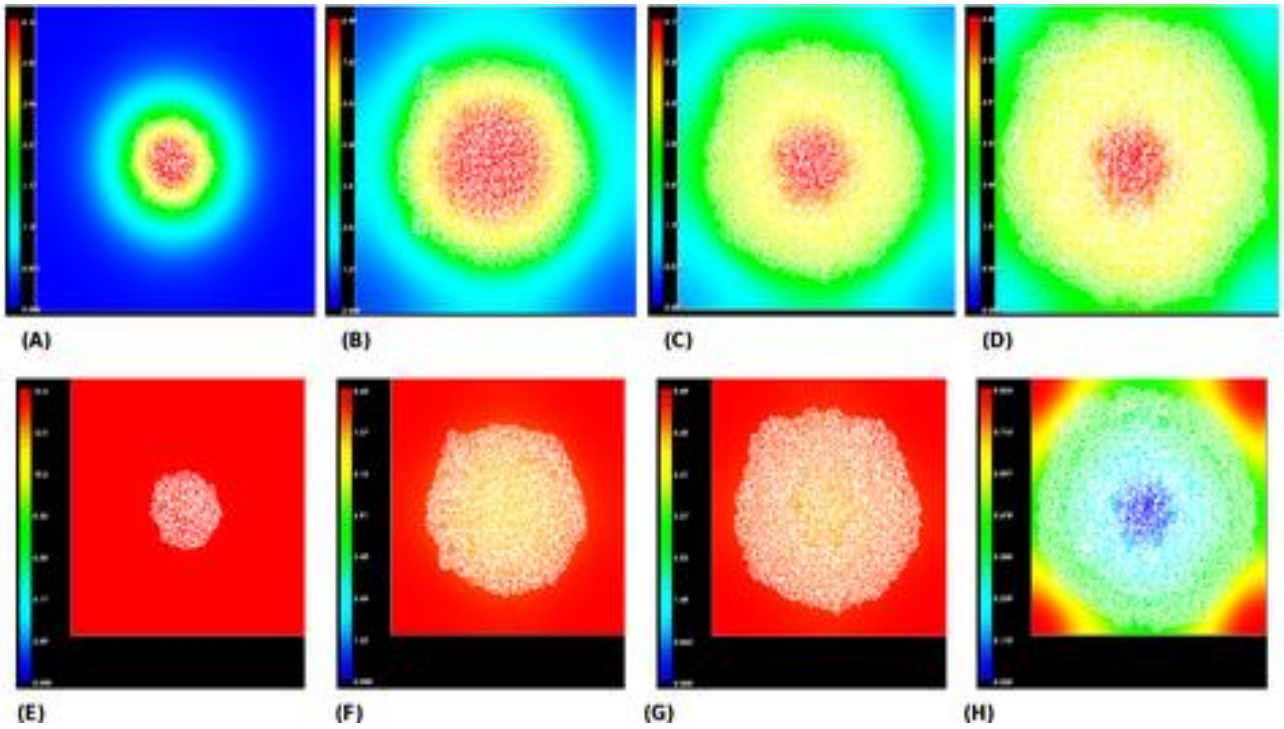

Figure 2.3-2 Chemical Gradient Using One Autoinducer Low EPS Production.
A-C show the gradient of autoinducer over the course of the biofilm development for the case of low EPS production. In A-B there is a well established gradient of AI with the center having the highest value. From B-D, the radius of high concentration (i.e, the red area) decreases, since the matrix producing cell type starts producing EPS. The EPS cells occupying the lattice do not secrete AI, therefore radius of AI decreases. E-H, shows the nutrient gradient. The nutrient is initial evenly distributed throughout the matrix and as the biofilm matures a gradient is established. At the final stage H the concentration of nutrient is lowest at the center leading to the observe dead cells as in figure 2.3-1.

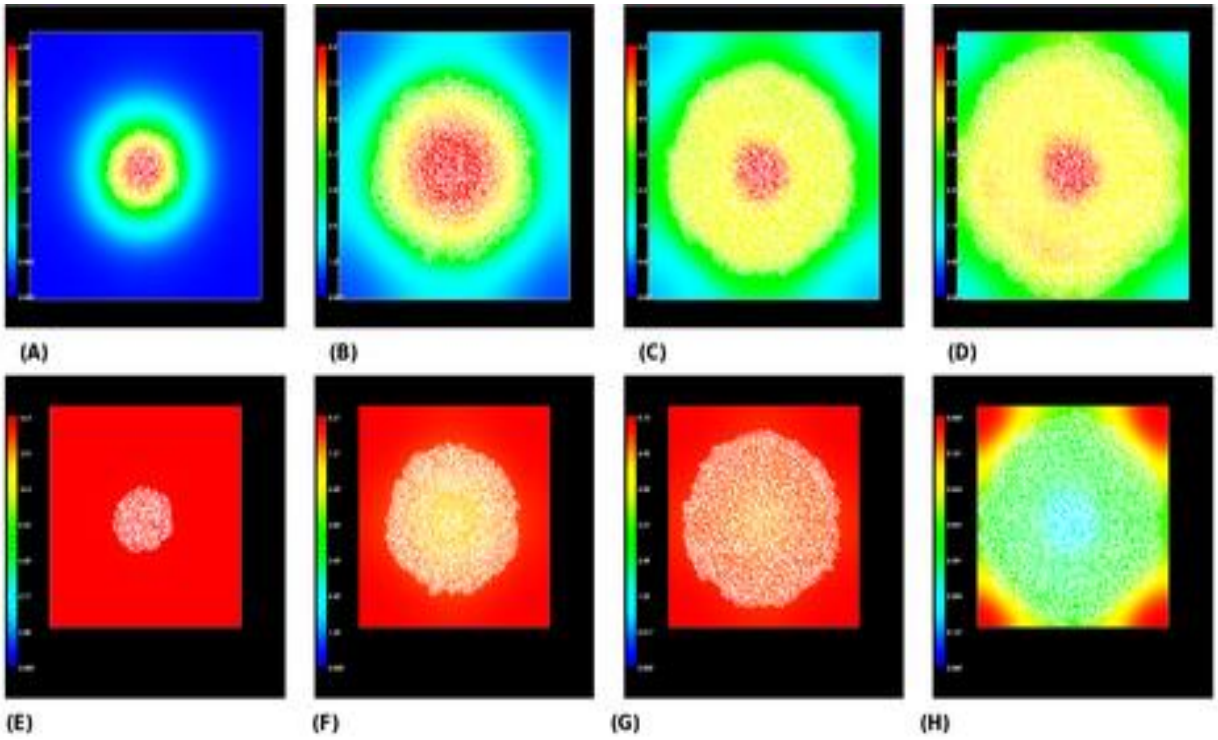

Figure 2.3-3 Chemical Gradient Using One Autoinducer Medium EPS Production.
A-C show the gradient of autoinducer over the course of the biofilm development for the case of Medium EPS production. The dynamics of the autoinducer is similar to what was observed in the case of low EPS production. Specifically, the concentration of autoinducer is highest in the center and the radius of highest concentration increases until EPS production begins then the highest level becomes localized to a smaller radius. The gradient is similar to what was observed in the case of low EPS production.

-

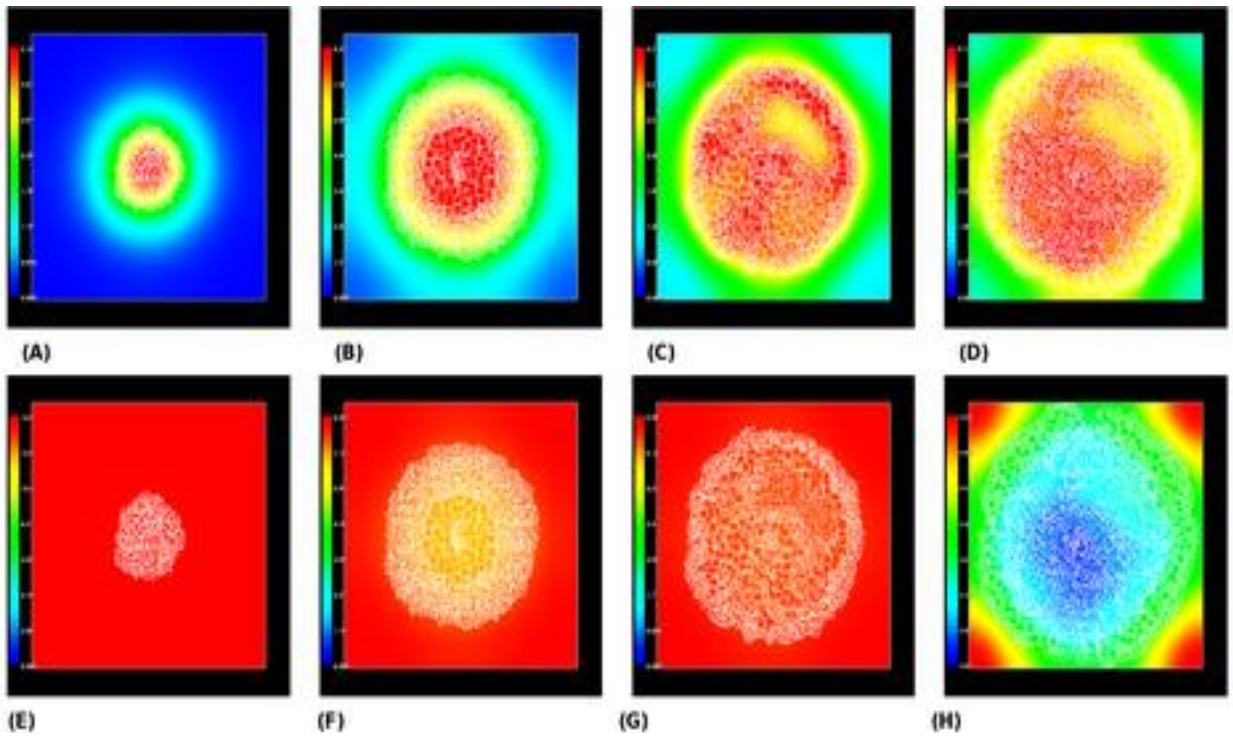

Figure 2.3-4 Chemical Gradient Using One Autoinducer High EPS Production.
A-C shows the gradient of autoinducer for the case of high EPS production. Initially the gradient is similar to what was observe in the case of low and medium EPS production. However, in C the gradient of high EPS production is different once EPS production occurs. Since in the case of high EPS production the EPS is localized to only certain areas of the biofilm. The other areas where the EPS is not present has matrix producing cells still producing AI but have not reached the necessary threshold to produce EPS. This leads to a higher concentration of AI throughout the biofilm.

EPS production rate influences spatial distribution but not temporal dynamics

From the simulations, we observe that the production rate of EPS has an effect on the biofilm. To examine the effects of the EPS production rate on the spatiotemporal dynamics, we varied the amount of EPS produced by matrix-producing cell once they reach T_2 the threshold. Figure 2.3-1 shows the snapshots for the simulated biofilm formation with low, medium and high EPS production rates. In figure 2.3.1, at t=44 hours, the compositions at the center of the biofilm once occupied by motile cells differ depending on the EPS production rate: at low EPS

production rate, the center is comprised of a cluster of dead cells and spore forming cells; at medium EPS production rate, the center of the biofilm is comprised of spore forming cells; at high EPS production rate, the center shows no clear delineation, instead EPS and spore forming cells are interspersed throughout.

The fractional compositions of the different phenotypes over time in figure 2.3-5 show that all three EPS production rates reproduce the phenotype transition points. The fractional composition differs slightly in the case of high EPS production rate. Specifically, the fraction of spore cells is greater at the end of the simulation for high EPS production rate. In our simulation the colony initially consist of only motile cells. In [58] the initially composition is hard to determine due to weak fluorescence. Once the method developed in[58] is able to identify the different phenotypes ($t > 18$ hrs) we observe the majority of the biofilm consist of motile cells. The matrix producing cells then become the majority phenotype in the colony and occupying more than half of the biofilm.

Later in the development of the biofilm the proportion of spore cells and low-fluorescent material form most of the biofilm. At the end of the experiment there is still a small proportion of motile and matrix producing cells. However, if the experiment were carried out longer we would expect all cells would die due to insufficient nutrition. Qualitatively the results obtained from the simulation and experiment agree. Specifically, motile cells form the majority of the young colony , in the case of the experiments the initial proportion is not represented graphically but stated in[58] and[61]. Most of the colony is later comprised of matrix producing cells that arise from motile cells. The proportion is slightly higher in the simulations than experiment.

As the biofilm matures an increase in spores and low-fluorescence material is observed. In the experiments there is a small proportion of spore cells and low-fluorescence material early in the development of the colony. The observed small proportion could be a result of the method not being able to accurately determine the phenotypes for $t < 18$ hours. In the simulation the proportion of spore cells is less than the experiment while the proportion of low-fluorescence material is higher than the values obtain from the experiment. This suggest that the thresholds on EPS and Spore could be improved.

We also observe for matrix producing cells the decline is not smooth as the experiment. The lack of smooth decline is likely due to the production of EPS. Since a pixel from each matrix producing cell is selected to produce EPS. If a large proportion of matrix producing cells reach the threshold simultaneously the overall proportion will decrease. Figures 2.3-1-2.3-5, suggest that the spatial dynamic of the biofilm is affected by the EPS production rate but the temporal dynamics is not.

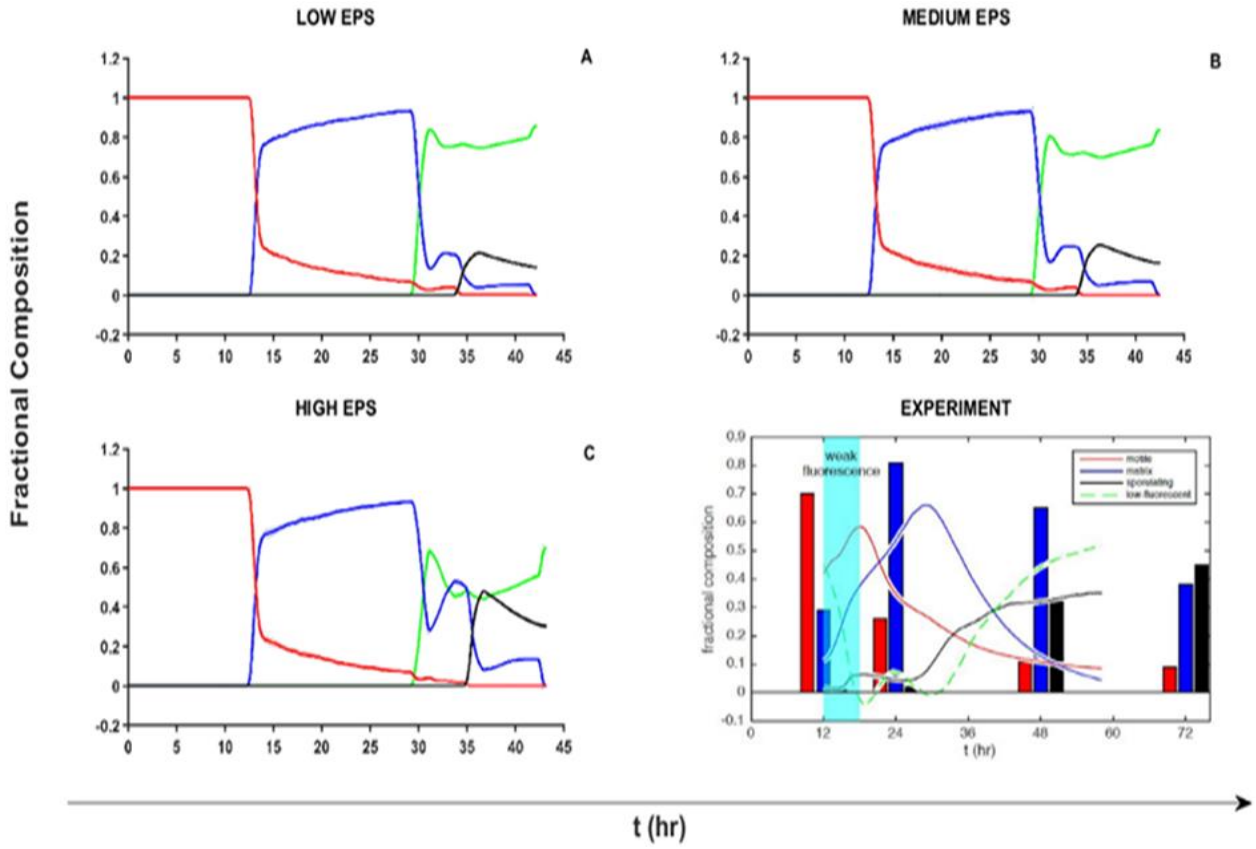

Figure 2.3-5 Fractional Composition of Different Phenotypes Using One Autoinducer. A-C represent the fractional composition of the motile(red), matrix producing(blue), spore(black) and low-fluorescent material (green) for the low, medium and high levels of EPS production respectively. The line chart represents the average of n=5 simulations. The graph labeled Experiment, gives a comparison of the fractional composition of experiment results from [58] (line chart)and [61] (bar chart). The results obtain from the simulations are in qualitatively agreement with the results of the line chart. In A-C we observe that the colony is initially comprised of motile cells. As the biofilm develops the majority of cells become matrix producing phenotypes. As the biofilm matures it is comprised of low fluorescence material. In the experiment the value of the matrix and motile cells never reach zero. However, in the simulations the value of the phenotypes drops to zero. We would expect this to happen if the experiment was monitored further. The experiment is not able to reproduce the dynamics of spore cells. In the experiment the value of spore cells gradually increases where as in the simulation the rise is sharper. The sharp rise is due to the threshold being reached simultaneously by a large proportion of cells.

Two autoinducers capture cell lineage and reorganize spatial location of dead cells.

Experimental evidence[46, 61] suggests a defined cell lineage exists within the B. Subtilis colony. Time-lapse microscopy revealed that motile cells switch to become matrix-producing cells and during further development sporulating cells were derived from matrix-

producing cells[61]. In addition to capturing the spatiotemporal dynamics we wanted to test if our model could reproduce the defined cell lineage. In our baseline simulations figure 2.3.1, spore forming cells developed from motile and matrix producing phenotypes, the proportion of spore forming cells that arise from motile and matrix phenotypes is listed in figure 2.3-7.

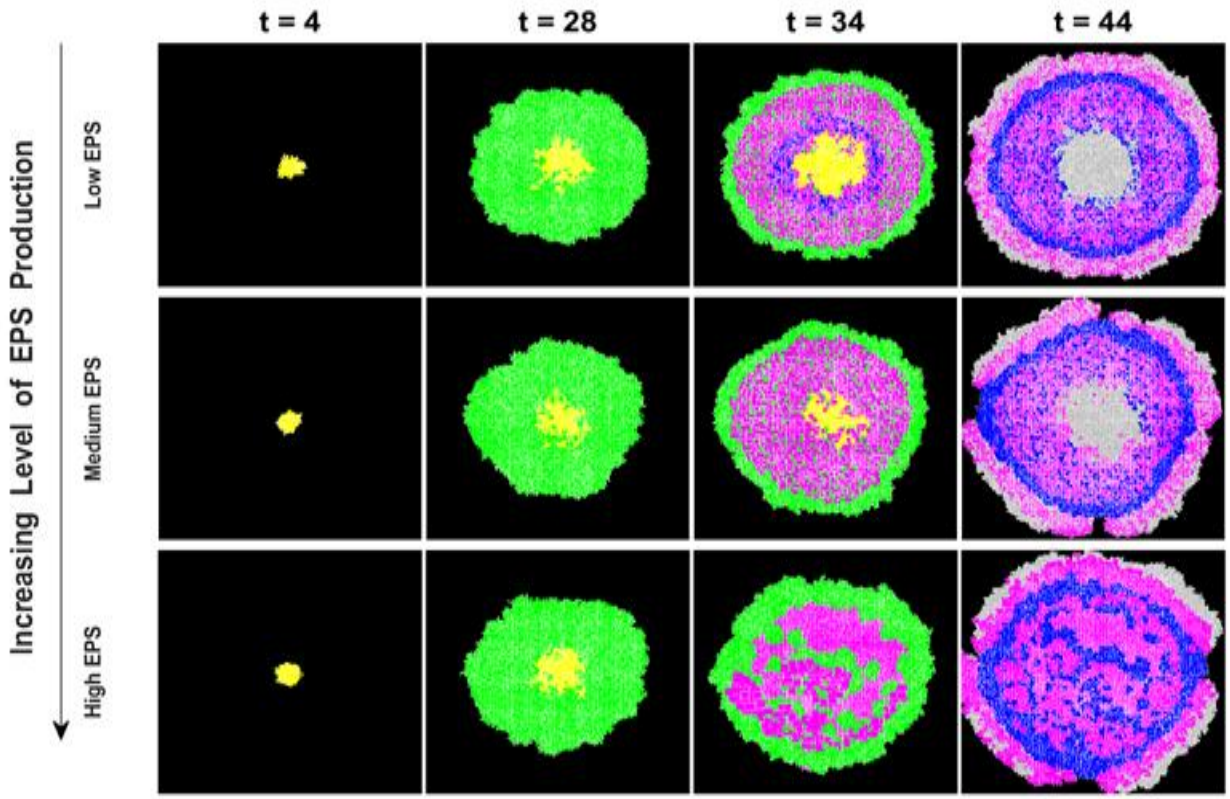

Figure 2.3-6 Spatial and Temporal Dynamics Using Two Auto Inducers.
With the addition of the second autoinducer the spatial and temporal dynamics of the biofilm observed in the case of one autoinducer is preserved. However, with the addition of the second autoinducer the center of the biofilm at the t=44 is now comprised of dead cells in the case of low and medium EPS production instead of a mixture of spores and dead cells. However, the case of high EPS production we still observe a patch distribution of EPS and spore cells throughout the biofilm.

To explain the discrepancy in the linage distribution between simulation and empirical observations, we carried out a parameter scan of the threshold values. However, the thresholds values obtained from the parameter scan that were able to reproduce the desired cell lineage

could not produce the correct spatiotemporal dynamics of the biofilm. This result suggested that an additional mechanism would be necessary to reproduce the observed cell lineage. It has been demonstrated that changes in phenotypes is caused by different autoinducers and often involve more than one autoinducers[13, 46, 57, 61, 106]. For example, sporulation is known to be under the control of at least two QS peptides[86]. Based on experimental evidence presented in[12, 13, 75] we hypothesize that adding a second autoinducer to our baseline model may reproduce the defined cell lineage.

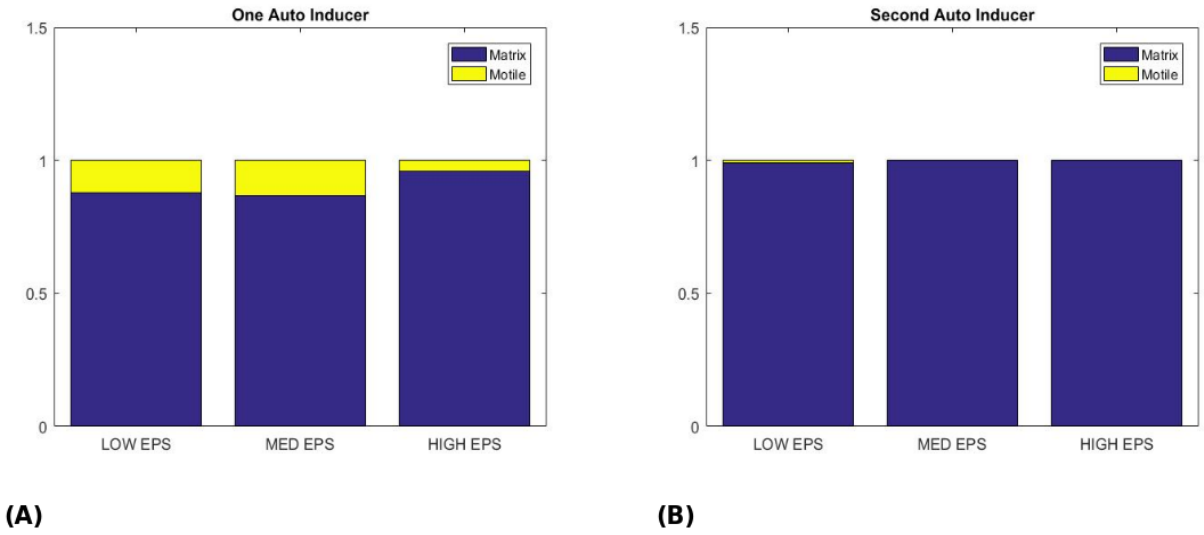

Figure 2.3-7 Cell Lineage Using One and Two Autoinducers.
The proportion of spore cells arising from motile cells in figure A when only one autoinducer is used is not in agreement with experiments in[61]. Specially in[61], presents strong evidence of a defined cell lineage where spore form from matrix producing cells. However, in the simulation where only one autoinducer is used we observe a spore cells forming from motile cells for all three levels of EPS production. After a parameter scan of threshold values we could not reproduce the distinct cell lineage discussed in[61] and also reproduce the spatiotemporal dynamics in[58]. We next decided to use a second autoinducer since it has been observed that different phenotypes are under the control of different signals during the development of a biofilm[56]. The second autoinducer in the model was produced by matrix producing cells. We then used the second autoinducer to establish the threshold concentration where cells would become spores (T_3). With the addition of the second autoinducer the spore forming cells arising from motile cells was highest at the low EPS production at less than two percent of the overall spore forming cells. When the EPS production is at the medium or high level. The spore forming cells that arise from motile cells are zero. This is in strong agreement with the cell lineage observed in[61].

To test this hypothesis, we allow the matrix producing cells to produce an additional autoinducer (A2). With the addition of A2, the threshold T_3 (spore threshold) now depends on the previous nutrient level and the level of A2. We found that in the simulations with the addition of A2, the spatial distribution of the phenotypes within the biofilm is affected (figure2.3-6): the center of the biofilm is now comprised of dead cells in the cases of low and medium EPS production rate. When the EPS production rate is high, the simulation reproduces the distribution observed in the case of one autoinducer.

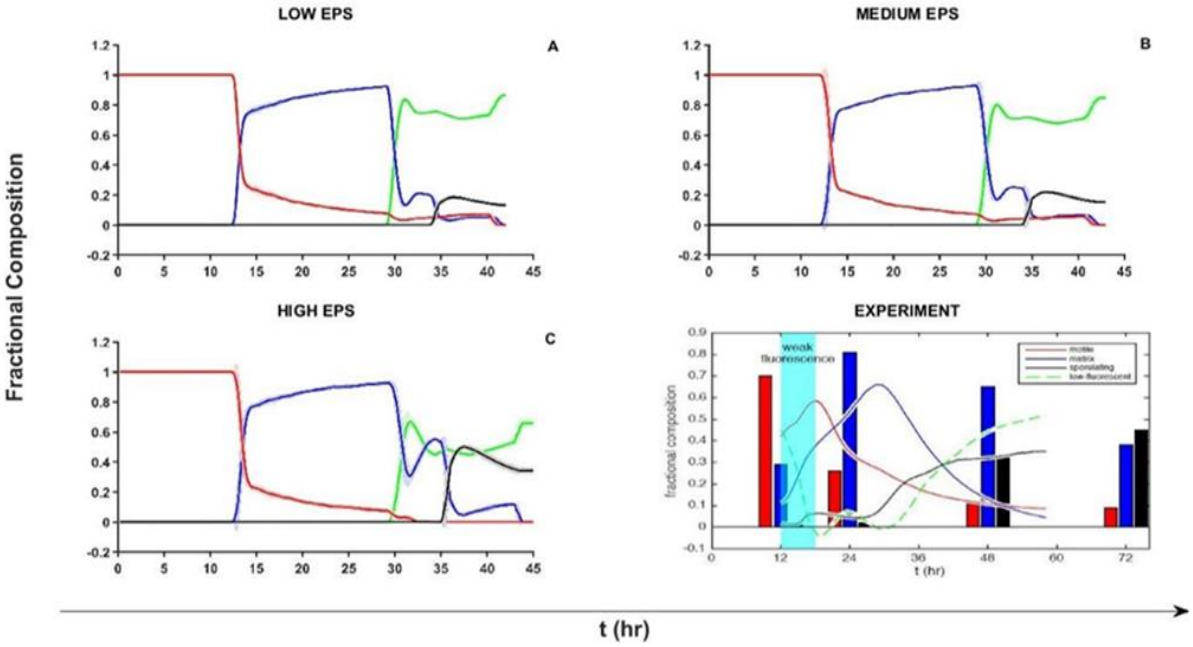

Figure 2.3-8 Fractional Composition Using Two Autoinducers.
The addition of a second autoinducer does not affect the dynamics of the fractional composition. The relative proportions remain the same as in the case of one autoinducer. Specifically, the relative proportion of the different cell types remain the same as in the experiment and the simulation with one autoinducer.

Figure 2.3-8 gives the fractional composition of the biofilm using two autoinducers at the low, medium and high EPS production rate. The dynamics as exhibited in A-C of the biofilm remains the same as the case of one autoinducer and the experiment. Specifically, the proportion exhibit the same qualitative behavior. Figure 2.3-8 of the simulations with two autoinducers at three different EPS production rate replicates the same proportions as the case with one autoinducer. When we examine the cell's lineage plotted in figure 2.3-7 the case with low EPS production rate, a small proportion ($< 2\%$) of the cells arise from motile cells. Furthermore, when the EPS production rate is medium or high, no spore forming cells emerge from motile cells. The lower rate of spore forming cells arising from motile cells suggest that the cell lineage observed experimentally is a consequence of more than one autoinducers.

The gradient of the two autoinducers and nutrient concentration is plotted in figure 2.3-9. Plots (A)-(D) represent the first autoinducer, (E)-(F) represents the nutrient and (I)-(L) represents the second autoinducer. From the plot, we observe that the inclusion of the second autoinducer produces a distinct chemical gradient. Specifically, the matrix producing cells establish a gradient of autoinducer independent of motile cells since motile cells are not capable of producing the second autoinducer but can only responded to it. By establishing a second gradient with the additional autoinducer. We are able to establish a threshold that will allow the majority of cells that become spores to arise from matrix producing cells while still exhibiting the spatiotemporal dynamics observed in the first simulation and experiment.

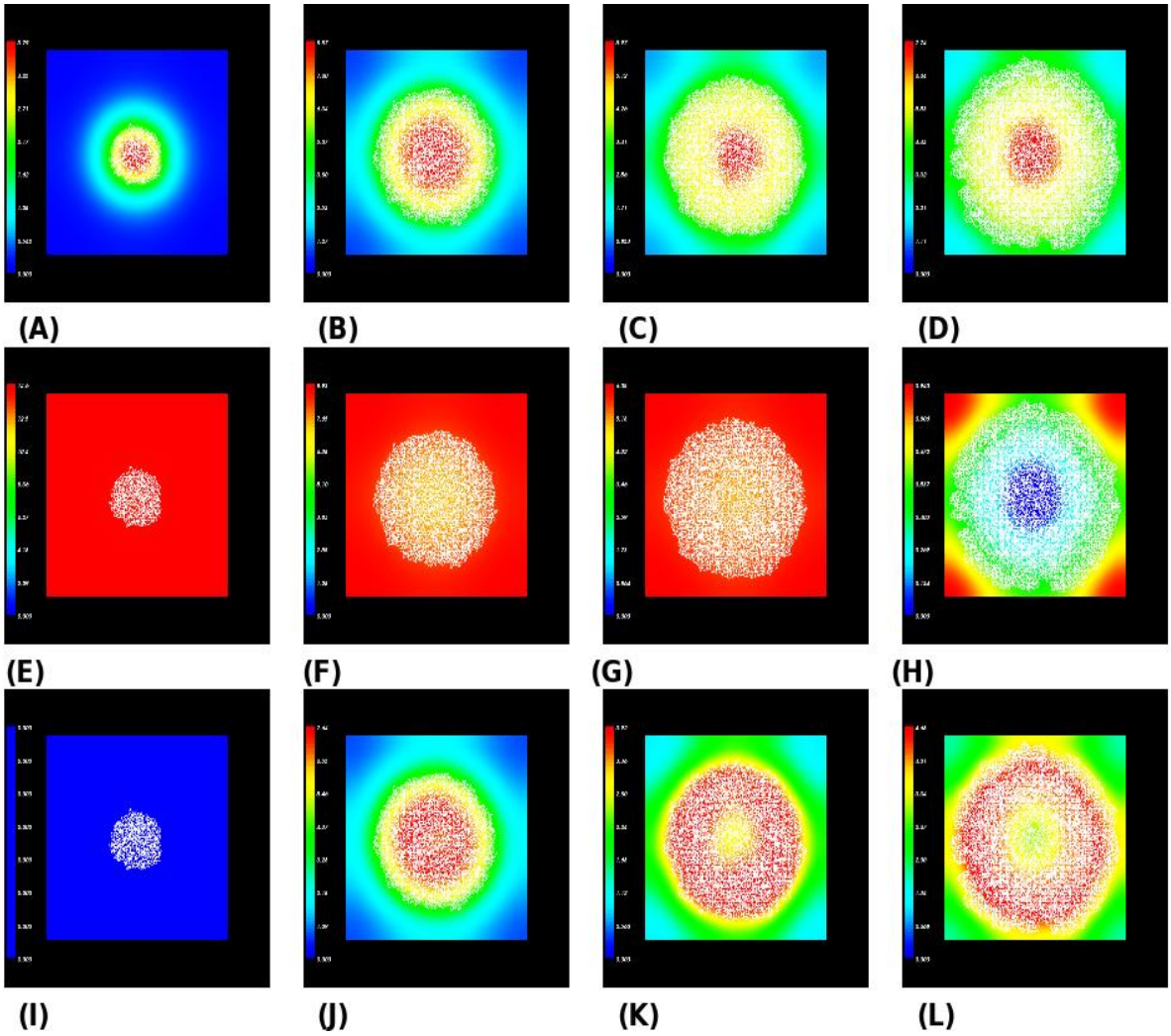

Figure 2.3-9 Chemical Gradient Using Two Autoinducers Low EPS Production.
The addition of a second autoinducer establishes a second gradient (I-L). The addition of the gradient allows us to establish a distinct region where the level of autoinducer and nutrient can reproduce the cell lineage, spatial and temporal dynamics observed in experiments.

Expansion of Biofilm Colony

We next examine the spatiotemporal dynamics of the biofilm expansion. From figures 2.3-1 and 2.3-6, we observe that in the simulation, the leading front of the expanding biofilm is occupied by different phenotypes. To better understand the contribution of the different phenotypes to the expansion of the biofilm, we examine the spatiotemporal distribution of phenotypes in the expanding biofilm using the model with two autoinducers. In figure 2.3-10 we

plot the average maximum distance from the center of the biofilm for all cells of a given phenotype, using the average of five replications. Panels A-C represent low, medium and high cases of EPS production, respectively.

For all three rates of EPS production we observe that the expansion of the colony is initially due to motile cells. Since early in the development phase, the levels of autoinducer and nutrient is below the threshold values required for the motile cells to differentiate to any of the other phenotypes. The expansion of the colony continues until the first set of thresholds is reached for differentiating to matrix producing cells. The expansion of the colony at all three levels of EPS production is then attributed to matrix producing cells. We reach this conclusion since the average of the maximum distance from the center of the biofilm is greater for the matrix-producing phenotype than the motile phenotype.

In case of low EPS production (A) the matrix producing phenotype has the greatest average distance until the threshold for spore formation is reached. Once the cells start forming spores, the average maximum distance from the center of the colony of the matrix-producing cell type becomes equal to the average max distance of the spore forming phenotype. From figure 2.3-6 and figure 2.3-10 we infer the equality of the distance between the two cell types is caused by matrix cell becoming spores. Once the distance becomes equal, we observe that a second expansion of the colony occurring due to the matrix-producing phenotype. Again, we make this assumption since the average maximum distance from the center of the colony is greatest for the matrix producing phenotype. The matrix producing cells remain furthest from the center until the end of the simulation. The spore cells have an average maximum distance that lies between the motile and matrix producing cells. The average maximum distance of the motile cells from the

center increase slightly from the beginning of the simulation until the end of the simulation when all nutrients are consumed.

In the case of medium EPS production panel B in figure 2.3-10, a similar development pattern is observed for the colony. Specifically, we have the matrix producing cells being furthest on average from the center of the colony. Followed by the average maximum distance of spore forming cells and matrix-producing cells being equal. Once this occurs the average maximum distance of the matrix producing cells is greater than the average maximum distance of the spore forming cells suggesting that the expansion of the colony is again due to matrix producing cells. When the EPS production is set to the highest level the initial colony expansion occurs due to motile cells and then is followed by an expansion due to matrix producing cells once the required threshold is reached. However, in the case of large EPS production a similar inference cannot be made. Figure 2.3-6 shows that, in the case of high EPS production, the spore forming cells are distributed in a few concentrated patches throughout the biofilm. Therefore, we are not able to make a similar inference as we did as in the case of low and medium EPS production.

From figure 2.3-6 and 2.3-10, we infer for EPS production at low or medium levels the spreading of the biofilm colony is first due to motile cells. Once the threshold for matrix producing cells is reached the expansion of the colony is due to the matrix producing phenotype. Expansion of the colony by the matrix-producing cells continues until another threshold is reached inducing cells to become spores. Once spore form from matrix-producers, a second expansion of the colony occurs. Specifically, the second expansion of the colony is a result of matrix-producing cells that did not become spore.

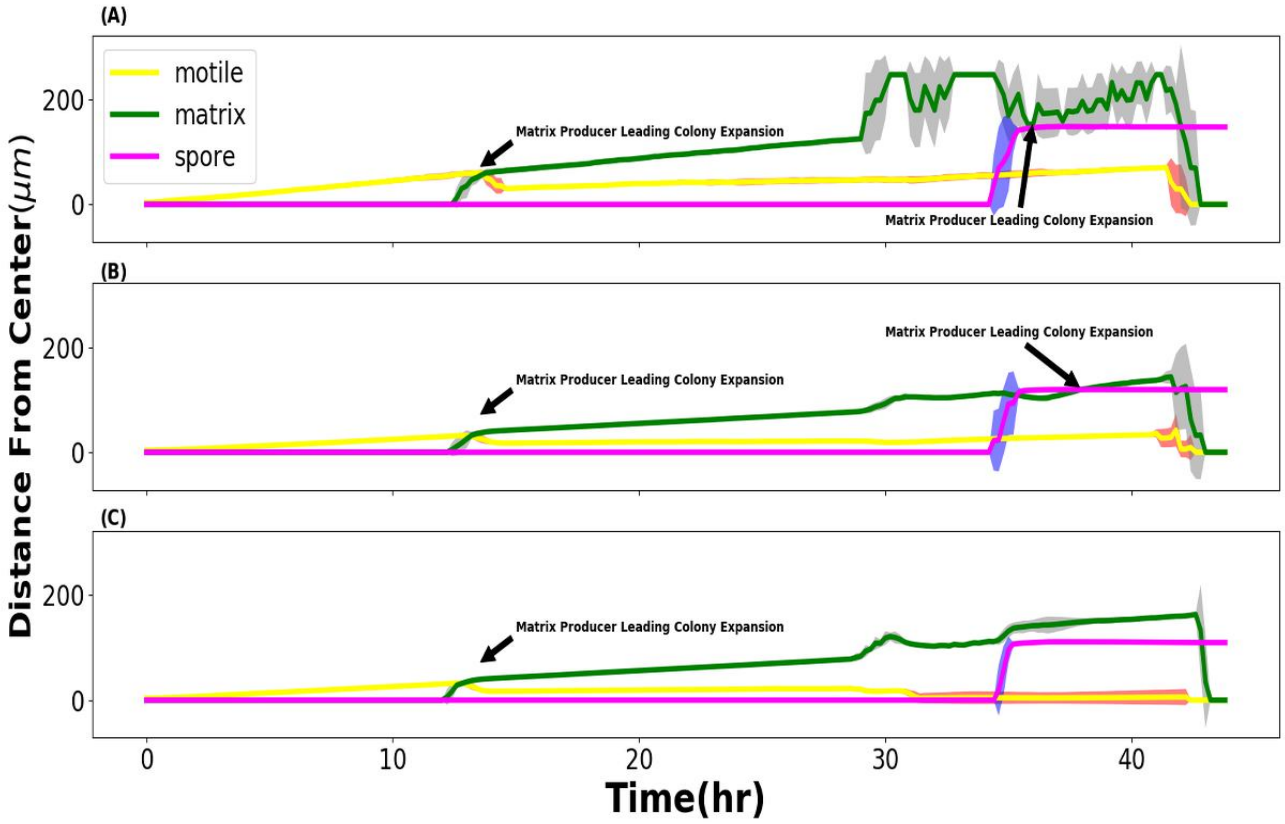

Figure 2.3-10 Distance from the Center of Biofilm of the Three Major Phenotypes. Figure A-B represents the maximum distance of each cell type from the center of the colony for n=5 replications at the low, medium and high EPS level of production. We observe the initial expansion of the colony by motile once the threshold T_1 to form matrix producing cells is reached. The matrix cells now have the maximum distance from the center of the colony. The biofilm develops until matrix producing cells become spore cells. At which time the we see an intersection of the lines for spore forming and matrix cells. We make the inference from figures 2.3-6 and the defined cell lineage established using two autoinducers. Once the spore forming cells arise from the matrix producing cells that have reached the necessary threshold. The matrix producing cells that have not become spores now lead the expansion of the biofilm.

.

Discussion

Phenotype switching is ubiquitous in microbes and is a strategy for ensuring the survival of the colony [89, 107]. A recent nondestructive method allows one to track the spatiotemporal dynamics of phenotype emergence, in *B. Subtilis* biofilm [58]. Despite the advantages over previous destructive methods, the new method cannot distinguish between dead cells and EPS. The non-destructive method instead groups them into one class of low fluorescent material, giving no information concerning the spatial distribution of them within the biofilm. Furthermore, the method gives no information on the early development of the colony and has poor predictive power later in the colony development [58]. To address these issues, we presented a mathematical and computational model to study phenotype switching exhibited by a *B. Subtilis* colony.

Our 2D agent-based model of colony formation is based on the GGH model with thresholds on two environment signals, nutrient and an autoinducer. The model used for the simulations reproduced the spatiotemporal dynamics observed in [58]. In addition, our simulations can distinguish the spatial distribution of EPS and dead cells. From the simulations, we observe dead cells are localized to the center or edge of the biofilm. The dead cells arise from cells that were either motile or matrix producing cells and did not become spore forming cells. From our simulations, we draw a few important conclusions.

First, to reproduce the spatiotemporal dynamics, it is necessary to couple QS and nutrient availability. Simulations that used a threshold on a single environmental que did not reproduce the spatiotemporal dynamics observed in the experiments. Previous results show that both QS and nutrient limitation play a role in initiating sporulation [108, 109]. Here we demonstrate that

the interdependence can explain spatial and temporal phenotypic differentiation throughout the development of a biofilm.

Second, to reproduce the cell lineage as well as the spatiotemporal patterning observed experimentally, a second autoinducer is required. When one autoinducer is present, we have spore cells arising from motile cells, contradicting the cell lineage from experiments[56]. Using a second autoinducer can be viewed as an evolutionary strategy of a microbe to ensure that only cells that are matrix producers and contribute to EPS production become spores that are able to become active under favorable conditions.

Finally, matrix-producing cells are responsible for the expansion of the biofilm. In figure 2.3-10 the average maximum distance of the matrix-producing cells from the center of the colony is greatest. The observation that the average maximum distance of matrix producing cells are furthest from the center along with the observation in figure 2.3-6 allows us to reach this conclusion. From figure 2.3-6 and 2.3-10 we observe that the expansion due to matrix-producing cells occurs at two different times during the development of the colony. The first expansion occurs after the threshold T_1 to become a matrix-producer is reached. The expansion of the colony by matrix-producing cells continues until the threshold for the spore phenotype is reached. Once this threshold is reached spore forming cells occupy an average maximum distance that is greater than the motile cells. After the spore forming cells appear a second expansion of the colony begins with the matrix forming cells that did not reach the required threshold to form spores. This expansion continues until the level of nutrient reaches zero and the matrix producing and motile cells die. This result is consistent with experiments that observe matrix-producing cells leading the expansion of the colony and that the expansion occurs during two different waves [59].

In conclusion, we have presented an agent-based model that incorporates thresholds on two important environmental ques, nutrient and autoinducer. Using the GGH model coupled with thresholds on these two variables, we reproduced the spatiotemporal dynamics exhibited experimentally. From the simulations we gained insight on the role EPS production has on the dynamics of the biofilm. In addition, our model allowed us to predict the distribution and ratio of dead cells and EPS separately. The model allowed us to gain insight on the role QS has on deciding cell fate and cell lineage. From the simulations, we hypothesize one role of having multiple autoinducer is to establish distinct cell lineage between cells responsible for producing EPS and cell that do not produce EPS. The distinction between the two cell types can be viewed as an evolutionary advantage to ensures only cells that produce EPS form spores.

The model gave us insight on the role environmental inputs have on cell fate. However, the changes were not as gradual as the experiment due to the threshold mechanism. We hope this model can be extended to incorporate subcellular dynamics along with environmental ques to reproduce the spatiotemporal dynamics of B. Subtilis in a way more consistent with experiments since an understanding of the constant interplay between environment signals and regulatory network is necessary to fully understand the role that either has in the development of a colony.

3 A COMPUTATIONAL MODEL OF BIOFILM DETACHMENT

3.1 Biofilm Dispersal

3.1.1 Background

Detachment occurs as the final stage of a three-stage process leading to the development of a biofilm. The first stage is characterized by irreversible attachment to a surface by using cohesive and adhesive force[110]. The next stage of development is the expansion of the colony due to growth and division of individual bacterium that are encased in the EPS[8, 111]. At the final stage bacterium and other material which constitute the biofilm such as EPS are detached from the colony.

To facilitate the detachment biofilms have developed a myriad of mechanism that allow detachment when conditions become unfavorable. Unfavorable conditions include the depletion of nutrients, increase of toxins and other environmental stresses [66, 112]. The three major mechanism used by bacteria to escape from a biofilm are desorption, detachment, and dispersion[113]. Although these terms refer to slightly different methods individual or clusters of bacteria leave a biofilm, in the literature they are used interchangeable and refer to an individual or cluster of bacterium cells leaving an established biofilm[114]. We will follow the convention of using the terms interchangeably.

The dispersal of biomass from a biofilm is categorized as either active or passive. When the dispersal of the biomass is due to external forces dispersal is categorized as being passive[115]. For example, biomass removed by shear force is considered a form of passive dispersal. Active dispersal on the other hand occurs as a direct consequence of activity within the biofilm.

Biomass dispersal can be further categorized into three broadly defined modes: seeding, sloughing or erosion[115]. Seeding is defined as the rapid release of cells from the biofilm and is considered a form active dispersal. Seeding is used by bacteria within a biofilm to colonize new areas and can occur due to either high or low nutrient availability. Erosion is the continuous release of single cells or small clusters of cells from a biofilm at low levels over the course of the formation of a biofilm. While sloughing refers to the sudden detachment of large portions of the biofilm[114, 116]. Erosion and sloughing can be classified as either active or passive where seeding is always active.

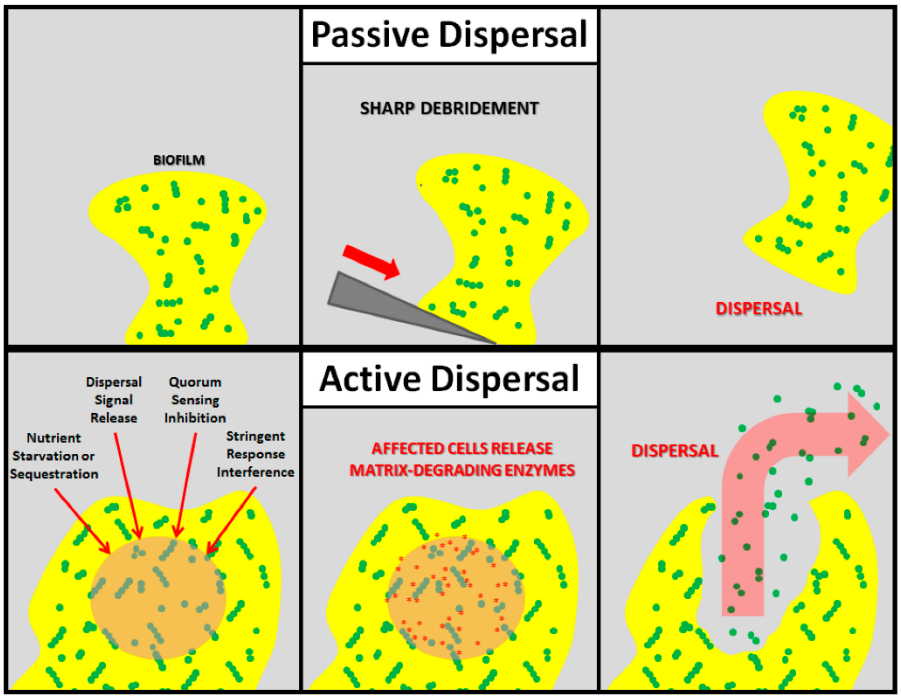

Figure 3.1-1 Active vs Passive Dispersal.
Figure 3.1-1 represents the two-mechanism causing dispersal in biofilm. The first passive occurs when some external force is applied to the biofilm causing the whole or partial removal of the biofilm. The second case is an illustration of active dispersal. In this case dispersal occurs as a direct consequence of stimulus provided by the bacterium within the biofilm. Figure reproduced with permission from [115].

Dispersal is also aided by environmental signals that enable bacterium within the biofilm to monitor their environment and release cells at an opportune time. An interesting example of environmental signal induced dispersal occurs when the level of nutrients available to a bacterium is used as a signal to disperse from biofilms[112]. The decision to disperse from the biofilm does not only occur at low levels of nutrients but can also be triggered at high levels. In addition, QS is generally thought to govern the assembly of biofilms when a population density becomes sufficient to warrant forming a colony. However, recent studies put forth evidence that QS contributes not only to the formation of biofilms but also to their disassembly[8, 26, 117]. Specifically, in most biofilms once a threshold concentrations of autoinducers is reached bacterium within the biofilm start to produce surfactants or enzymes that weaken the cohesive forces that hold the biofilm together[26]. The weaken of the bonds within the biofilm enable bacteria embedded in the matrix to escape an increase the likelihood of survival of a biofilm.

3.1.2 Mathematical Models of Detachment

Mathematical Models of biofilm dispersal have included both continuum and discrete models. In this section, I will give an overview of some of the important models that have been used to study the dispersal process. One of the earliest models to successfully incorporate detachment was the continuum model presented in [118], where biofilm detachment was trigged by the thickness of the biofilm. In their model, Wanner and Gujer introduce a term σ that measured the detachment velocity of biomass from the biofilm based on the thickness of the biofilm. Although the model improved on previous models of biofilms by adding a mechanism to account for biomass detachment. The detachment mechanism used did not account for the heterogeneity observed experimentally during the different phases of biofilm development. Specifically, the early model could not account for bacterial attachment, growth and detachment.

Later continuum models of detachment included detachment occurring as a result of fluid flow and shear stress[119]. Although, later Continuum models incorporated different detachment mechanisms. They did not allow for the observed emergent properties and dynamics of the biofilm to be attributed to the physical interactions between the bacterium forming the colony. Furthermore, due to the limitation of continuum models the chemical and biological processes leading to detachment could not be included as contributions from individual bacterium.

To overcome the shortcomings of continuum models, cellular automata and individual-based models were developed to model biofilms. The main advantage of using individual and automata models is that they allow for the macroscopic properties of a biofilm to emerge from microscopic interactions between individual cells and their environment. Baclab presented an early Cellular Automata computer model that incorporated detachment that was dependent on the concentration of a detachment inducing chemical. Baclab modelled chemical reactions taking place in the biofilm by using deterministic differential equations and diffusion equations. While using a stochastic cellular automata model for cell division, detachment and movement.

In the Baclab model, at any time point of the simulation, the state of the system is represented using the following three arrays: $S = \{C_s(x, y, z)\}$ denoting the concentration of the limiting substrate, $F = \{C_F(x, y, z)\}$ denoting the concentration of the detachment factor and B=$\{B(x, y, z)\}$, denoting the occupation state at location (x, y, z). In Baclab simulations, concentrations of the limiting substrate and detachment factor are updated using differential equations. While the updates of the occupation state $B(x, y, z)$, are made using cellular automata rules. Detachment in Baclab occurs if $C_F > C_{max}$ at a cell's location, where C_{max} is a predetermined threshold concentration of the detachment factor or if a cell is no longer attached

to the substratum. The model incorporates detachment factor production and cellular activity through the following reaction term:

$$r_F(C_s, X) = \begin{cases} 0, & if\ B = Null\ Identity\ Pointer \\ k * C_s, & if\ B \neq Null\ Identity\ Pointer \end{cases}$$

The parameter k denotes the detachment factor production coefficient. B represents an identity pointer to a vector, $I_{bacterium}$, containing all relevant information about an individual bacterium. The first order expression in C_s correlate the detachment factor production with the cellular activity of a cell. With the assumption that when a cell is in a starved state, energy is conserved and extra cellular chemicals are not actively produced.

The expression is substituted into the reaction diffusion equation:

$$0 = D_i\left(\frac{\partial^2 C_i}{\partial x^2} + \frac{\partial^2 C_i}{\partial y^2} + \frac{\partial^2 C_i}{\partial z^2}\right) + r_i(C_s, X)$$

where C_i is the detachment factor concentration C_F.

The algorithm governing detachment is illustrated in figure 3.1-2 and corresponds to the following sequence of operations adopted from [120]. 1, Initializes the surface with N_c randomly placed spherical colonies of radius R_c. Each cell within the colonies is inoculated with a random amount of substrate relative to division denoted by M, where M is chosen from a uniform $(0, m_n)$ distribution. 2, generates the substrate distribution for the current time step, t, by finding the steady-state solution to the reaction diffusion equation. 3, the detachment factor distribution is generated for the current time step, t, by again finding the steady-state solution to the reaction diffusion equation. 4, for each cube in the spatial domain Γ, determine if it is occupied by a bacterium. If the cube is unoccupied, nothing further is done with that volume element at the current time step. If the cube is occupied, further calculations are performed. 5, Each bacterium consumes substrate based on (2) and the local concentration. The cumulative amount of substrate

consumed for each cell, since its last division, is then updated. 6, Determine if C_F in the cube is above the detachment factor threshold, $C_{F,max}$. 7, Remove the bacterium in the current cube and any additional bacteria in other cubes according to the detachment rule specified. Additionally, identify and remove any floating clusters of bacteria. 8, Check if the bacterium has consumed enough substrate to divide. 9, Create a new bacterium neighboring the parent and leave excess substrate (not required for the creation of a daughter cell) with the parent bacterium according to the rules specified. 10, Move forward in time by Δt based on the events that occurred in steps 4–9.

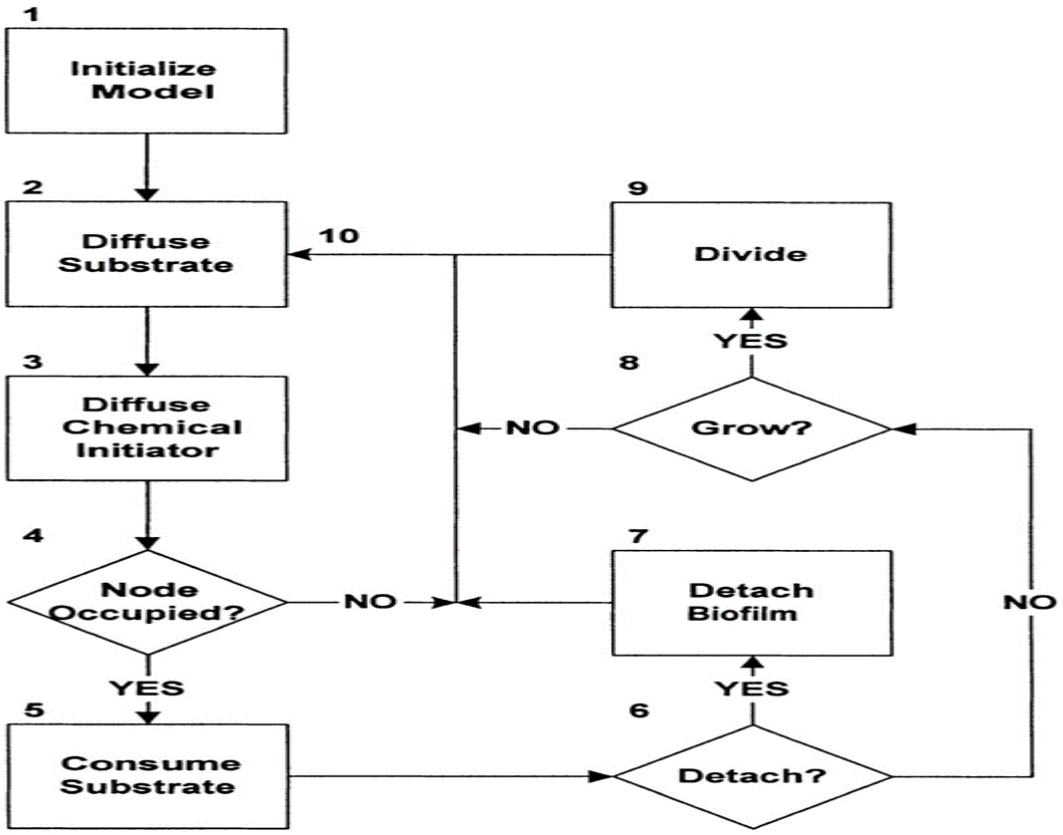

Figure 3.1-2 Detachment Rules Used in Baclab.
Illustration of a typical simulations using Baclab. A full explantation of each step is giving above. Figure reproduced with permission from [120].

The widely popular individual-based model presented in [121] was extended to incorporate biomass detachment. To incorporate detachment, a continuous speed detachment function denoted $\boldsymbol{F}_{\mathrm{det}}$ was introduced to calculate the local biomass erosion. $\boldsymbol{F}_{\mathrm{det}}$ can depend on measured biofilm mechanical properties, on local biomass EPS composition, on the distance to the solid support, or the local concentration of detachment-inducing chemical species[30]. For a point **x** on the biofilm surface, the retraction speed of the biofilm is expressed as

$$\frac{d\mathbf{x}}{dt} = -\boldsymbol{F}_{det}(\mathbf{x})\mathbf{n}(\mathbf{x})$$

Where $\boldsymbol{F}_{det}(\mathbf{x})$ is defined as the value of the detachment speed function at point **x** and $\mathbf{n}(\mathbf{x})$ as vector normal to the biofilm at **x.** The model is valid for both 2D and 3D simulations.

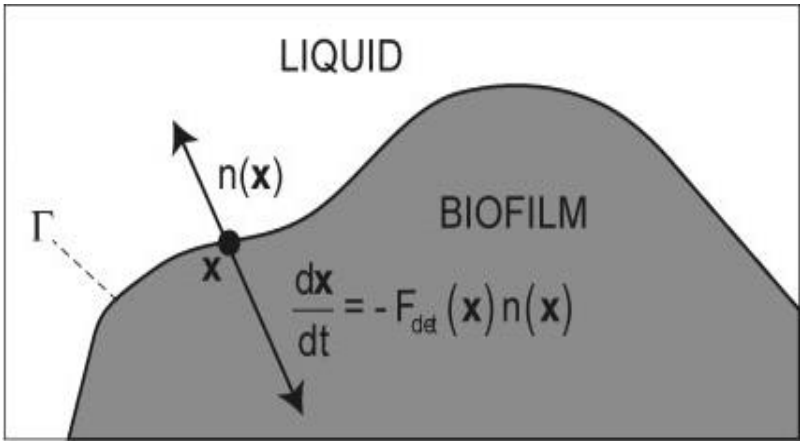

Figure 3.1-3 Biomass Detachment as Implemented in the Particle Based Model.
*The surface detachment rate at a point (**x**) placed at the biofilm interface results from the product of local values of the detachment speed function, F_{det}, and the vector normal to the surface at that point (**n(x)**), as described by the above equation. Reproduced from[30] with permission.*

The continuum, cellular automata, and individual-based models discussed have been modified to include a myriad of detachment mechanism. However, detachment due to quorum sensing has not been incorporated until recently. In[122] a model of QS induced biofilm detachment is first proposed. The authors use an established continuum model with a predefined dispersal rate to model detachment. In their model, once an autoinducer threshold is reached cells disperse from the biofilm at a predefined rate. Their model is a step in the right direction since it incorporates a universal signal produced by a myriad of bacterium. However, their modelling approach does not provide information on the effect individual cells reacting to quorum sensing induced detachment has on the emergent structure of the biofilm. Furthermore, the model being a continuum model does not explicitly model EPS and instead subsumes EPS in the term representing cells comprising the biofilm.

To gain a better understanding of the role of QS induced detachment has on a biofilm. We present an agent based model to study QS induced biofilm detachment in an environment with no shear force. We explicitly include EPS and model detachment that is dependent on QS. In our model biofilm detachment is induced by the weakening of adhesion or cohesion between cell types within the biofilm.

3.2 Agent Based Model of QS Induced Biofilm Dispersal

3.2.1 Cellular Potts Implementation

Modified Hamiltonian

Experiments point to the weakening of cohesive bonds in a biofilm leading to dispersal, either through the secretion of enzymes such as a biosurfactant or other endogenously produced chemical compounds[123-130]. In this chapter a model of detachment is presented that allows the weakening of the cohesion/adhesion forces in the biofilm under the control of QS. Specifically, in our model once a certain threshold level of an autoinducer is exceed, the cohesive forces in the biofilm will start to weaken initiating detachment of cells from the biofilm.

The weaken of the cohesive force is done by including a cohesiveness weakening factor $\mathcal{D}$ that depends on the local autoinducer concentration $a(x,t)$. We take this approach since experimental evidence suggest that biofilm detachment is dependent on the concentration of secreted enzymes that weaken their cohesive bonds [126, 129, 131]. The regulatory mechanisms that govern the production of these enzymes are themselves QS dependent[8, 124, 132, 133]. To introduce this effect in our model we modify the $\mathcal{H}_{boundary}$ term in the Hamiltonian of the CPM. Specially, we include an expression $\mathcal{D} * a(x,t)$, we can think of $\mathcal{D}$ as detachment factor relating autoinducer production and cohesion[120].

Given us,

$$J'\left(\tau\left(\sigma(\vec{\imath})\right),\tau\left(\sigma(\vec{\jmath})\right)\right) = J\left(\tau\left(\sigma(\vec{\imath})\right),\tau\left(\sigma(\vec{\jmath})\right)\right) + \mathcal{D} * a(x,t)$$

The increase in the values of J' corresponding to weakening of cell cohesion and occurs once an autoinducer threshold τ_2 is achieved.

Cell Growth and Division

In our model, the rate of cell growth and division depends on the local nutrient concentration, $n(x,t)$. In our simulation, each cell initial occupies a 5×5 pixels and 1 pixel is set equal to 2 μm. A cell with adequate nutrient will continue to increase its volume until twice its target volume V_t is reached at which time the cell divides. The division occurs instantaneously creating two daughter cells of the same type with the target volume set equal to one half the parent's target volume $V_t/2$. The direction of division is chosen at random to ensure that there is no bias in any direction on the lattice therefore reducing anisotropy. The bacterium in our model respond to glucose and grow at a rate proportional to its concentration.

$$\frac{dV_t}{dt} = \alpha * n(x,t)$$

EPS Production

EPS production is ubiquitous across bacteria species and serves as hallmark of biofilm formation[2, 14, 46, 47, 66, 134, 135]. In our model EPS is represented as a discrete cell type with its production governed by QS[12, 64, 135-137]. EPS is produced once a certain threshold level of autoinducer is reached [10, 12, 57, 87, 138]. This threshold is referred to as τ_1. EPS cells are represented as a generalized cell type with size proportionally to the target volume of a bacterium cell[96]. If a cell in our model is in an upregulated state it will produce EPS cells as follows: a boundary pixel is randomly selected from a cell which is upregulated, that pixel location then becomes the center of the EPS particle with a predetermined target volume and surface area.

Since the production of EPS is metabolically costly to the EPS producer[139, 140]. To account for the extra cost associated with EPS production the consumption rate of nutrient is doubled for cell producing EPS[141]. The amount of EPS produced is varied by adjusting the parameter π:

$$r_{EPS} = \pi * bacterium\ volume$$

Detachment

In our model biomass detaches from the biofilm due to weakened cohesion or by cell death. Weakening of the cohesive strength between cell types occurs once the autoinducer reaches a threshold value denoted by τ_2. In the simulations, once biomass is detached from the biofilm they are removed from the simulation domain. Since the simulation occur on a lattice which is a regular repeated graph. We use a graph-based algorithm, specifically the depth-first search algorithm to identify detached cells. Bacteria and EPS cell are connected to the substratum in two ways. They can be directly connected meaning they rest on top of the substratum or they can be connected through other bacteria cells or EPS that are connected to the substratum.

We implement detachment as follows:

1. For a cell $\sigma(i)$ excluding the medium and source, we construct a dictionary using $\sigma(i)$ as a key and its neighbors that share a common surface area as values. We then have for each cell a dictionary where the cell indexes $\sigma(i)$ can be viewed as vertices and the list of values associated with that cell index as vertices connected to it by a path.
2. A graph is then constructed using the dictionaries obtain from part 1.
3. We next check the graph obtain in part 2 for components that are not connected using the depth first search algorithm [142]. The substratum is used as the starting node instead of a randomly selected cell to ensure that the starting node is a part of the biofilm. If a cell were

randomly selected cell it is possible that the selected cell is detached from the biofilm. Using the substratum as the root ensures that this does not occur.

4. Finally, if a cell is not connected it is deleted and removed from the simulation domain.

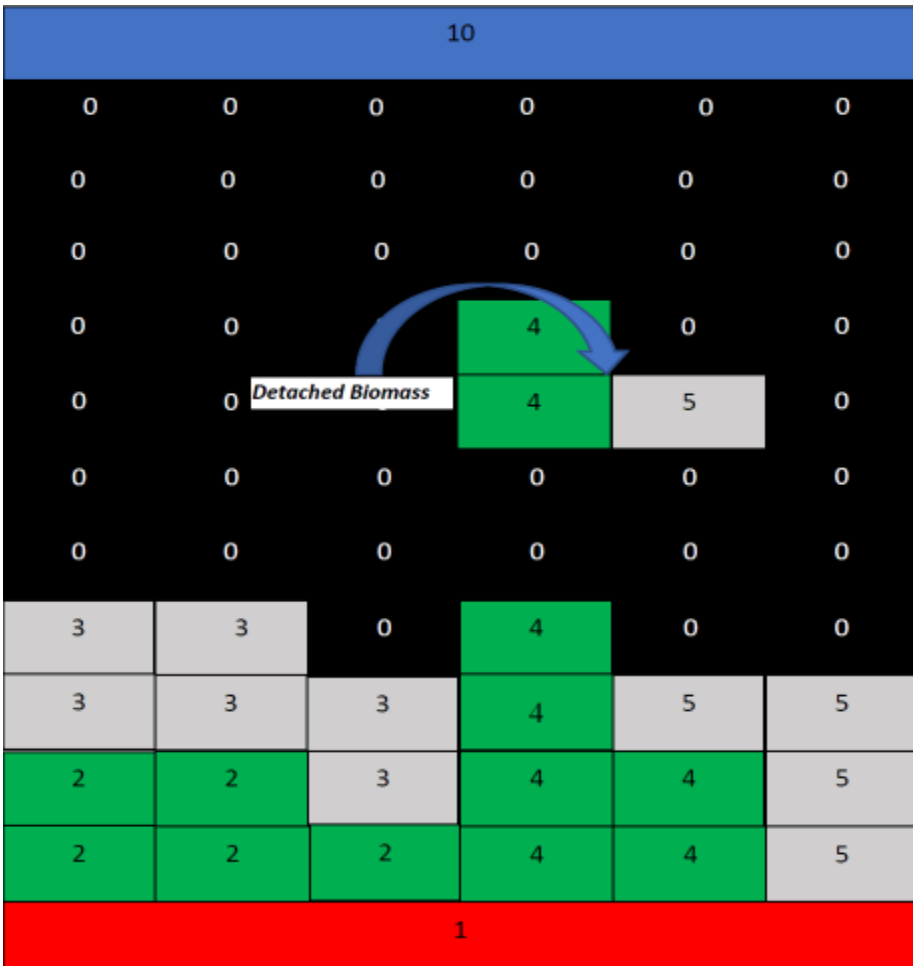

Figure 3.2-1 Biofilm Detachment.
The figure is an illustration of a detached biomass composes of bacterium (green) and cell (gray). The rest of the colony is attached to the substratum (red) once detached the biomass will be deleted from the simulation domain. The medium (black) and source(blue) are also represented.

Chemical Fields

The evolution of glucose and autoinducer concentrations are modeled using the following reaction-diffusion equations.

$$\frac{\partial n}{\partial t} = D_n \nabla^2 \mathrm{n} - \lambda_n n + S$$

$$\frac{\partial a}{\partial t} = D_a \nabla^2 \mathrm{a} - \lambda_a a + (\alpha + \beta) a$$

Where $n(\boldsymbol{x}, t)$ denotes the local concentration of glucose, D_n represents the coefficient of diffusivity of the nutrient, λ_n represents the coefficient of decay. The term $S = S(\boldsymbol{x}, t)$ describes the input of nutrient at a constant rate ϕ_n from a source located at the top of the simulation domain. This is done to simulate biofilm growing in the wild, medical devices, or oral cavity where a constant source of nutrient is available [134]. The first two terms for the autoinducer can be interpreted the same as we did for nutrient. The third term represents the addition of autoinducer by the cells that produced autoinducer at a basal rate α and when upregulated produced at a rate $(\alpha + \beta)$. The diffusion coefficient D_a and , D_n are rescaled to take into account presence of microbial cells and EPS [97].

Simulation Domain

The simulation domain Ω represents a square lattice with length $l_x = 150$ and width $l_y = 200$ in pixels. In our simulation 1 pixel is set equal to 2 μm. This gives us a simulation domain corresponding to 300 μm in the horizontal direction and 400 μm in the vertical direction. The substratum in our model is located at the bottom of the simulation domain and is impermeable to both biomass, autoinducer and nutrient substrate. Therefore, we set homogeneous von Neumann boundary conditions $\partial n = \partial a = 0$ at the substratum for both autoinducer and nutrient substrate. The simulation domain represents a small portion of a larger

domain in which the biofilm grows such as would be found in nature, implanted medical device or as part of a larger bioreactor. This assumption allows us to set periodic boundary conditions at the sides $x_{min} = 0$ and $x_{max} = 150$ for both autoinducer and nutrient substrate. At the top of the simulation domain $y_{max} = 200$, we set Dirichlet boundary condition to represent nutrient constantly being added to the simulation domain. The boundary condition at the top of the simulation domain is set to zero allowing the simulation to account for the removal of autoinducers and establish a diffusion gradient within the biofilm and simulation domain.

Table 3.2-1 Parameter Values

Parameter	Value	Units	Reference
D_{ComX}	2.2×10^{-6}	cm^2/sec	[98]
ComX synthesis Rate	1×10^4	$nMhr^{-1}$	[98]
ComX Degradation Rate Constant	0.693	hr^{-1}	[98]
$D_{Glucose}$	6.7×10^{-6}	cm^2/sec	[97]
Glucose Uptake rate	$Varied$		Estimated
$\mathcal{D}$	$10,100$		Estimated
$J_{BAC,BAC}$	20		Estimated
$J_{EPS,EPS}$	-5		Estimated
$J_{BAC,EPS}$	-5		Estimated
$J_{BAC,SUB}$	5		Estimated
$J_{EPS,SUB}$	-5		Estimated

3.3 Results

3.3.1 Aim of Study

The cohesive and adhesive strength exhibited by biofilms is a factor in their resilience to treatment and removal[19, 130, 143]. One explanation put forth to explain the resilience exhibited by biofilms is they are overdesigned. Specifically, in [19] the authors demonstrate the property of biofilm resilience by measuring the factor of safety of a biofilm. The factor of safety as defined by the authors is the ratio of measured cohesive strength to the estimated fluid stress excreted on the biofilm. The factor of safety values calculated for biofilms ranged from 330 to 55,00. When taking in comparison to engineered structures that usually have a factory of safety < 10, the authors argue that biofilms are overdesigned and it is the overdesign of biofilms that lead to them being resilient to removal. Given the role cohesive forces have in the recalcitrant behavior exhibit by biofilms, suggest that if one's aim is to disassemble a biofilm. The focus should be on the adhesive bonds holding the biofilm together specifically, the cell-cell, EPS-EPS, and cell-EPS bonds.

In carrying out this research we seek the answer to several questions. First is it possible to induce dispersal by focusing on weakening a single interaction? QS not only coordinates the assembly of a biofilm, but is used by some species to coordinate the disassembly of the biofilm as it matures[26, 127, 137, 144]. This leads to the second question, what is the role of quorum sensing in dispersal and its effect on the biofilm's structure? In addition, we seek to gain an understanding of what advantages does QS regulated EPS production have over EPS production that is not QS regulated. To better understanding the role of adhesion and quorum sensing regulated EPS production and biofilm dispersal we use the Cellular Potts model as described above.

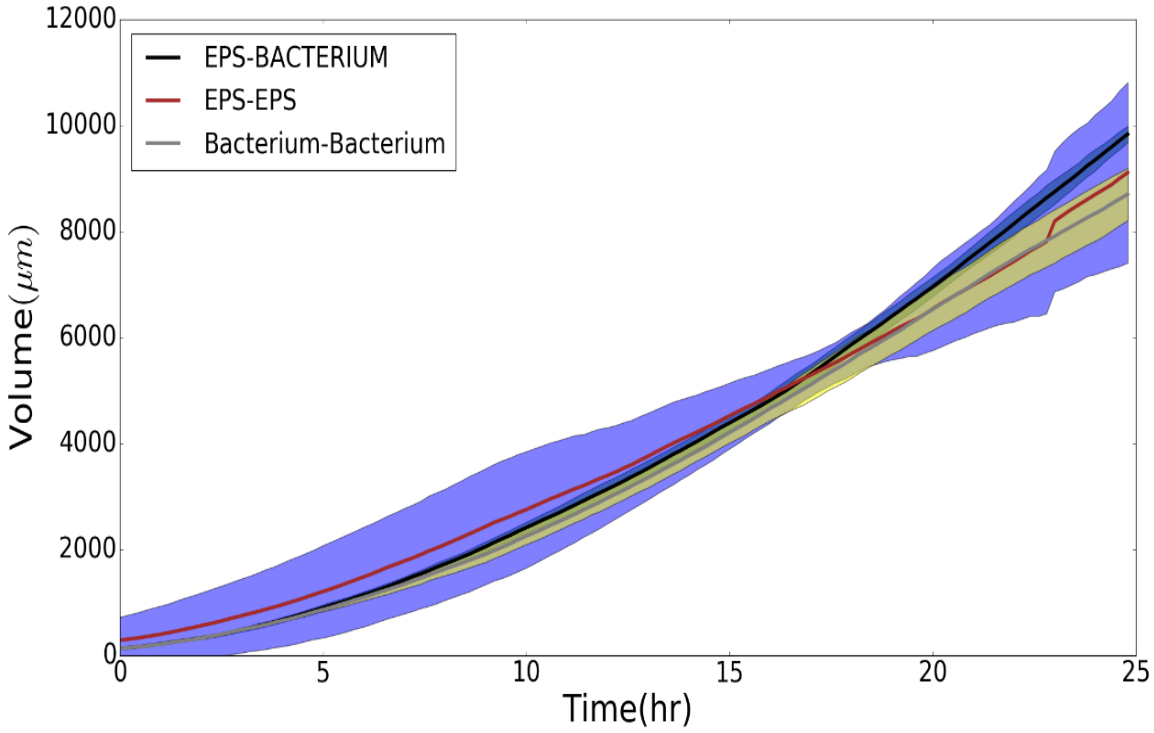

Figure 3.3-1. Initial Attempt to Initiate Dispersal Using Individual Adhesion Terms. When each term is weakened the biomass of the biofilm increases indicating that focusing on an individual term will not be enough to induce dispersal of biomass from the biofilm. The shaded continuous error bars represent a 95% confidence interval around the mean value of the five simulations.

Results

To simulate the growth of a biofilm, at the start of the simulation cells are placed on a substratum located at the bottom of the simulation domain. We start out simulation by assuming that there are no dispersed cells, upregulated cells, EPS or autoinducer in the simulation domain. As the simulation is initiated the cells located on the substratum grow and divide due to consuming nutrients and secrete autoinducer at a basal rate. The production at the basal rate continues until a threshold τ_1 is reached at which time a bacterium will switch from being down-regulated to up-regulated[145]. When a cell is up-regulated it produces the autoinducer at a rate

one order of magnitude greater than cells that are down-regulated[146]. The threshold τ_1 once exceed also allows a cell to produce EPS.

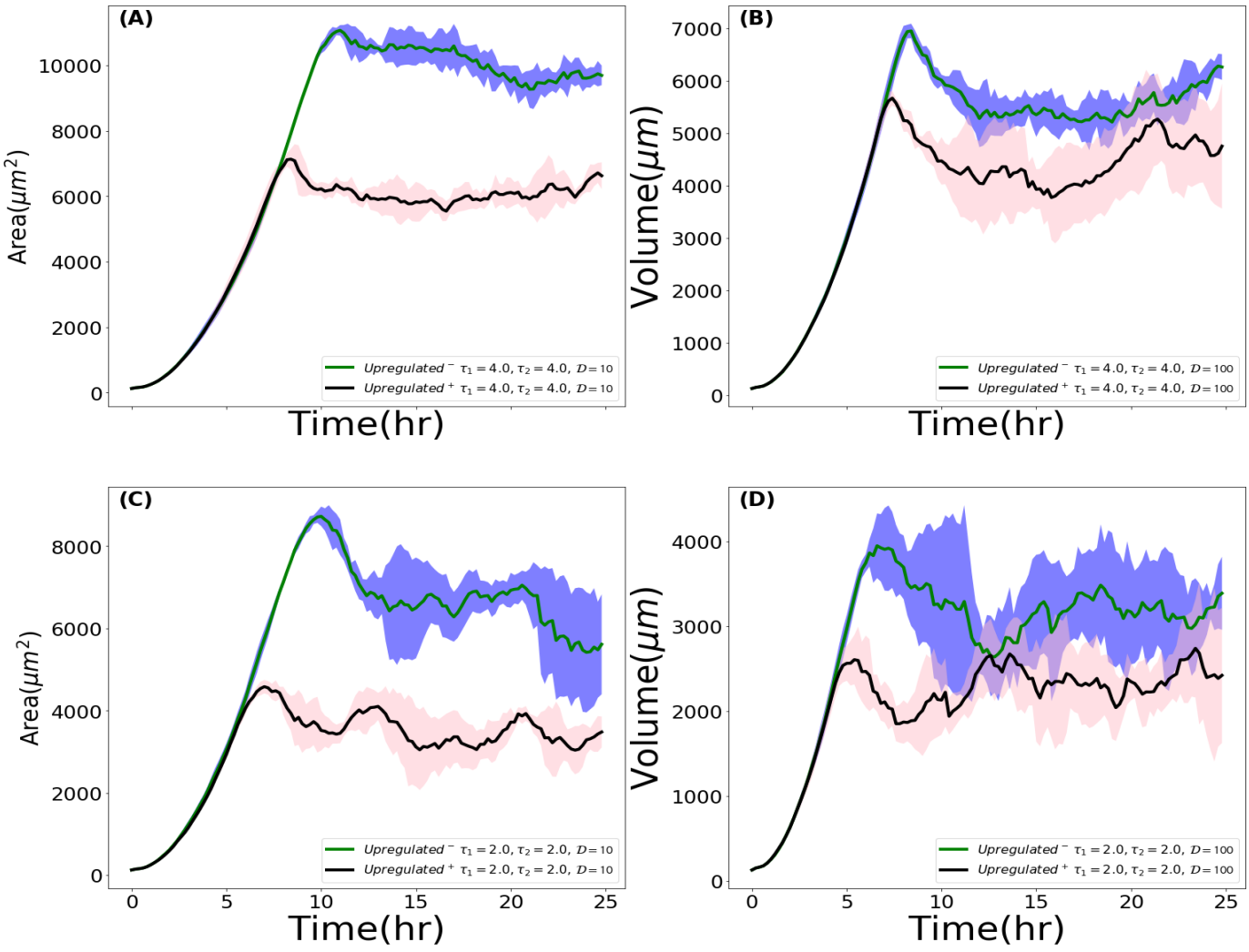

Figure 3.3-2 $upregulated^+$ and $upregulated^-$ Using Equal Values on Both Thresholds. Figures A and B represent the case when $\tau_{1,2} = 4\mu M$. While figures C and D represent the case when $\tau_{1,2} = 2\mu M$. From the figures we observe $upregulated^+$ (black line) biofilms exhibit a lower maximum biomass than biofilms that $upregulated^-$ (green line). This occurs for all possible thresholds τ_1. Furthermore, biofilms with a larger value of τ_1 produce biofilms that have a larger biomass than biofilms with a smaller value of τ_1. When biofilms with that have the same value of τ_1 are compared biofilms with a higher value of $\mathcal{D}$ have dispersal events that occur at an earlier time than biofilms with a smaller value of $\mathcal{D}$. The shaded continuous error bars represent a 95% confidence interval around the mean value of the five simulations.

Biofilms with cells that become upregulated are denoted $upregulated^{+}$ while biofilms comprised of cells that are unable to produce an increased rate of autoinducer are termed $upregulated^{-}$. To better understand the role of cell-cell, cell-EPS, and EPS-EPS adhesion a second threshold τ_2, is introduced that once exceed will weaken the adhesion/cohesion of the biofilm.

To exam the effects of cohesion, we simulate a biofilm growing and attempt to induce dispersal. We first test the hypothesis that dispersal can be induced by weakening an individual term in our model. We focus on the individual terms: $J_{BAC,BAC}$, $J_{EPS,EPS}$, and $J_{BAC,EPS}$ to test our hypothesis. We set the threshold τ_1, τ_2 equal to $2\mu M$ allowing for the growth of the smallest biofilm in our model and $\mathcal{D} = 100$ the highest detachment value used in our simulations. We set these values because if we cannot induce dispersal on a smaller biofilm with a high detachment factor we reason that we will not be able to do so on a larger biofilm. From figure 3.3.1 we observe the biofilm's volume increased as an approximate linear function for each case. Our observation indicates focusing on weakening an individual interaction will not induce dispersal of cells from the biofilm. Each plot presented in figure 3.31 represents the average of five simulations. The shaded continuous error bars represent a 95% confidence interval around the mean value of the five simulations.

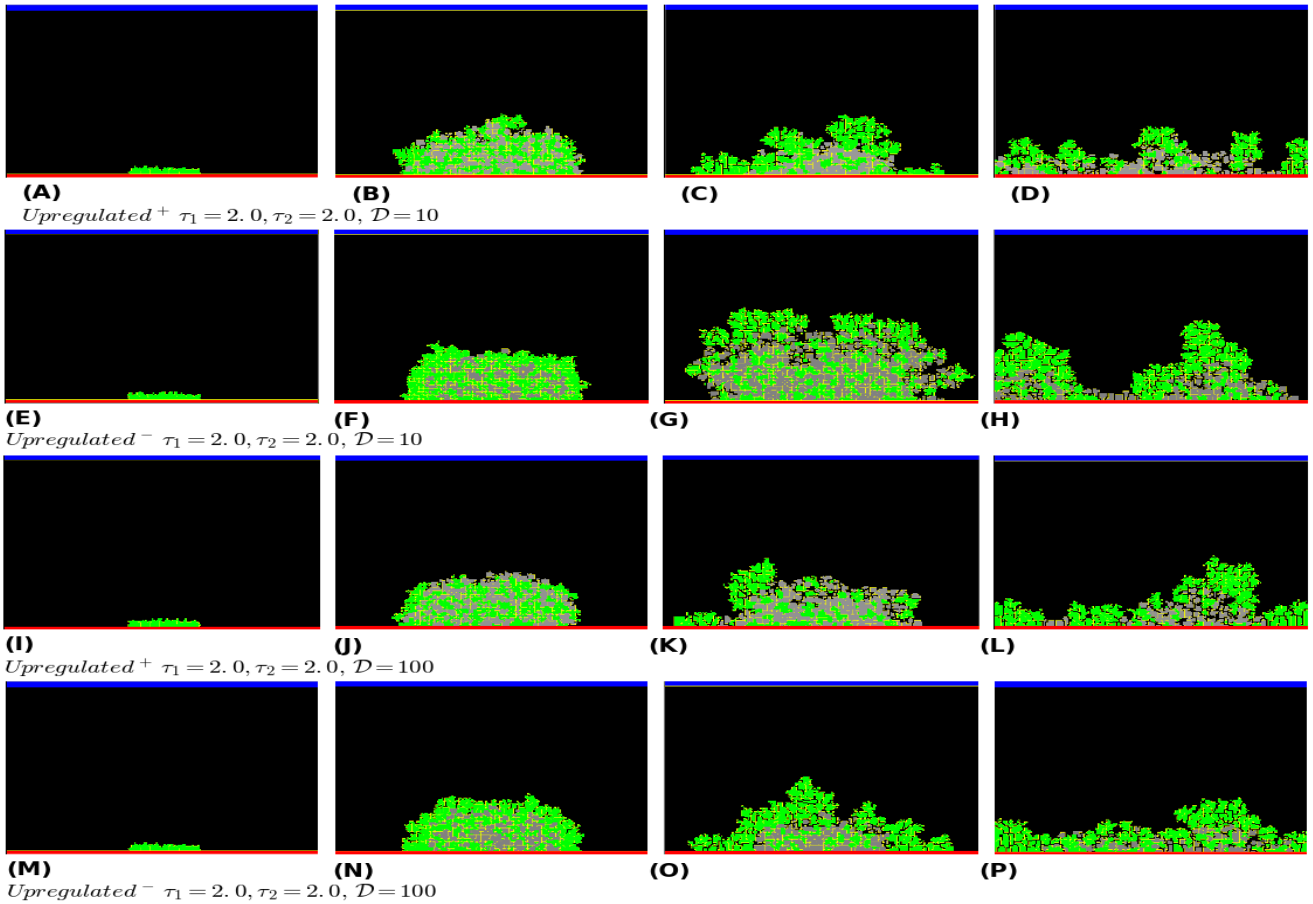

Figure 3.3-3 Biofilm Morphology.
Figures A-P represents the morphology of the biofilm when different values of the detachment factor $\mathcal{D}$ and for the case when $\tau_{1,2} = 2\mu M$. Green colored cells represent bacterium cells and grey represent EPS. The blue bar at the top represent the nutrient source. The first column represents the initial layout of the cells on the substratum. The second column B, F, J, and N represent a mature biofilm before cells are dispersed. The third column C, G, K, and O represent dispersal of cells from the biofilm while the final column represents the final state of the biofilm. The morphology of $\tau_{1,2} = 4\mu M$ is similar and therefore not plotted.

Since weakening individual terms does not induce dispersal, we next focus on weakening all terms to induce dispersal. In fig 3.3.2 A-D, we plot the growth of a biofilm for the case $\tau_{1,2} = 2\mu M$ and $\tau_{1,2} = 4\mu M$ while varying the values of the detachment factor $\mathcal{D}$. The thresholds were selected to examine the effects of dispersal and EPS production. Specifically, we wanted to examine the consequences of a biofilm having the same threshold on EPS production and

making the decision to disperse cells. We set the values of $\mathcal{D} = 10$ and $\mathcal{D} = 100$ and observe biofilms lacking upregulated cells $upregulated^{-}$ reach a higher average maximum biomass than biofilms with upregulated cells $upregulated^{+}$. In the case where $\mathcal{D} = 10$, we observe $upregulated^{+}$ biofilms reach an average maximum biomass that is one half of the biofilm with cells that cannot be upregulated $upregulated^{-}$. When $\mathcal{D} = 100$, the average maximum size of the $upregulated^{-}$ biofilms are greater than $upregulated^{+}$ biofilms. These observations lead us to conclude that one of the possible mechanism biofilms use to regulate their size is the upregulation of cells after a certain threshold is reached.

We next examine the time to dispersal for the different thresholds. For $\tau_{1,2} = 2\mu M$ and $\mathcal{D} = 10$, biofilms with $upregulated^{+}$ cells start to disperse at an average time of $hr = 6$ while cells in the $upregulated^{-}$ biofilms start to disperse at average time of $hr = 8$. From figure 3.3-2(D) when $\mathcal{D} = 100$ the first dispersal event occurs at $hr = 5$ for $upregulated^{+}$ and $hr = 6$ for $upregulated^{-}$ biofilms. The thresholds are then increased to $\tau_{1,2} = 4\mu M$. When we compare the $upregulated^{+}$ biofilms to $upregulated^{-}$ biofilms for $\mathcal{D} = 10$ and $\mathcal{D} = 100$ we observe similar dynamics as the case $\tau_{1,2} = 2\mu M$. Suggesting that upregulation of cells within the biofilm is a mechanism used by biofilms to reduce their size rapidly. In addition, we observe that for either threshold when $\mathcal{D} = 100$ the biofilms have values later in the simulation that are more variable leading to confidence intervals for the $upregulated^{-}$ and $upregulated^{+}$ overlapping.

To give a visual representation of the morphology of the biofilm we plot $\tau_{1,2} = 2\mu M$ for different values of $\mathcal{D}$ in figures 3.3-3. The plots represent the initial layout of cells on the substratum figure 3.3-3 panels A, E, I, and M. In figures 3.3-3 panels B, F, J, and N represents the state during the biofilms growth where the threshold to produces EPS is reached. Panels C,

G, K, and O in figure 3.3-3 illustrate the initiation of dispersal of cells from the biofilm. While the last column represents the final state of the biofilm. From figures 3.3-3 panels C and G, the $upregulated^-$ biofilm is larger than the $upregulated^+$ biofilm for the same value of $\mathcal{D}$. When the value of $\mathcal{D}$ is increased to 100 in figures 3.3-3 panels K and O, the difference in biomass between the $upregulated^-$ and $upregulated^+$ biofilm becomes less distinct as suggested by figure 3.3-2 panel D. From the last column, we observe that after cells are dispersed from the biofilm the cells spread on the surface of the substratum and continues to grow and produce EPS if the threshold for EPS production is satisfied.

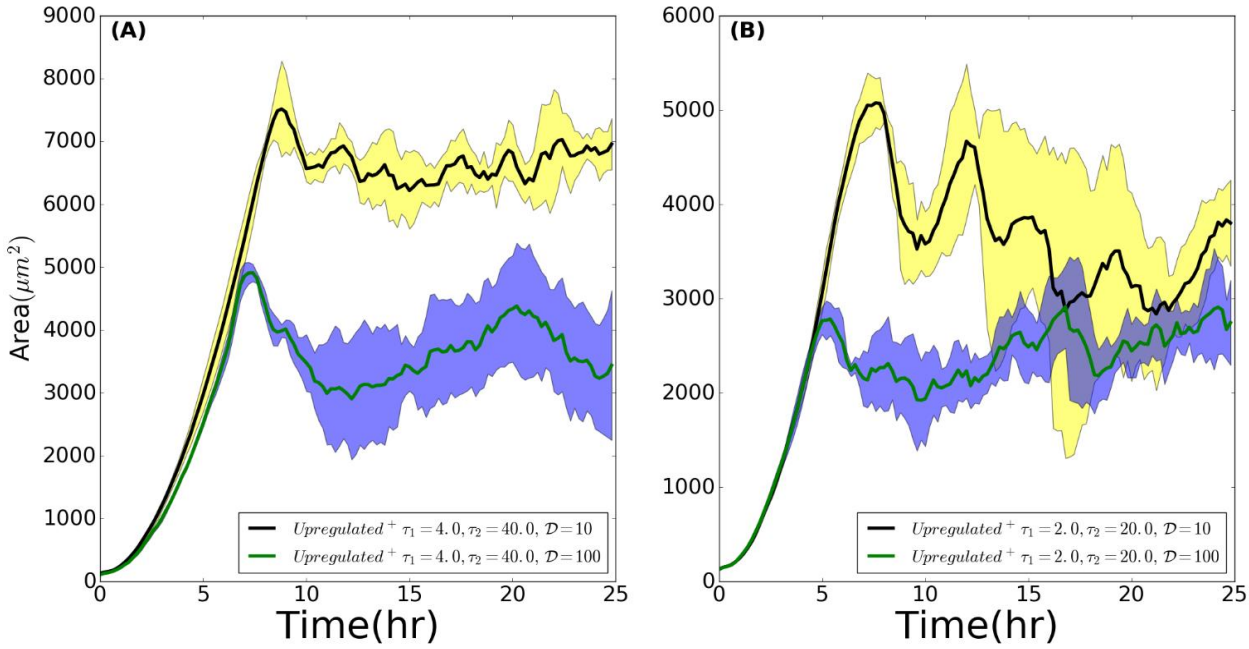

Figure 3.3-4 $Upregulated^+$ Using and Increased Value for Second Threshold. Figure 3.3-4 gives the temporal plot of the biomass of biofilms grown with different τ_1, τ_2 and detachment values D. The black line graph represents biofilms with $\mathcal{D} = 10$ while the green line represents biofilms with $\mathcal{D} = 100$. Figure A plots the biomass of biofilms when $\tau_1 = 4\mu M and\ \tau_2 = 40\mu M$. While figure B plots the temporal biomass of biofilms with $\tau_1 = 2\mu M and\ \tau_2 = 20\mu M$. From the plots we observe biofilms with $\tau_1 = 4\mu M$ reached a higher maximum biomass when compared with biofilm where $\tau_1 = 2\mu M$. Furthermore, for both figure A and B, biofilms with the higher detachment factor had cells that were dispersed at an earlier time.

We next focus on $upregulated^{+}$ biofilms which represent the experimentally observed behavior of cells in a biofilm. From figure 3.3.4 A-B, we observe that for $\tau_1 = 20\mu M$ and $\tau_1 = 40\mu M$ biofilms with $\mathcal{D} = 100$ have lower maximum biomass than biofilms with $\mathcal{D} = 10$. We attribute the lower maximum biomass to dispersal of cells occurring earlier than biofilms with $\mathcal{D} = 10$, since higher detachment factor causes earlier dispersal. When $\tau_1 = 2\mu M$ the biomass of the biofilm exhibits variability that is greater than what is observed when $\tau_1 = 4\mu M$. The greater variability causes the confidence interval $\mathcal{D} = 10$ and $\mathcal{D} = 100$ to overlap and do not exhibit the clear separation over the simulation time course when $\tau_1 = 4\mu M$.

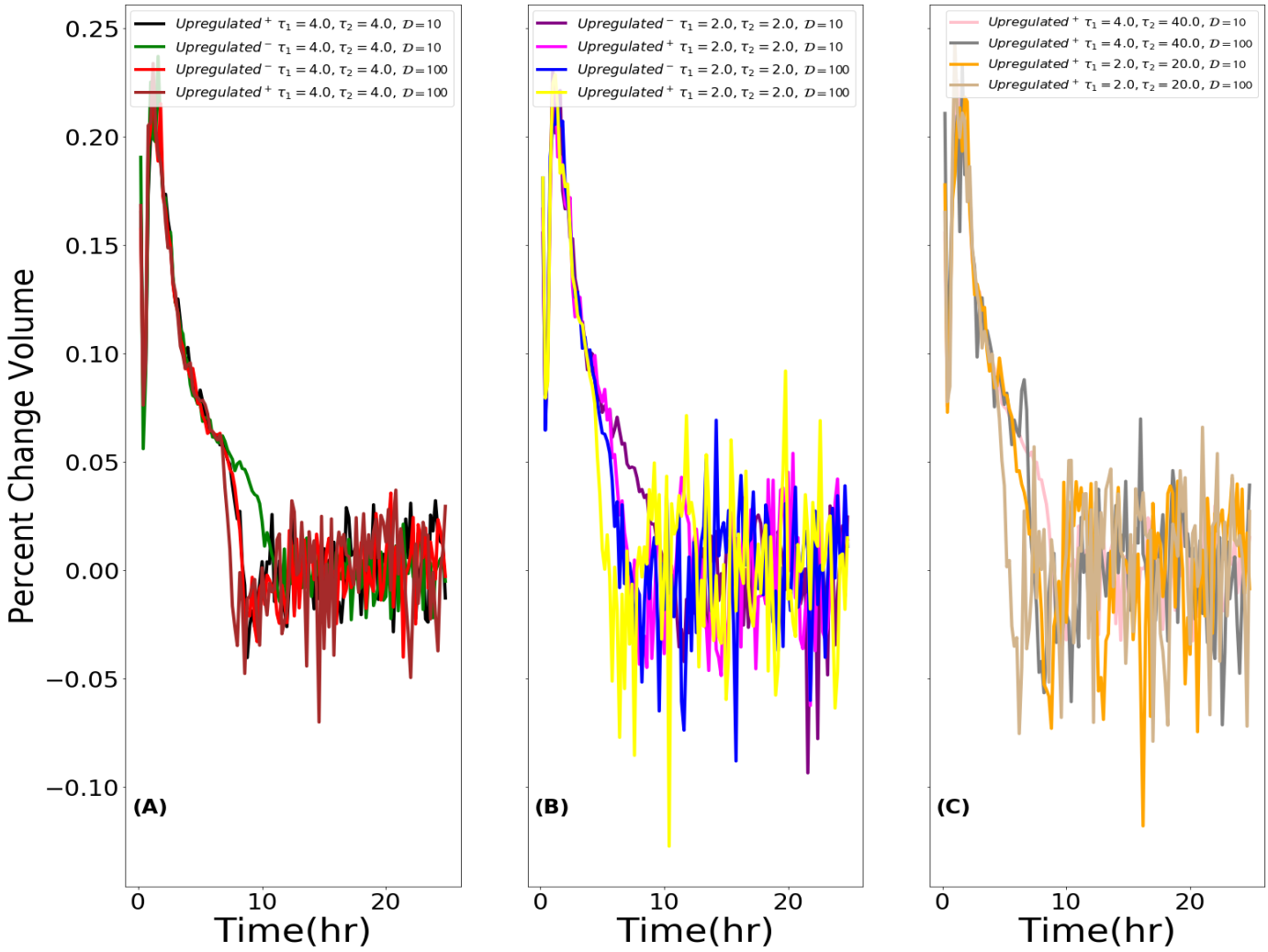

Figure 3.3-5 Loss of Biomass.
Figures A-C represent the change in biomass of the simulated biofilms. Figure A shows the loss of biomass for biofilms with $\tau_{1,2} = 4\mu M$ and for different values of the detachment factor. In figure A, the greatest loss of biomass was exhibited in biofilms where the detachment factor was set to 100 (red and maroon lines). In figure B, when $\tau_{1,2} = 2\mu M$ the same results held with the largest detachment occurring when $\mathcal{D} = 100$. In figure C, the largest detachment occurs when $\tau_1 = 2\mu M$ and $\tau_2 = 20\mu M$ with $\mathcal{D} = 100$. When we compare $\tau_1 = 4\mu M$ and $\tau_2 = 40\mu M$ biofilms the largest dispersal event again occurs when $\mathcal{D} = 100$

To better understand the dispersal dynamics exhibited by the biofilms, we measure the change in the biomass of the biofilm over the duration of the simulation. In figure 3.3.5 we plot the average percentage change in biomass for n=5 simulations for the parameter values listed. When comparing figure 3.3-5 A-B, biofilms with $\tau_1 = 4\mu M$ exhibit less biomass loss than

biofilms with $\tau_1 = 2\mu M$. The largest dispersal event observed is when $\tau_1 = 2\mu M$ and $\tau_2 = 2\mu M$ and $\mathcal{D} = 100$ with over 10% of the biofilm detached from the colony. Furthermore, we observe that cells with $\tau_1 = 2\mu M$ and $\mathcal{D} = 100$ experienced the greatest biomass loss. In figure 3.3-5 C, when the threshold is increased to $\tau_2 = 20\mu M$ and $\tau_2 = 40\mu M$ the highest loss in biomass occurs when $\mathcal{D} = 10$. Table 3.3-1 list the number of dispersal events for n=5 replication of simulated biofilm growth. From the table we see that biofilms with $\mathcal{D} = 100$ have a greater number of dispersal events than biofilms with $\mathcal{D} = 10$ except when $\tau_{1,2} = 2\mu M$ and the cells are capable of being upregulated. The largest difference in the number of dispersal events occurs when $\tau_1 = 4\mu M$and $\tau_2 = 40\mu M$. Figure 3.3-5 and table 3.3-1, leads us to conclude that increasing $\mathcal{D}$ causes earlier dispersal events therefore leading to overall more dispersal events. However, the detachment factor is not able to predict the size of the biomass that will be dispersed from the biofilm.

Table 3.3-1 Total Number of Dispersal Events

$\boldsymbol{\tau_1, \tau_2}$	Upregulated	$\mathcal{D} = 10$	$\mathcal{D} = 100$
2,2	+	48	45
2,2	-	38	46
4,4	+	41	46
4,4	-	42	45
2,20	+	39	41
4,40	+	32	45

The ratio of EPS to total biomass over the simulated growth of the biofilm is given in fig 3.3-6. Biofilms grown with $\tau_1 = 2\mu M$, fig 3.3-6B, have EPS occupying a larger fraction of the total biomass than biofilms with $\tau_1 = 4\mu M$, fig 3.3-6A. Due to the lower threshold value placed on cells to become upregulated and produce EPS. From fig 3.3-6A we see the maximum biofilm occupancy of EPS with $\tau_1 = 4\mu M$ is less than 50% of the overall biofilm. However, from figure 3.3-2 the overall volume of biofilms with $\tau_1 = 4\mu M$ has a higher maximum volume and

maintains a higher volume over the simulation. When we increase $\tau_2 = 20\mu M$ and $\tau_2 = 40\mu M$ biofilms with a detachment factor of $\mathcal{D} = 10$ have EPS occupying a great fraction of the biofilm than EPS with the detachment value set to $\mathcal{D} = 100$. In addition, for a given value of detachment factor biofilms with a lower τ_1 are composed of more EPS than biofilms with high τ_1. These observations lead us believe QS regulated EPS production can be used as a timing mechanism by biofilms. Specifically, a quorum regulated threshold can be used to ensure that the biofilm attain a high volume if desired while not having to pay the cost associated with secreting EPS at an earlier stage in development. This would confer an advantage to biofilm since it is now able to attain a high volume, obtain the protection of EPS but at a lower metabolic cost if the threshold τ_1 to produce EPS is high.

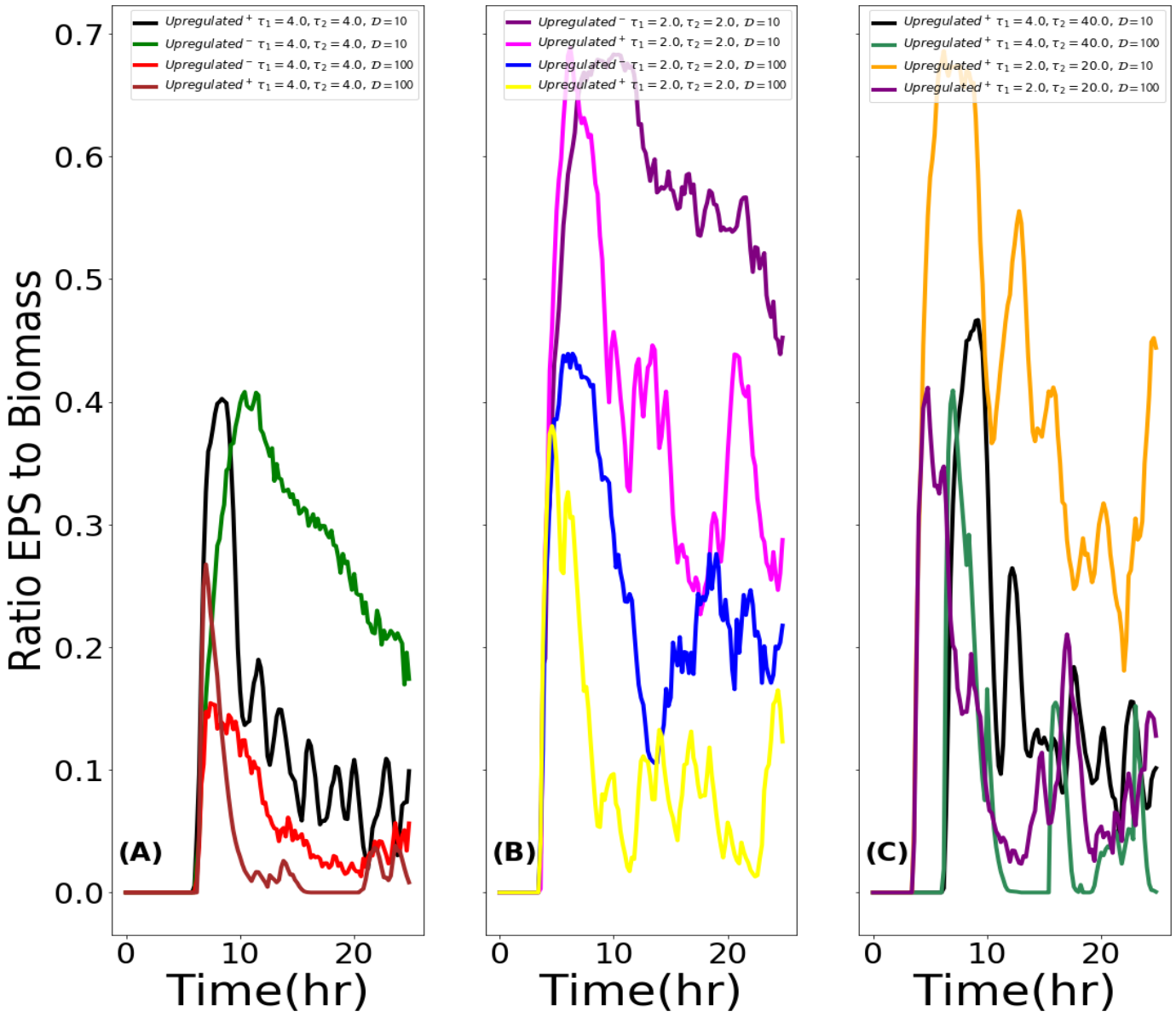

Figure 3.3-6 Fractional EPS Composition.
Figure A represents the amount of EPS in the biofilm when $\tau_{1,2} = 4\mu M$. The biofilms in figure A that $upregulated^+$ (black and maroon) have EPS occupying a greater fraction of the biomass than biofilm that are $upregulated^-$ (green and red). In figure B, $upregulated^-$ (maroon and blue) biofilms have EPS occupying a greater fraction of the biofilm when compared with $upregulated^+$ biofilms (yellow and pink). Figure C represents biofilms with τ_2 increased to $\tau_2 = 20\mu M$ and $\tau_2 = 40\mu M$. Biofilms with $\tau_1 = 2\mu M$(yellow and maroon) have EPS occupying a higher fraction of the biofilm than biofilms with $\tau_1 = 4\mu M$(black and green) for a given value of $\mathcal{D}$.

We next examine the dynamics of the biofilm under the conditions where the amount of EPS produced by the upregulated cells is decreased to half the original amount. When the EPS produced by a cell is proportional to its target volume we denote this as EPS^{+} when it is set to half the cells target volume EPS^{-}. In fig 3.3.7, we plot $EPS^{+}$and EPS^{-} biofilms for the thresholds listed. When $\tau_1 = 2\mu M$ yields biofilms with a smaller volume than $\tau_1 = 4\mu M$. When $\tau_1 = 2\mu M$ or $\tau_1 = 4\mu M$ the EPS^{+} biofilm reach a greater overall volume for the value of the detachment factor selected. The biofilms with $\mathcal{D} = 10$ also reach a larger maximum volume than the case when $\mathcal{D} = 100$ for the respective choice of τ_1. Suggesting the amount of EPS produced by a biofilm is another mechanism biofilms can use to regulate their size.

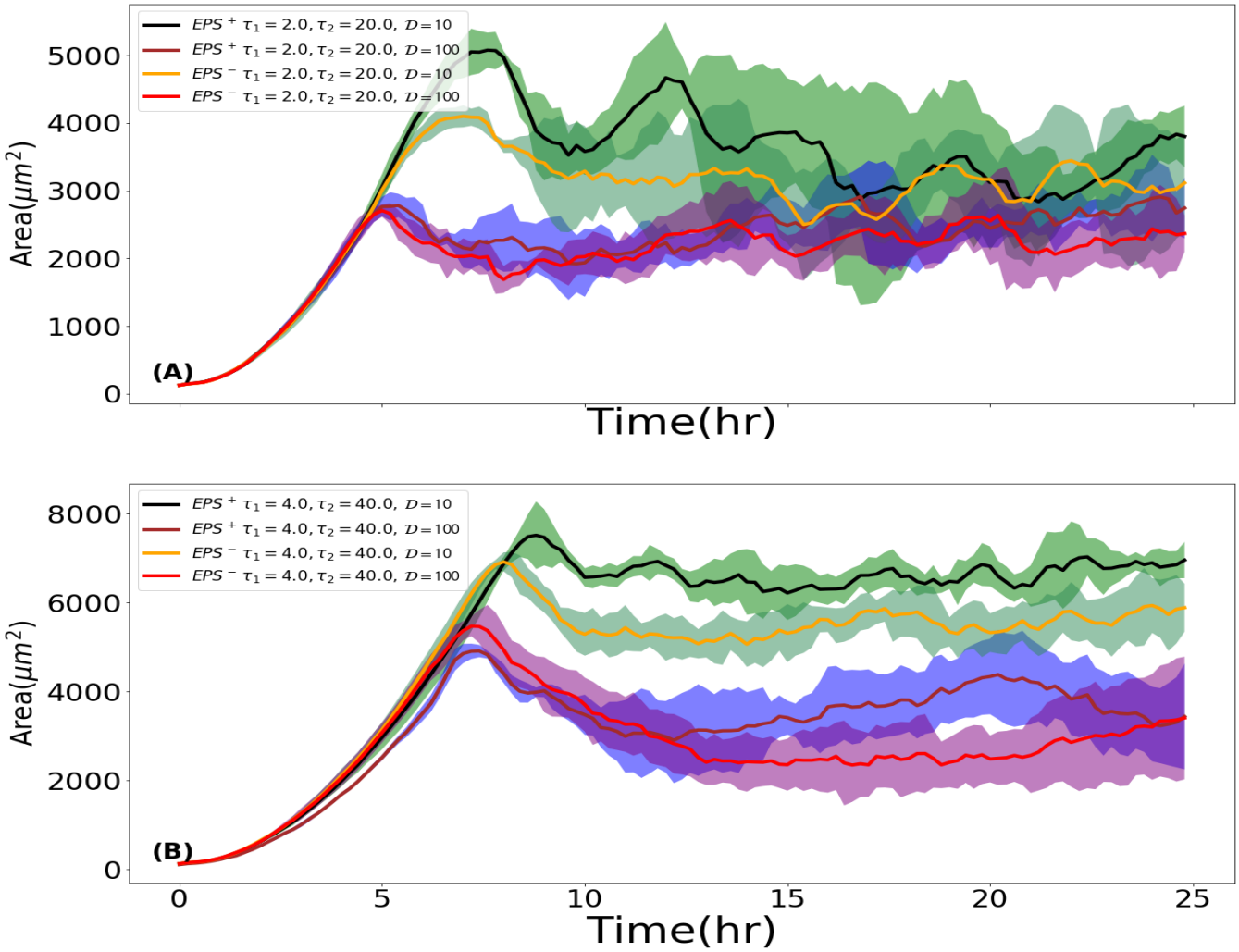

Figure 3.3-7 EPS^{+} VS EPS^{-}
Comparison of the case where matrix producing cells produce EPS at half the regular rate. When $\tau_1 = 2\mu M$ EPS^{+}biofilms (black and maroon) reach a maximum biomass value that is higher than EPS^{-}. The same behavior is observed when $\tau_1 = 4\mu M$. Biofilms with a higher value of detachment factor $\mathcal{D}$=100(maroon and red) reach a lower maximum biomass and lower biomass over the simulated growth period as observed in the previous simulated biofilms.

3.4 Conclusion

As pointed out in [130] Reducing biofilm cohesive (or adhesive) strength of a biofilm is the most important strategies to understand if we aim to better control them. Specifically, in [130] the authors discuss weakening cohesive forces could (1) allow prevailing hydrodynamic shear to remove biofilm, (2) increase the efficacy of designed interventions for removing biofilms, (3) enable phagocytic engulfment of softened biofilm aggregates, and (4) improve phagocyte mobility and access to biofilm. To this end we examine the effects of weakening cohesive forces of cells within the biofilm. Specifically, we incorporate thresholds on QS and dispersal in our model to understand QS the importance if any of quorum sensing induced EPS production and detachment.

From our simulation we conclude that QS regulated autoinducer production and detachment can be viewed as growth balancing mechanism enabling the biofilm to regulate their maximum size by producing EPS and dispersing cells. Specially, biofilms that included cells that were able to upregulate and increase their production of autoinducer had a smaller maximum size that was reached earlier than biofilm that were deficient of upregulated cells. Indicating that upregulation of autoinducer production as a mechanism used by biofilms to regulate their size. Biofilms that regulate their size in this manner have the advantage that they are able to have more nutrient and produce less waste due to smaller number of cells in the biofilm. In addition, we observe the timing of the dispersal is regulated by the value of the detachment factor. Biofilms where the detachment factor was set to $\mathcal{D} = 100$ had dispersal events occurring earlier than biofilms with $\mathcal{D} = 10$ for the thresholds selected. We hypothesize that early dispersal can also be used as a mechanism by the biofilm to ensure nutrient for the rest of the population to grow.

Incorporating thresholds on EPS production leads to different biofilm composition. Specifically, low thresholds on upregulating autoinducer and EPS production leads to biofilms where EPS comprises higher fraction of total biomass. We hypothesis having threshold regulated EPS production is used by the biofilm to ensure that it has reached an adequate size that warrants the costly production of EPS. Specifically, a threshold on EPS production maybe considered a mechanism for switching to a mode of EPS production once a certain number of cells is present. The production of EPS enhances protection from environmental insults ensuring the bacteria can protect themselves efficiently[141].

The plots of the temporal changes in the biomass indicate that the biofilms reach a steady state value as they mature. However, from figure 3.3-3 we see that we cannot make the claim of a steady state value of the overall biomass. The biofilm as it matures spreads horizontally along the substratum and some cells although not part of the initial biofilm accounted for when calculating the overall biomass since they are attached to the substratum. For future models, we would use another method to account for detached biomass that does not include using the substratum. Therefore, allowing us not to count these values in the overall biomass.

4 CONCLUSIONS AND FUTURE WORK

4.1 Conclusion

The behavior of biofilms is known to be under the control of not only cellular networks but also signals in their environment. Levels of autoinducer, Ph levels, nutrient and waste have been observed to effect the behavior of biofilms. The effect occurs from the initial stage of attachment of planktonic cells to a surface, intermediate stages such as phenotypic differentiation and cells dispersal, and ultimately the death. The environment signal that has been studied the most is quorum sensing due to it regulating a myriad of behaviors.

QS although widely studied, its interaction with other environmental signals is not fully understood. Furthermore, studies point to threshold values as causing certain behavior exhibited by biofilms but do not illustrate how the different threshold can lead to emergent properties exhibited in biofilms. Specifically, the spatial and temporal patterning formed by biofilms. In addition, models that are presented to model biofilms do not use QS to explain the phenotypic variation exhibited in biofilms. In addition, papers that present experimental evidence demonstrating the effects of QS threshold do not measure the values of the threshold and how they relate to the morphology of the biofilm. In our model we aim to fill these gaps.

Specifically, we aim to better understand the role QS has on the emergent property exhibited by biofilms by incorporating thresholds in an established agent based model. We want to better understand how biofilms use thresholds to govern the behavior that is observed experimentally. In particular, our model seeks to understand if using thresholds on QS and other environmental signals we can reproduce the spatiotemporal patterning exhibited in a lab strain of B. Subtilis. We next study QS thresholding as it relates to dispersal of cells in a biofilm.

Incorporating thresholds on QS and the nutrient level in the CPM, we reproduce the spatiotemporal pattern exhibited in the lab strain of B. Subtilis. From our simulations we discovered that it is necessary to use two autoinducer signals and a signal on the nutrient level. Leading us to use three thresholds to reproduce the results that were observed in the experiments. We next focused on gaining a better understanding of the QS and its role in cell dispersal. To gain an understand of the dispersal events we again incorporated a threshold on the autoinducer and EPS production. Using a threshold on these values allowed us to make inferences on the possible reasons a biofilm would want to upregulate production of EPS and autoinducer as discussed in the literature. Specifically, we found that biofilms that upregulate cells reach an overall smaller maximum size than biofilms that are not capable of upregulating autoinducer production. We hypothesize that upregulating autoinducer production is a mechanism used by cells to manage the size of the biofilm. We next incorporated thresholds on detachment. Specifically, we used a threshold that once exceeded would cause the cohesion between cell types in our model to weaken and allowing cells to disperse from the biofilm. We set a detachment factor that determines the strength of the weakening of the bonds. From our simulation we found that higher detachment factor led to dispersal of cells at an earlier time in the simulation than lower values. Suggesting another mechanism biofilms use to regulate their size.

Although, we gained insight on the behavior of biofilms using our model on detachment it has a significant shortcoming. Specifically, cells that are not connected to the main biofilm contribute to the overall biomass since they are attached to the substratum. Therefore, we cannot make predictions regarding the steady state behavior of the biofilms. In the model we proposed to explain the spatiotemporal distribution of phenotypes.

Despite the improvements needed to be made to the models they are capable of providing insight into the QS mechanism underlying some of the behaviors we observe in biofilms and is an advancement in the field of modeling biofilms. The model emphasizes thresholds on environmental factors which are the keys to driving the gene regulatory network affecting gene expressions in microbes. Thresholds are often discussed in biofilm literature but their interdependence hardly examined. Specifically, how does the increase or decrease in a threshold value affect the development of a colony and what are the advantages or disadvantages of having a threshold on certain activities such as EPS production or phenotype differentiation.

The model presented here tries to answer these questions in a novel way using an agent-based model and threshold values on some of the often-discussed environmental ques mentioned in literature. Using thresholds on autoinducers we reproduced the spatiotemporal dynamics exhibited in a colony of B. Subtilis. To the best of my knowledge this is the first time this has been done. Furthermore, our model separates the biofilm into EPS and bacterial components an attribute that is not common in many models but is necessary for a complete understanding of biofilm. The separation of EPS and bacterium component will prove useful in future studies that may include treatment with antibiotics. The inclusion of detachment although not new in biofilm modelling detachment as it relates to cohesion and QS has not been incorporated into a model of biofilms.

4.2 Future Work

Agent based modelling of biofilms is a promising field. There are still many questions that need to be answered. A multiscale model incorporating the gene regulatory networks that lead to autoinducer signals and the activation of a quorum will provide a better understanding not only of phenotypic variations exhibited in biofilms but also the important mechanism of biofilm dispersal. Furthermore, incorporating gene regulatory networks will allow one to understand how environmental signals such as nutrient or Ph levels effect the development of a biofilm. In addition to adding gene regulatory network to our model. Including an additional species of bacterium to the CPM would allow us include multispecies competition and division of labor by species.

REFERENCES

1. Donlan, R.M., *Biofilms: microbial life on surfaces.* Emerging infectious diseases, 2002. **8**(9): p. 881.
2. Lopez, D., H. Vlamakis, and R. Kolter, *Biofilms.* Cold Spring Harb Perspect Biol, 2010. **2**(7): p. a000398.
3. Donlan, R.M., *Biofilm Formation A Clinically Relevant Microbiological Process.* Clinical Infectious Diseases, 2001. **33**(1387-1392).
4. James, G.A., et al., *Biofilms in chronic wounds.* Wound Repair Regen, 2008. **16**(1): p. 37-44.
5. Singh, P.K., et al., *Quorum-sensing signals indicate that cystic fibrosis lungs are infected with bacterial biofilms.* Nature, 2000. **407**(6805): p. 762.
6. Sehar, S. and I. Naz, *Role of the Biofilms in Wastewater Treatment*, in *Microbial Biofilms - Importance and Applications*. 2016.
7. Mattei, M.R., et al., *Continuum and discrete approach in modeling biofilm development and structure: a review.* J Math Biol, 2017.
8. Kostakioti, M., M. Hadjifrangiskou, and S.J. Hultgren, *Bacterial biofilms: development, dispersal, and therapeutic strategies in the dawn of the postantibiotic era.* Cold Spring Harb Perspect Med, 2013. **3**(4): p. a010306.
9. Lappin-Scott, H.M. and J.W. Costerton, *Microbial biofilms.* Vol. 5. 2003: Cambridge University Press.
10. Bassler, M.B.M.a.B.L., *Quorum Sensng in Bacteria.* Annual Review ofMicrobiology, 2001 **55**: p. 165-199.

11. Li, Y.H. and X. Tian, *Quorum sensing and bacterial social interactions in biofilms.* Sensors (Basel), 2012. **12**(3): p. 2519-38.

12. Lopez, D., H. Vlamakis, and R. Kolter, *Generation of multiple cell types in Bacillus subtilis.* FEMS Microbiol Rev, 2009. **33**(1): p. 152-63.

13. Shank, E.A. and R. Kolter, *Extracellular signaling and multicellularity in Bacillus subtilis.* Curr Opin Microbiol, 2011. **14**(6): p. 741-7.

14. Hobley, L., et al., *Giving structure to the biofilm matrix: an overview of individual strategies and emerging common themes.* FEMS Microbiol Rev, 2015. **39**(5): p. 649-69.

15. Garrett, T.R., M. Bhakoo, and Z. Zhang, *Bacterial adhesion and biofilms on surfaces.* Progress in Natural Science, 2008. **18**(9): p. 1049-1056.

16. Kirmusaoglu, S., *Staphylococcal Biofilms: Pathogenicity, Mechanism and Regulation of Biofilm Formation by Quorum-Sensing System and Antibiotic Resistance Mechanisms of Biofilm-Embedded Microorganisms*, in *Microbial Biofilms - Importance and Applications*. 2016.

17. Steinberg, N. and I. Kolodkin-Gal, *The Matrix Reloaded: Probing the Extracellular Matrix Synchronizes Bacterial Communities.* J Bacteriol, 2015.

18. Koo, H. and K.M. Yamada, *Dynamic cell-matrix interactions modulate microbial biofilm and tissue 3D microenvironments.* Curr Opin Cell Biol, 2016. **42**: p. 102-112.

19. Aggarwal, S., P.S. Stewart, and R.M. Hozalski, *Biofilm Cohesive Strength as a Basis for Biofilm Recalcitrance: Are Bacterial Biofilms Overdesigned?* Microbiol Insights, 2015. **8**(Suppl 2): p. 29-32.

20. Taglialegna, A., I. Lasa, and J. Valle, *Amyloid Structures as Biofilm Matrix Scaffolds.* J Bacteriol, 2016. **198**(19): p. 2579-88.

21. Ma, L., et al., *Assembly and development of the Pseudomonas aeruginosa biofilm matrix.* PLoS Pathog, 2009. **5**(3): p. e1000354.

22. Flemming, H.-C., *The perfect slime.* Colloids and Surfaces B: Biointerfaces, 2011. **86**(2): p. 251-259.

23. Rutherford, S.T. and B.L. Bassler, *Bacterial quorum sensing: its role in virulence and possibilities for its control.* Cold Spring Harb Perspect Med, 2012. **2**(11).

24. Romeo, T., *Bacterial biofilms*. Vol. 322. 2008: Springer.

25. Passos da Silva, D., et al., *An Update on the Sociomicrobiology of Quorum Sensing in Gram-Negative Biofilm Development.* Pathogens, 2017. **6**(4).

26. Solano, C., M. Echeverz, and I. Lasa, *Biofilm dispersion and quorum sensing.* Curr Opin Microbiol, 2014. **18**: p. 96-104.

27. Stewart, P.S. and J. William Costerton, *Antibiotic resistance of bacteria in biofilms.* The Lancet, 2001. **358**(9276): p. 135-138.

28. Stewart, P.S., *Mechanisms of antibiotic resistance in bacterial biofilms.* Int J Med Microbiol, 2002. **292**(2): p. 107-13.

29. Roy, V., B.L. Adams, and W.E. Bentley, *Developing next generation antimicrobials by intercepting AI-2 mediated quorum sensing.* Enzyme Microb Technol, 2011. **49**(2): p. 113-23.

30. Xavier Jde, B., C. Picioreanu, and M.C. van Loosdrecht, *A general description of detachment for multidimensional modelling of biofilms.* Biotechnol Bioeng, 2005. **91**(6): p. 651-69.

31. Chambless, J.D. and P.S. Stewart, *A three-dimensional computer model analysis of three hypothetical biofilm detachment mechanisms.* Biotechnol Bioeng, 2007. **97**(6): p. 1573-84.

32. Liebal, U.W., et al., *How mathematical modelling elucidates signalling in Bacillus subtilis.* Mol Microbiol, 2010. **77**(5): p. 1083-95.

33. Dockery, J.D. and J.P. Keener, *A mathematical model for quorum sensing in Pseudomonas aeruginosa.* Bull Math Biol, 2001. **63**(1): p. 95-116.

34. Chopp, D.L., et al., *A mathematical model of quorum sensing in a growing bacterial biofilm.* J Ind Microbiol Biotechnol, 2002. **29**(6): p. 339-46.

35. Mattei, M.R., et al., *Continuum and discrete approach in modeling biofilm development and structure: a review.* J Math Biol, 2018. **76**(4): p. 945-1003.

36. Ermentrout, G.B., and Leah Edelstein-Keshet, *Cellular Automata Approaches to Biological Modeling.* Journal of theoretical Biology, 1993. **160**.

37. Bussemaker, H.J., *Analysis of a pattern-forming lattice-gas automaton: Mean-field theory and beyond.* Physical Review E, 1996. **53**(2): p. 1644-1661.

38. Graner, F., and James A. Glazier., *Simulation of biological cell sorting using a two-dimensional extended Potts model.* Physical review letters 1992. **69**(13).

39. Scianna, M. and L. Preziosi, *Multiscale Developments of the Cellular Potts Model.* Multiscale Modeling & Simulation, 2012. **10**(2): p. 342-382.

40. McCoy, B.M. and T.T. Wu, *The two-dimensional Ising model*. 2014: Courier Corporation.

41. Steinberg, M.S., *Does differential adhesion govern self‐assembly processes in histogenesis? Equilibrium configurations and the emergence of a hierarchy among*

populations of embryonic cells. Journal of Experimental Zoology, 1970. **173**(4): p. 395-433.

42. Preziosi, M.S.a.L., *Cellular Potts Models Multiscale Extensions and Biological Applications.pdf.* CRC Press, 2013.
43. Scianna, M. and L. Preziosi, *Cellular Potts Models: Multiscale Extensions and Biological Applications*. 2013: Chapman and Hall/CRC.
44. J. W. Costerton, P.S.S., E. P. Greenberg, *Bacterial Biofilms: A Common Cause of Persistent Infections.* Science, 1999. **284**: p. 1318-1322.
45. Murphy, J.T., R. Walshe, and M. Devocelle, *A computational model of antibiotic-resistance mechanisms in methicillin-resistant Staphylococcus aureus (MRSA).* J Theor Biol, 2008. **254**(2): p. 284-93.
46. Vlamakis, H., et al., *Sticking together: building a biofilm the Bacillus subtilis way.* Nat Rev Microbiol, 2013. **11**(3): p. 157-68.
47. Flemming, H.C. and J. Wingender, *The biofilm matrix.* Nat Rev Microbiol, 2010. **8**(9): p. 623-33.
48. Merle E. Olson, H.C., Douglas W. Morck, Andre G. Buret, Ronald R. Read, *Biofilm bacteria: formation and comparative susceptibility to antibiotics.* The Canadian Journal of Veterinary Research, 2002. **66**(2): p. 86.
49. Donlan, R.M. and J.W. Costerton, *Biofilms: Survival Mechanisms of Clinically Relevant Microorganisms.* Clinical Microbiology Reviews, 2002. **15**(2): p. 167-193.
50. Flemming, H.-C., *Microbial Biofouling: Unsolved Problems, Insufficient Approaches, and Possible Solutions*, in *Biofilm Highlights*. 2011. p. 81-109.

51. Fux, C.A., et al., *Survival strategies of infectious biofilms.* Trends Microbiol, 2005. **13**(1): p. 34-40.

52. Kussell, E. and S. Leibler, *Phenotypic diversity, population growth, and information in fluctuating environments.* Science, 2005. **309**(5743): p. 2075-8.

53. Grote, J., D. Krysciak, and W.R. Streit, *Phenotypic Heterogeneity, a Phenomenon That May Explain Why Quorum Sensing Does Not Always Result in Truly Homogenous Cell Behavior.* Appl Environ Microbiol, 2015. **81**(16): p. 5280-9.

54. Schreiber, F., et al., *Phenotypic heterogeneity driven by nutrient limitation promotes growth in fluctuating environments.* Nat Microbiol, 2016. **1**(6): p. 16055.

55. Kearns, D.B. and R. Losick, *Cell population heterogeneity during growth of Bacillus subtilis.* Genes Dev, 2005. **19**(24): p. 3083-94.

56. Lopez, D. and R. Kolter, *Extracellular signals that define distinct and coexisting cell fates in Bacillus subtilis.* FEMS Microbiol Rev, 2010. **34**(2): p. 134-49.

57. Cairns, L.S., L. Hobley, and N.R. Stanley-Wall, *Biofilm formation by Bacillus subtilis: new insights into regulatory strategies and assembly mechanisms.* Mol Microbiol, 2014. **93**(4): p. 587-98.

58. Wang, X., et al., *Probing phenotypic growth in expanding Bacillus subtilis biofilms.* Appl Microbiol Biotechnol, 2016. **100**(10): p. 4607-15.

59. Srinivasan, S., et al., *Matrix production in Bacillus subtilis biofilms is localized to a propagating front.* bioRxiv preprint 2017: p. 14.

60. Wang, X., S. Meng, and J. Han, *Morphologies and phenotypes in Bacillus subtilis biofilms.* J Microbiol, 2017. **55**(8): p. 619-627.

61. Vlamakis, H., et al., *Control of cell fate by the formation of an architecturally complex bacterial community.* Genes Dev, 2008. **22**(7): p. 945-53.

62. Tasaki, S., M. Nakayama, and W. Shoji, *Morphologies of Bacillus subtilis communities responding to environmental variation.* Dev Growth Differ, 2017. **59**(5): p. 369-378.

63. K. P. Lemon, A.M.E., H. C. Vlamakis, C. Aguilar, and R. Kolter, *Biofilm Development with an Emphasis on Bacillus subtilis.* Current Topics in Microbiology and Immunology 2008.

64. Aguilar, C., et al., *Thinking about Bacillus subtilis as a multicellular organism.* Curr Opin Microbiol, 2007. **10**(6): p. 638-43.

65. Romero, D., et al., *Amyloid fibers provide structural integrity to Bacillus subtilis biofilms.* Proc Natl Acad Sci U S A, 2010. **107**(5): p. 2230-4.

66. Driks, A., *Tapping into the biofilm: insights into assembly and disassembly of a novel amyloid fibre in Bacillus subtilis.* Mol Microbiol, 2011. **80**(5): p. 1133-6.

67. Setlow, P., *Spores of Bacillus subtilis: their resistance to and killing by radiation, heat and chemicals.* J Appl Microbiol, 2006. **101**(3): p. 514-25.

68. Grossman, A.D., *Genetic networks controlling the initiation of sporulation and the development of genetic competence in Bacillus subtilis.* Annual review of genetics, 1995. **29**(1): p. 477-508.

69. Kumar, A. and T.R. Singh, *A quantitative study of gene regulatory pathways in Bacillus subtilis for virulence and competence phenotype by quorum sensing.* Syst Synth Biol, 2013. **7**(1-2): p. 33-9.

70. Maamar, H., A. Raj, and D. Dubnau, *Noise in gene expression determines cell fate in Bacillus subtilis.* Science, 2007. **317**(5837): p. 526-9.

71. Stiegelmeyer, S.M. and M.C. Giddings, *Agent-based modeling of competence phenotype switching in Bacillus subtilis.* Theor Biol Med Model, 2013. **10**: p. 23.

72. Jabbari, S., J.T. Heap, and J.R. King, *Mathematical modelling of the sporulation-initiation network in Bacillus subtilis revealing the dual role of the putative quorum-sensing signal molecule PhrA.* Bull Math Biol, 2011. **73**(1): p. 181-211.

73. De Jong, H., et al., *Qualitative simulation of the initiation of sporulation in Bacillus subtilis.* Bull Math Biol, 2004. **66**(2): p. 261-99.

74. Narula, J., et al., *Ultrasensitivity of the Bacillus subtilis sporulation decision.* Proc Natl Acad Sci U S A, 2012. **109**(50): p. E3513-22.

75. López, D., et al., *Structurally diverse natural products that cause potassium leakage trigger multicellularity in Bacillus subtilis.* Proceedings of the National Academy of Sciences, 2009. **106**(1): p. 280-285.

76. Ben-Jacob, E., et al., *The physics of bacterial decision making.* Front Cell Infect Microbiol, 2014. **4**: p. 154.

77. *Reaction–diffusion modelling of bacterial colony patterns.*

78. Zhang, T., *Modeling Biofilms: From Genes to Communities.* Processes, 2017. **5**(4).

79. von Bronk, B., A. Gotz, and M. Opitz, *Complex microbial systems across different levels of description.* Phys Biol, 2018. **15**(5): p. 051002.

80. Vishnoi, M., et al., *Triggering sporulation in Bacillus subtilis with artificial two-component systems reveals the importance of proper Spo0A activation dynamics.* Mol Microbiol, 2013. **90**(1): p. 181-94.

81. Fujita, M. and R. Losick, *Evidence that entry into sporulation in Bacillus subtilis is governed by a gradual increase in the level and activity of the master regulator Spo0A.* Genes Dev, 2005. **19**(18): p. 2236-44.

82. Lopez, D., et al., *Paracrine signaling in a bacterium.* Genes Dev, 2009. **23**(14): p. 1631-8.

83. Jung, J., et al., *Improvement of surfactin production in Bacillus subtilis using synthetic wastewater by overexpression of specific extracellular signaling peptides, comX and phrC.* Biotechnol Bioeng, 2012. **109**(9): p. 2349-56.

84. Michiko M. Nakano, R.M., Adam Myers, Jane Curry, Alan D. Grossman, and Peter Zuber, *srfA Is an Operon Required for Surfactin Production, Competence Development, and Efficient Sporulation in Bacillus subtilis.*

85. Auchtung, J.M., C.A. Lee, and A.D. Grossman, *Modulation of the ComA-dependent quorum response in Bacillus subtilis by multiple Rap proteins and Phr peptides.* J Bacteriol, 2006. **188**(14): p. 5273-85.

86. Rai, N., R. Rai, and K.V. Venkatesh, *Quorum Sensing in Competence and Sporulation*, in *Quorum Sensing vs Quorum Quenching: A Battle with No End in Sight*. 2015. p. 61-64.

87. Lopez, D., et al., *Structurally diverse natural products that cause potassium leakage trigger multicellularity in Bacillus subtilis.* Proc Natl Acad Sci U S A, 2009. **106**(1): p. 280-5.

88. Zhang, W., et al., *Nutrient depletion in Bacillus subtilis biofilms triggers matrix production.* New Journal of Physics, 2014. **16**(1).

89. McKenney, P.T., A. Driks, and P. Eichenberger, *The Bacillus subtilis endospore: assembly and functions of the multilayered coat.* Nat Rev Microbiol, 2013. **11**(1): p. 33-44.

90. Schultz, D., et al., *Deciding fate in adverse times: sporulation and competence in Bacillus subtilis.* Proc Natl Acad Sci U S A, 2009. **106**(50): p. 21027-34.

91. Barbieri, G., et al., *CodY regulates expression of the Bacillus subtilis extracellular proteases Vpr and Mpr.* J Bacteriol, 2015. **197**(8): p. 1423-32.

92. Handke, L.D., R.P. Shivers, and A.L. Sonenshein, *Interaction of Bacillus subtilis CodY with GTP.* J Bacteriol, 2008. **190**(3): p. 798-806.

93. Serror, Pascale, and Abraham L. Sonenshein, *CodY Is Required for Nutritional Repression of Bacillus subtilis Genetic Competence.* JOURNAL OF BACTERIOLOGY, 1996. **178**(20): p. 5910–5915.

94. Swat, M.H., et al., *Multi-scale modeling of tissues using CompuCell3D.* Methods Cell Biol, 2012. **110**: p. 325-66.

95. Graner, F. and J.A. Glazier, *Simulation of biological cell sorting using a two-dimensional extended Potts model.* Physical review letters, 1992. **69**(13): p. 2013.

96. Staudt, C., et al., *Volumetric measurements of bacterial cells and extracellular polymeric substance glycoconjugates in biofilms.* Biotechnol Bioeng, 2004. **88**(5): p. 585-92.

97. Stewart, P.S., *Diffusion in Biofilms.* Journal of Bacteriology, 2003. **185**(5): p. 1485-1491.

98. Pai, A. and L. You, *Optimal tuning of bacterial sensing potential.* Mol Syst Biol, 2009. **5**: p. 286.

99. Thomas Boland and a.F.J.S. Robert A. Latour, *Molecular Basis of Bacterial Adhesion.* Handbook of Bacterial Adhesion: Principles, Methods, and Applications, 2000.

100. Kreth, J. and M.C. Herzberg, *Molecular Principles of Adhesion and Biofilm Formation,* in *The Root Canal Biofilm*. 2015. p. 23-53.

101. Aggarwal, S., E.H. Poppele, and R.M. Hozalski, *Development and testing of a novel microcantilever technique for measuring the cohesive strength of intact biofilms.* Biotechnol Bioeng, 2010. **105**(5): p. 924-34.

102. Ahimou, F., et al., *Biofilm cohesiveness measurement using a novel atomic force microscopy methodology.* Appl Environ Microbiol, 2007. **73**(9): p. 2897-904.

103. Lau, P.C., et al., *Absolute quantitation of bacterial biofilm adhesion and viscoelasticity by microbead force spectroscopy.* Biophys J, 2009. **96**(7): p. 2935-48.

104. Burdett, I. D., T. B. Kirkwood, and J. B. Whalley, *Growth Kinetics of Individual Bacillus subtilis Cells and Correlation with Nucleoid Extension.* Journal of Bacteriology, 1986. **167**(1): p. 219-230.

105. Wang, X., G. Wang, and M. Hao, *Modeling of the Bacillus subtilis Bacterial Biofilm Growing on an Agar Substrate.* Comput Math Methods Med, 2015. **2015**: p. 581829.

106. Cornforth, D.M., et al., *Combinatorial quorum sensing allows bacteria to resolve their social and physical environment.* Proc Natl Acad Sci U S A, 2014. **111**(11): p. 4280-4.

107. Mirouze, N. and D. Dubnau, *Chance and Necessity in Bacillus subtilis Development.* Microbiol Spectr, 2013. **1**(1).

108. Lazazzera, B.A., *Quorum sensing and starvation: signals for entry into stationary phase.* Current Opinion in Microbiology, 2000. **3**(2): p. 177-182.

109. *Purification and characterization of an extracellular peptide factor that affects two different developmental pathways in Bacillus subtilis.*

110. Allison, D.G., *Community structure and co-operation in biofilms*. 2000: Cambridge University Press.

111. Uppuluri, P. and J.L. Lopez-Ribot, *Go Forth and Colonize: Dispersal from Clinically Important Microbial Biofilms.* PLoS Pathog, 2016. **12**(2): p. e1005397.

112. Hunt, S.M., et al., *Hypothesis for the role of nutrient starvation in biofilm detachment.* Appl Environ Microbiol, 2004. **70**(12): p. 7418-25.

113. Petrova, O.E. and K. Sauer, *Escaping the biofilm in more than one way: desorption, detachment or dispersion.* Curr Opin Microbiol, 2016. **30**: p. 67-78.

114. Kaplan, J.B., *Biofilm dispersal: mechanisms, clinical implications, and potential therapeutic uses.* J Dent Res, 2010. **89**(3): p. 205-18.

115. Fleming, D. and K.P. Rumbaugh, *Approaches to Dispersing Medical Biofilms.* Microorganisms, 2017. **5**(2).

116. Barraud, N., S. Kjelleberg, and S.A. Rice, *Dispersal from Microbial Biofilms.* Microbiol Spectr, 2015. **3**(6).

117. Romeo, T., *When the party is over: a signal for dispersal of Pseudomonas aeruginosa biofilms.* J Bacteriol, 2006. **188**(21): p. 7325-7.

118. Gujer, O.W.W., *A multispecies biofilm model.* Biotechnology and Bioengineering 1986. **28 i**(3).

119. Duddu, R., D.L. Chopp, and B. Moran, *A two-dimensional continuum model of biofilm growth incorporating fluid flow and shear stress based detachment.* Biotechnol Bioeng, 2009. **103**(1): p. 92-104.

120. Hunt, S.M., et al., *A computer investigation of chemically mediated detachment in bacterial biofilms.* Microbiology, 2003. **149**(Pt 5): p. 1155-63.

121. Kreft, J.-U., et al., *Individual-based modelling of biofilms.* Microbiology, 2001. **147**(11): p. 2897-2912.

122. Emerenini, B.O., et al., *A Mathematical Model of Quorum Sensing Induced Biofilm Detachment.* PLoS One, 2015. **10**(7): p. e0132385.

123. Xu, H. and Y. Liu, *d-Amino acid mitigated membrane biofouling and promoted biofilm detachment.* Journal of Membrane Science, 2011. **376**(1-2): p. 266-274.

124. Boles, B.R., M. Thoendel, and P.K. Singh, *Rhamnolipids mediate detachment of Pseudomonas aeruginosa from biofilms.* Mol Microbiol, 2005. **57**(5): p. 1210-23.

125. Landini, P., et al., *Molecular mechanisms of compounds affecting bacterial biofilm formation and dispersal.* Appl Microbiol Biotechnol, 2010. **86**(3): p. 813-23.

126. Nijland, R., M.J. Hall, and J.G. Burgess, *Dispersal of biofilms by secreted, matrix degrading, bacterial DNase.* PLoS One, 2010. **5**(12): p. e15668.

127. Boles, B.R. and A.R. Horswill, *Agr-mediated dispersal of Staphylococcus aureus biofilms.* PLoS Pathog, 2008. **4**(4): p. e1000052.

128. Araujo, L.V.d., et al., *Rhamnolipid and surfactin: Anti-adhesion/antibiofilm and antimicrobial effects.* Food Control, 2016. **63**: p. 171-178.

129. Zezzi do Valle Gomes, M. and M. Nitschke, *Evaluation of rhamnolipid and surfactin to reduce the adhesion and remove biofilms of individual and mixed cultures of food pathogenic bacteria.* Food Control, 2012. **25**(2): p. 441-447.

130. Stewart, P.S., *Biophysics of biofilm infection.* Pathog Dis, 2014. **70**(3): p. 212-8.

131. Dusane, D.H., et al., *Rhamnolipid mediated disruption of marine Bacillus pumilus biofilms.* Colloids Surf B Biointerfaces, 2010. **81**(1): p. 242-8.

132. Dunny, G.M., and Bettina AB Leonard, *Cell-Cell Communication in Gram-Positive Bacteria.* Annual Reviews in Microbiology, 1997. **51**(1): p. 527-564.

133. Abee, T., et al., *Biofilm formation and dispersal in Gram-positive bacteria.* Curr Opin Biotechnol, 2011. **22**(2): p. 172-9.

134. Costerton, J., *biofilm primer.* 2007.

135. Vu, B., et al., *Bacterial extracellular polysaccharides involved in biofilm formation.* Molecules, 2009. **14**(7): p. 2535-54.

136. Sauer, K., et al., *Pseudomonas aeruginosa Displays Multiple Phenotypes during Development as a Biofilm.* Journal of Bacteriology, 2002. **184**(4): p. 1140-1154.

137. Kim, S.M., et al., *LuxR homologue SmcR is essential for Vibrio vulnificus pathogenesis and biofilm detachment, and its expression is induced by host cells.* Infect Immun, 2013. **81**(10): p. 3721-30.

138. Fujita, M., J.E. Gonzalez-Pastor, and R. Losick, *High- and low-threshold genes in the Spo0A regulon of Bacillus subtilis.* J Bacteriol, 2005. **187**(4): p. 1357-68.

139. Xavier, J.B., *Social interaction in synthetic and natural microbial communities.* Mol Syst Biol, 2011. **7**: p. 483.

140. Ashleigh S. Griffin, S.A.W.a.A.B., *Cooperation and competition in pathogenic bacteria.* Nature, 2004. **430**(7003): p. 1021-4.

141. Frederick, M.R., et al., *A mathematical model of quorum sensing regulated EPS production in biofilm communities.* Theor Biol Med Model, 2011. **8**: p. 8.

142. Tarjan, Robert., *Depth-first search and linear graph algorithms.* SIAM journal on computing 1.2 (1972): 146-160.

143. Jabbouri, S. and I. Sadovskaya, *Characteristics of the biofilm matrix and its role as a possible target for the detection and eradication of Staphylococcus epidermidis associated with medical implant infections.* FEMS Immunol Med Microbiol, 2010. **59**(3): p. 280-91.

144. J. Maxwell Dow, L.C., Kim Findlay, Yong-Qiang He, Jia-Xun Feng, and Ji-Liang Tang, *Biofilm dispersal in Xanthomonas campestris is controlled by cell– cell signaling and is required for full virulence to plants.* PNAS 2003. **100**(19): p. 10995.

145. Efendiev, M., *Evolution equations arising in the modelling of life sciences*. Vol. 163. 2013: Springer Science & Business Media.

146. Von Bodman, Susanne Beck, Doris R. Majerczak, and David L. Coplin., *A negative regulator mediates quorum-sensing control of exopolysaccharide production in Pantoea stewartii subsp. stewartii.* Proceedings of the National Academy of Sciences, 1998. **95**.